Geosciences Journal
Vol. 8, No. 2, p. 211–264, June 2004

Depositional processes of late Quaternary sediments in the Yellow Sea: a review

Sung Kwun Chough* — *School of Earth and Environmental Sciences, Seoul National University, Seoul 151-747, Korea*
Hee Jun Lee — *National Research Laboratory for Coastal Sedimentary Dynamics, Korea Ocean Research and Development Institute, Ansan, P.O.Box 29, Seoul 425-600, Korea*
Seung Soo Chun — *Faculty of Earth Systems and Environmental Sciences, Basic Science Institute, Chonnam National University, Gwangju 500-757, Korea*
Young Jae Shinn — *School of Earth and Environmental Sciences, Seoul National University, Seoul 151-747, Korea*

ABSTRACT: This review focuses on the depositional processes of late Quaternary sediments in the eastern Yellow Sea, an epicontinental sea with a flat and broad seafloor (less than 100 m in water depth) and extensive tidal flats along the southeastern coast. The Yellow Sea was subaerially exposed during the last glacial period when sea level was about 120 m below the present level. During erosional retreat of shorefaces and river mouths, sedimentation was largely controlled by high-amplitude rise in sea level, forming transgressive sheets (echo type 1-3a) and sediment ridges (echo types 2-1 and 2-2) with extensive development of ravinement surfaces. The distribution of surface sediments reflects an interplay of sediment input from the surrounding landmass and the hydrodynamic regime in response to sea-level rise. Muddy sediments in the central part represent the Huanghe-River source and form a highstand sheet (echo type 1-3b). Large birdfoot-like sand bodies off the Jiangsu coast also represent highstand deposits when sea level reached the present position at about 6 ka. In the southeastern part of the Yellow Sea, sediments are dominated by sand ridges (echo types 2-1, 2-2 and 2-3), largely shaped by tidal currents. The southwestern corner of the Korean Peninsula is dominated by a thick deposit of mud, the Heuksan mud belt. The muds largely originate from the Geum River, whose distribution is controlled by strong southward coastal currents. In the coastal regions of the southeastern Yellow Sea, sedimentation is controlled by a combined effect of waves and tides with distinctive seasonalities in sedimentary facies owing to the monsoonal climate: tide-dominated mud deposition in summer and wave-dominated sand deposition/erosion in winter. Winter storms play a role in sedimentation on intertidal flats. Quantitative monitoring of sediment transport suggests that the textural variation results from the overwhelming role of winter waves superimposed on tidal currents in pulling sands and resuspending muds. Due to low sedimentation rate, the tidal flats formed retrogradational, coarsening-upward pattern during the Holocene sea-level rise.

Key words: Yellow Sea, Quaternary sediments, depositional processes, tidal flats, sediment transport

1. INTRODUCTION

The Yellow Sea forms an epicontinental sea (ca. 500,000 km^2 in area) surrounded by the landmass of China and Korea and is arbitrarily bordered to the East China Sea by a line connecting Jeju Island and south of Changjiang River mouth (Fig. 1). The sea is characterized by a flat and broad seafloor with an average water depth of 55 m. The seafloor deepens toward the north-south trending axis that lies in the eastern part of the sea, reaching more than 100 m in water depth in the vicinity of Jeju Island (Fig. 1). The western part of the sea includes deltas of the Huanghe River and the isobaths are parallel to the coastline, whereas the eastern part is fringed by numerous islands, estuaries and tidal flats. Tidal sand ridges are ubiquitous in water depth of about 70 m. Off the Jiangsu coast, the shallow and flat seafloor forms in water depth of 50 m and slopes gently eastward to the central part of the sea (Fig. 1).

The Yellow Sea was subaerially exposed during the last glacial period when sea level was lowered by about 120 m below the present level (Fairbanks, 1989; Chough et al., 2000). In the central part of the sea, marine transgression initiated at about 12–11 ka (Wang et al., 1985; Kim and Kennett, 1998) and sea level reached the present position at about 6 ka (Chough et al., 2000). Depositional processes of Quaternary sediments have largely been controlled by changes in sea level in concert with spatio-temporal variations in water-mass circulation and along-shore and seasonal currents, waves and tidal currents (Chough et al., 2000; Park et al., 2000; Lee and Chu, 2001). High amplitude sea-level rise had especially strong influence on sedimentation during erosional retreat of shorefaces and river mouths when pre-Holocene deposits were intensively eroded to form transgressive sheets and sediment ridges (Lee and Yoon, 1997; Jin et al., 2002). As the rate of sea-level rise decreased, depositional processes were affected by sediment supply, topography and prevailing currents (Jin and Chough, 1998; Park et al., 2000; Liu et al., 2002).

At the turn of the new millennium, major improvements have been made in the acquisition of high-resolution seismic data and deep cores, especially in the eastern part of the Yellow sea (Fig. 2). The high-resolution Chirp profiles were obtained in a closely-spaced pattern, enabling surface sediment distribution to be related with subsurface echo types (Chough et al., 2002). Combined with deep drill cores and age dates, these data help understand depositional processes of late Quaternary sediments in sequence stratigraphic per-

*Corresponding author: sedlab@snu.ac.kr

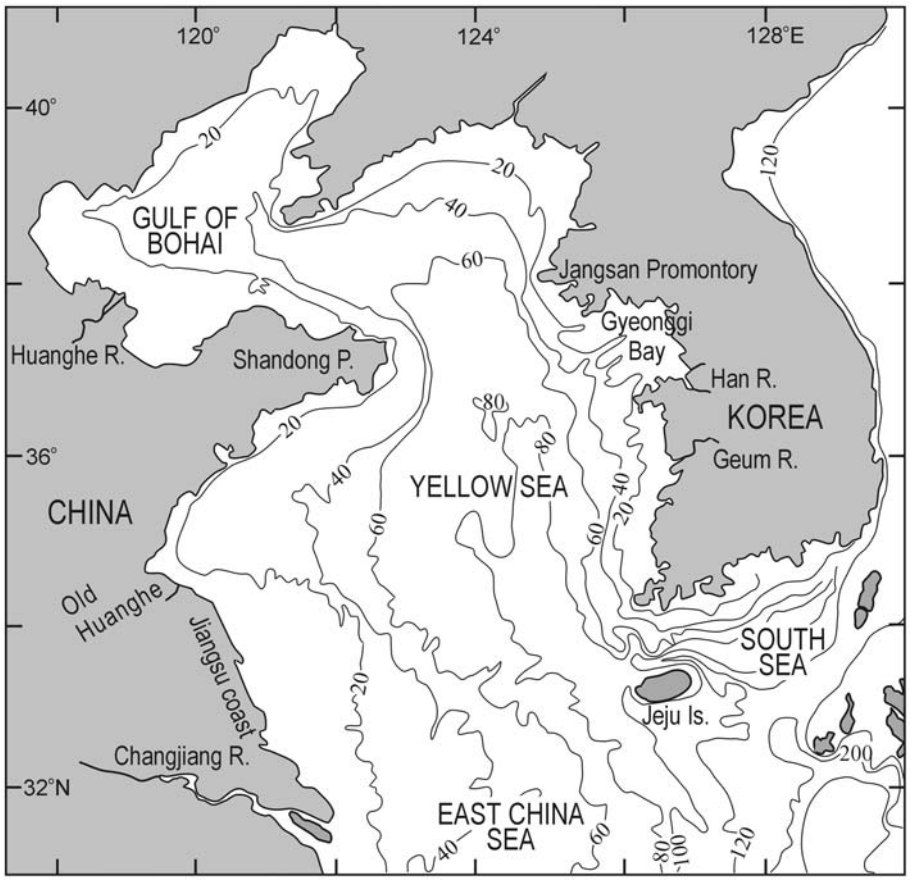

Fig. 1. Bathymetry of the Yellow Sea. Contours in meters.

spectives. This review provides a state-of-the-art summary of the distribution, origin and sink of late Quaternary sediments, depositional processes in response to sea-level changes and their controlling factors in the Yellow Sea. The emphasis is also placed on depositional processes on tidal flats along the coastline of the Korean Peninsula.

2. OCEANOGRAPHIC SETTING

The Yellow and Bohai seas are affected by warm and saline oceanic currents and less saline coastal currents in a basin-wide scheme of a cyclonic gyre (Fig. 3). In general, the former flow northward whilst the latter flow southward. On the east side of the Yellow Sea, the Kuroshio and Tsushima warm currents and the Yellow Sea warm current (YSWC) dominate, whereas various coastal currents prevail in the Chinese shallow waters (Fig. 3). Coastal currents flow southward along the west coast of Korea particularly during winter (Fig. 3). In the southern Yellow and East China seas, pronounced coastal currents switch their current direction seasonally, i.e., southward in winter and northward in summer, although the direction of the offshore Taiwan warm current is constantly northward (Fig. 3). In particular, during the summertime flooding season, the northward Taiwan warm current meets the discharge of the Changjiang River forming the "Changjiang diluted water (CDW)" off the river mouth. The CDW extends southeast- to eastward and may reach the offshore west of Jeju Island during peak floods (Guan, 1994). Nonetheless, the major current patterns in the Bohai, Yellow and East China seas remain more or less consistent regardless of season (Guan, 1994).

A seasonal cold water mass (Yellow Sea cold water) occurs in the lower water column of the central Yellow Sea during the warm half of the year (April–November) (Su and Weng, 1994). It is characterized by lower temperature and higher salinity compared with those of surrounding waters and varies in distribution and volume with season. It is considered that the Yellow Sea cold water derived from the surface water of the previous winter sinking through a cooling process. In contrast, the origin of the YSWC is still controversial. A variety of theories are suggested, including a simple branch of the Tsushima warm current or the Taiwan warm current (Beardsley et al., 1985; Guan, 1994) and an upwind current by the northerly winds of the winter monsoon (Hsueh and Romca, 1986; Park, 1986; Mask et al., 1998). There is also debate on hydraulic behavior of the YSWC, a question as to whether it is a persistent mean current or an intermittently generated current (Guan, 1994; Lie et al., 2001). The coastal current along the Korean coast, reinforced by strong northerly winds during late fall and winter, flows southward and then eastward through the Jeju

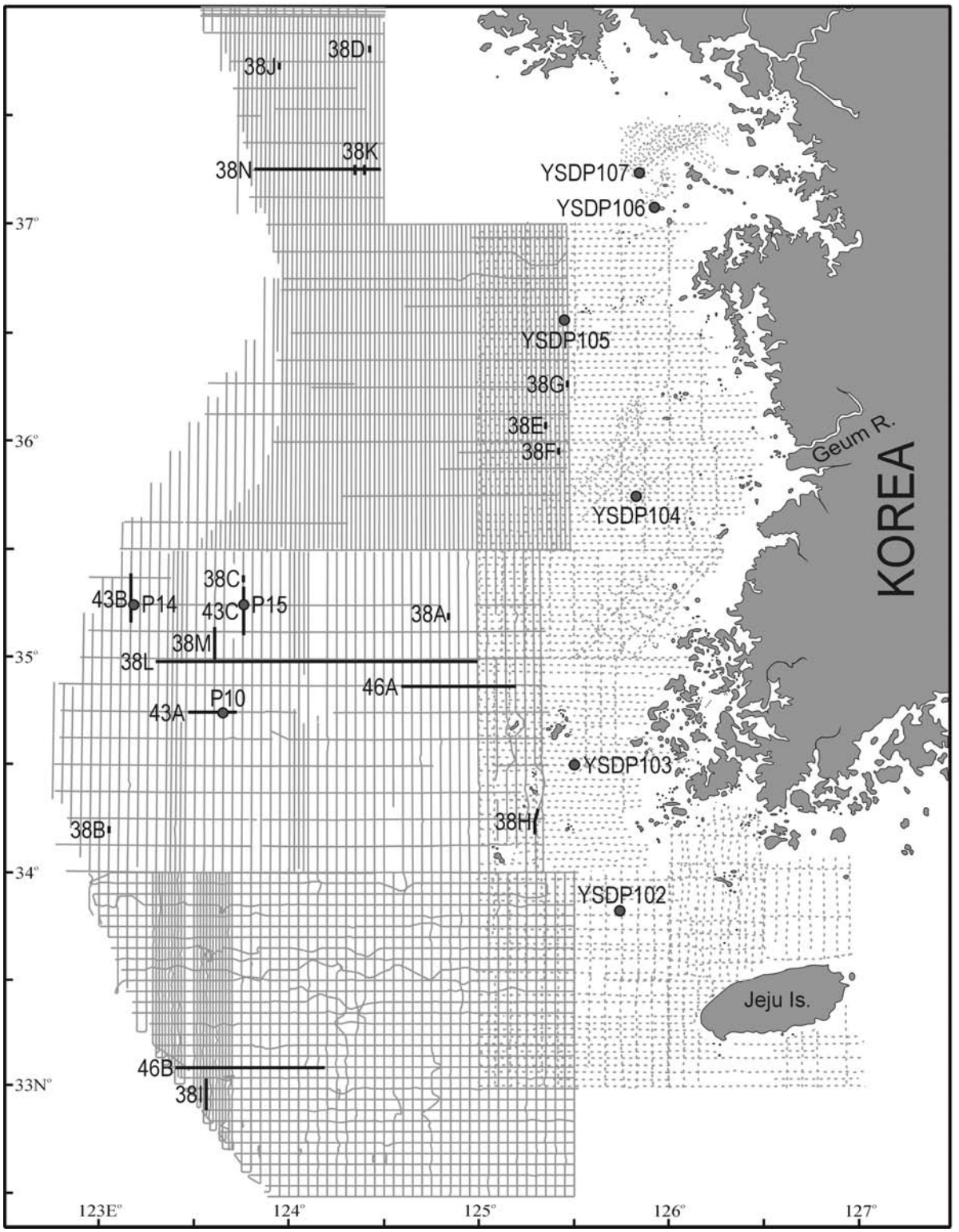

Fig. 2. Tracklines of Chirp subbottom profiles (solid lines) acquired by National Oceanographic Research Institute (NORI), and air-gun, sparker and 3.5 kHz seismic profiles (dotted lines) acquired by Korea Institute of Geoscience and Mineral Resources (KIGAM). Numbered thick lines are tracks of the cited figures. Numbered circles denote locations of piston and drill cores.

Strait (Fig. 3). Diluted by summer runoff and chilled by outbreaks of cold air, the Korean coastal current forms a strong and stable thermohaline front embracing the coastal archipelago including Heuksan Island off the southwestern-coast of Korea (Lie, 1985; Guan, 1994).

The Yellow Sea is dominated by a semidiurnal tidal

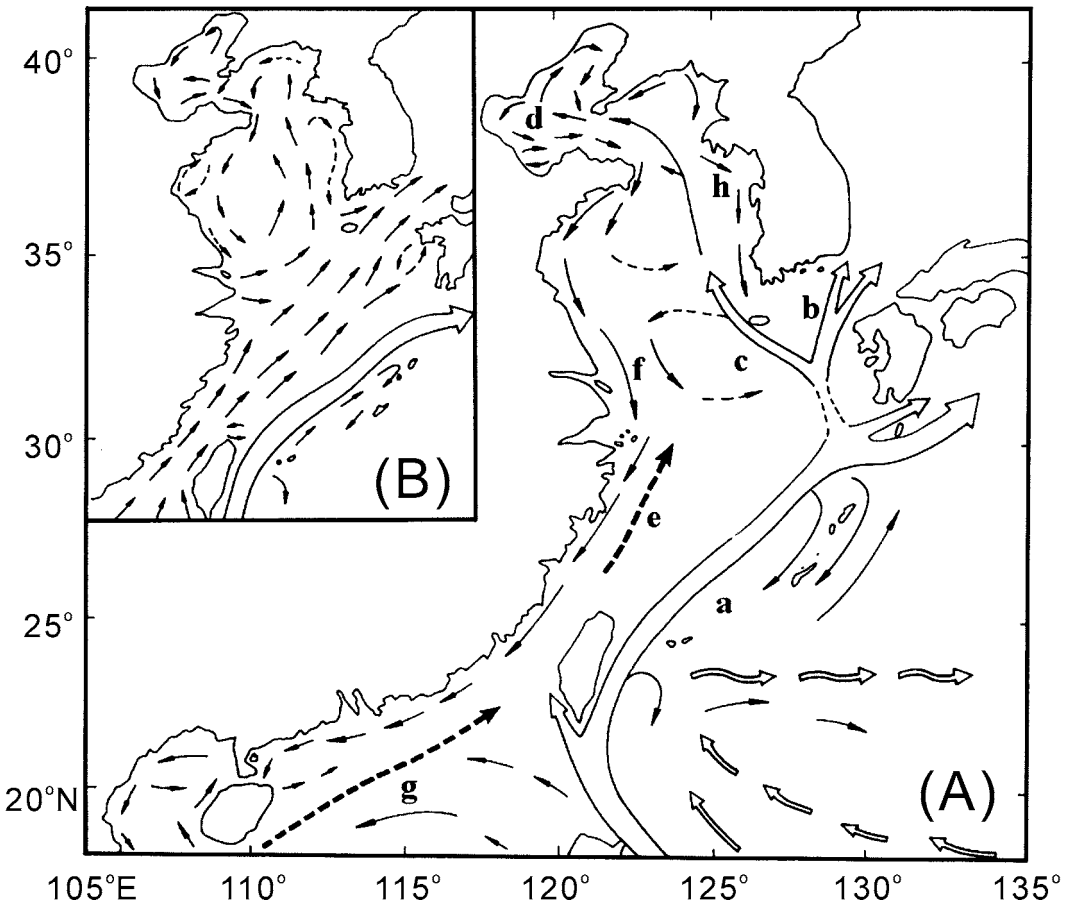

Fig. 3. Schematic diagram illustrating major current systems in the Bohai, Yellow and East China seas and adjacent areas for winter (A) and summer (B). a, Kuroshio; b, Tsushima warm current; c, Yellow Sea warm current; d, Bohai Sea circulation; e, Taiwan warm current; f, China coastal current; g, South China Sea warm current; h, South Korea coastal current. Modified after Guan (1994).

regime with a tidal range exceeding 4 m in many coastal areas (Choi, 1980). Strong tidal currents are largely rotary with the long axis of the tidal ellipse oriented NE–SW in the mid-eastern part (north of 35°30′N) and N–S to NW–SE in the southeastern part of the sea, respectively (Fig. 4) (Choi, 1980; Larsen et al., 1985; Lee and Jung, 1999). Tidal current ellipses also display a distinctive radial pattern near the Jiangsu coast and a rectilinear pattern in the Changjiang River mouth (Li et al., 2001; Uehara et al., 2002). In contrast, relatively high ellipticity of tidal currents is observed in the east of Changjiang River mouth. Tidal currents readily exceed 1 m/s in the nearshore and gradually diminish offshore, trending N–S in the central Yellow Sea (Larsen et al., 1985). The inferred paleotidal current model shows that the tidal current at 10 ka was stronger and oscillated more rectilinearly than it does today (Uehara et al., 2002). As the sea level rose, the region of intense tidal bottom stress migrated from around Jeju Island toward the southwestern coast of Korea and along the retreat path of the paleo-Changjiang River mouth, suggesting that tidal processes played a significant role in reworking and deposition of sediments (Uehara and Saito, 2003).

3. SURFACE SEDIMENT DISTRIBUTION

The Yellow Sea receives a great quantity of sediments discharged through the adjacent rivers, especially the Huanghe (1.08×10^9 tons/yr) and Changjiang (ca. 5×10^9 tons/yr) rivers (Milliman and Meade, 1983; Milliman et al., 1985). The Huanghe River is a major agent in providing recent muddy sediments to the Yellow Sea, as revealed by numerous provenance studies based on geochemical analysis (Yang et al., 2003b). Huanghe River-derived deltaic muddy sediments (9–15% of sediment discharge) are transported southward and accumulate in the central Yellow Sea (CYSM in Fig. 5) (Milliman et al., 1985; Lee and Chough, 1989; Alexander et al., 1991; Park and Khim, 1992). Echo-character mapping and sediment coring have revealed that the mud unit is up to 6 m thick and thins out southeastward (Shinn et al., 2004). A thick clinoform mud deposit occurs at the eastern tip of the Shandong-Peninsula, referred to as the Shandong mud wedge (SMW in Fig. 5). According to Liu et al. (2002), it was mostly deposited early in the Holocene (prior to 9.0 cal. ka) before the Huanghe River mouth shifted to the Bohai Sea, which is the reason why the Shan-

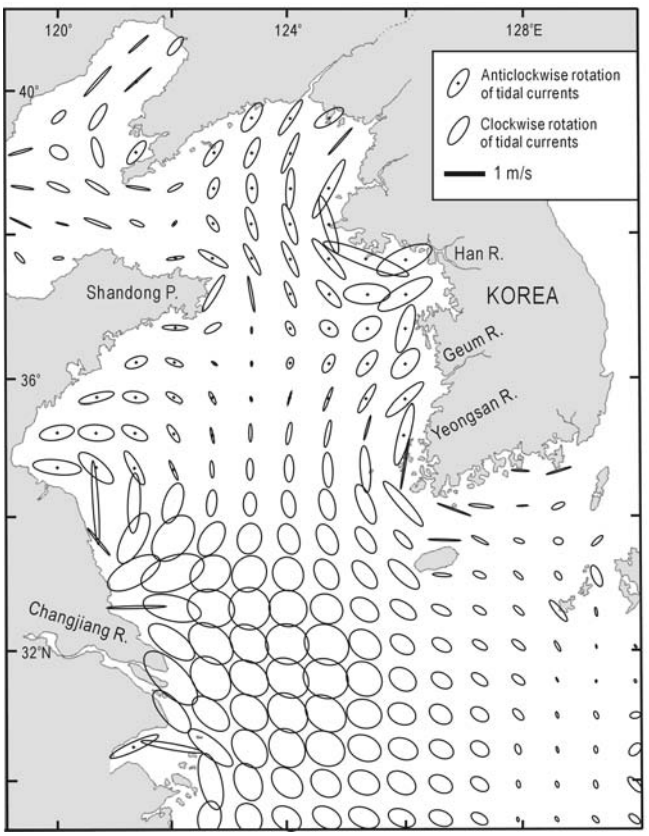

Fig. 4. M_2 tidal model of the Yellow Sea. After Choi (1980) and Lee and Jung (1999).

dong mud wedge is not connected to the present Huanghe River delta. Large birdfoot-like sand bodies occur north of the Changjiang River mouth off the Jiangsu coast, which formed prior to the southward shift of the river mouth by tidal-current winnowing (Wang and Aubrey, 1987). On the contrary, Li et al. (2001) concluded that the sand bodies were deposited during the regressive phase of sea level and formed by tidal currents and longshore transportation of sands from the abandoned Huanghe and modern Changjiang deltas. Further north, along the Jiangsu coast, muddy sand, sandy mud and mud were deposited by the old Huanghe River delta prior to 1855. These sediments have been partly winnowed by waves and tidal currents and acted as a source of the mud patch southwest of Jeju Island (Nittrouer et al., 1984; DeMaster et al., 1985; Milliman et al., 1985). Changjiang River-derived sediments are mostly confined to the south and seasonally transported offshore by a plume event. The east of Changjiang River mouth is covered with sandy sediments (Yangtze sand shoal: YSS), either relict sands of continental shelf (Emery, 1968) or an active offshore tidal sand sheet (Liu, 1997).

The Korean rivers discharge relatively small amounts of sediments into the eastern Yellow Sea (Chough et al., 2000). The fine-grained sediments largely derived from the Geum River (discharge, 5.6×10^6 tons/yr) are transported southward, forming a distinct mud belt, the Heuksan mud belt, in water depth of 20–70 m (Chough et al., 2000) (Fig. 5). Although

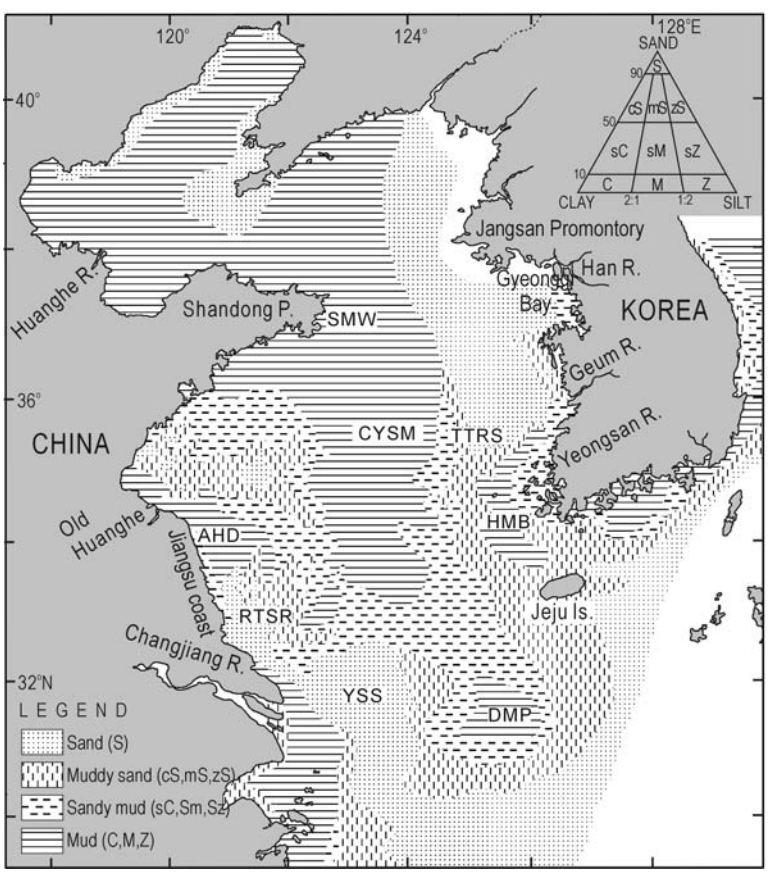

Fig. 5. Surface sediment distribution in the Yellow Sea and adjacent seas (after Lee and Chough, 1989). Sediment classification according to Folk's (1954) scheme. SMW, Shandong mud wedge; CYSM, central Yellow Sea mud; TTRS, transgressive tidal ridge and swale; HMB, Heuksan mud belt; AHD, abandoned Huanghe delta; RTSR, regressive tidal sand ridge; YSS, Yangtze sand shoal; DMP, distal mud patch.

it is known that fine-grained sediments largely originate from the Geum River, along with other small-scale rivers and coastal erosion, an integrated study of the origin and depositional processes of this mud belt is warranted (see section 4.2) (Lee and Chough, 1989; Jin and Chough, 1998; Park et al., 2000; Lee and Chu, 2001). Ridge-and-swale topography is dominant in the inner-middle shelf area of the eastern Yellow Sea. A thin sheet of sand drapes erosional ridges in the nearshore area, which appear to have originated from erosion of older deposits by energetic tidal activity during the period of post-glacial transgression (Jung et al., 1998; Jin and Chough, 2002; Kim, 2003). Some ridges, located far offshore, are considered to be depositional in origin as a result of sand migration, as represented by southwestward-dipping internal reflectors (Kim, 2003). The origin and evolution of these ridges in the eastern Yellow Sea remain explained.

4. SOURCE, TRANSPORT AND SINK OF MODERN SEDIMENTS

4.1. Synoptic Picture

The Yellow Sea receives enormous amounts of terrigenous sediments from the landmasses of both China and Korea via a number of rivers (Lee and Chough, 1989). Extensive geochemical and mineralogical studies have elucidated varying sources of the Holocene sediments in the Yellow Sea (Chough et al., 2000). Among the riverine sources, fine-grained sediments of the Huanghe River dominate the Yellow Sea either by fresh input from the Bohai Sea or by reworking of the former Huanghe deposits (Old Huanghe Delta) off the Jiangsu province (Fig. 5). A voluminous Huanghe River-derived mud deposit in the central Yellow Sea is considered to have been prograding southward since the early Holocene (Alexander et al., 1991; Liu et al., 2002). It is known that some of the Huanghe suspended sediments have traveled farther south and to be deposited on the seafloor south of Jeju Island (Fig. 5). The Changjiang River, despite its gigantic discharge of fresh water into the sea (900 km^3/yr; Milliman and Meade, 1983), contributes only scanty amounts of sediments mostly during the summer flooding season (Lee and Chough, 1989). The Changjiang plume toward the southeastern Yellow Sea is unlikely to extend to the north of Jeju Island (cf. Lie et al., 2003; see also Section 2). Instead, most of the Changjiang sediments are transported southward along the coast to the East China Sea (Fig. 6). This dispersal system of the Changjiang River may provide a key to a persistent issue about the origin of the Heuksan mud belt (HMB) encompassing the southwestern coast of Korea (Fig. 7) (Park et al., 2000; Lee and Chu, 2001). Nonetheless, because the river mouth has been continually shifted southward to its present position, the Changjiang River might have been a significant earlier source of sediments for the southwestern Yellow Sea (Yang et al., 2002).

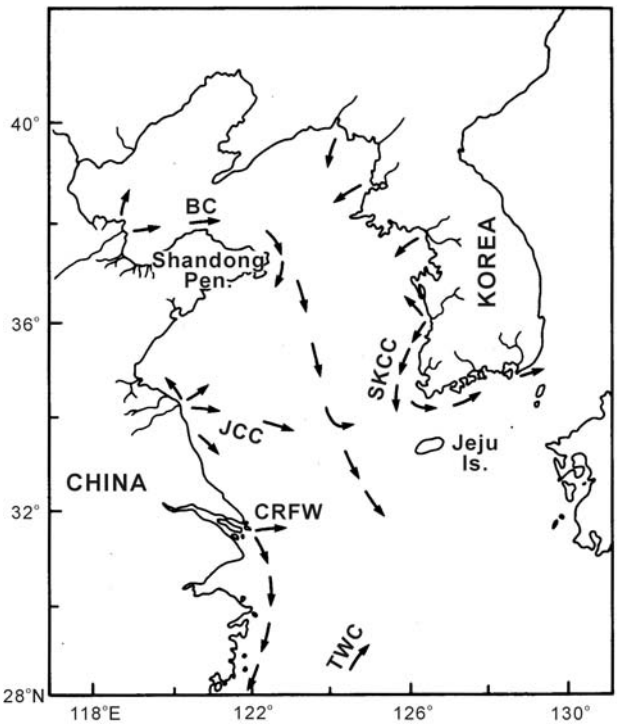

Fig. 6. Schematic dispersal patterns (arrows) of recent sediments in the Yellow Sea. BC, Bohai current; JCC, Jiangsu coastal current; CRFW, Changjiang River freshwater; TWC, Taiwan warm current; SKCC, South Korean coastal current. After Lee and Chough (1989).

In the eastern Yellow Sea, some of the major Korean rivers have consistently controlled sedimentary processes in the coastal area and inner shelves. A variety of hydrographic and clay mineral investigations have shown that the suspended plume from the Geum River is vigorously transported southward by combined wind-generated and tidal currents during winter. In summer, the plume effects tend to be restricted to coastal areas (particularly tidal flats) adjacent to the river mouth and somewhat extend northward in a flood-dominant tidal regime. However, the flux of suspended sediments in the offshore area seems to be at least an order of magnitude lower than the wintertime counterpart, according to the extensive suspended sediment measurements in the HMB (Lee and Chu, 2001). A reconnaissance survey of suspended sediment concentrations had suggested that part of the suspended sediments in action on the relatively wide, shallow terrain flanked seaward by the HMB in the southeastern Yellow Sea may be further transported to the southern coast of Korea during winter (Wells, 1988). Compared with offshore environments, the complex coastline with numerous tidal flats has been artificially modified in many places by the construction of seawalls and dykes typified by the huge Saemangeum dyke (Choi and Lee, 2003; Eo and Kim, 2003). The associated loss of coastal sinks might trigger unexpected adjustments of sedimentary

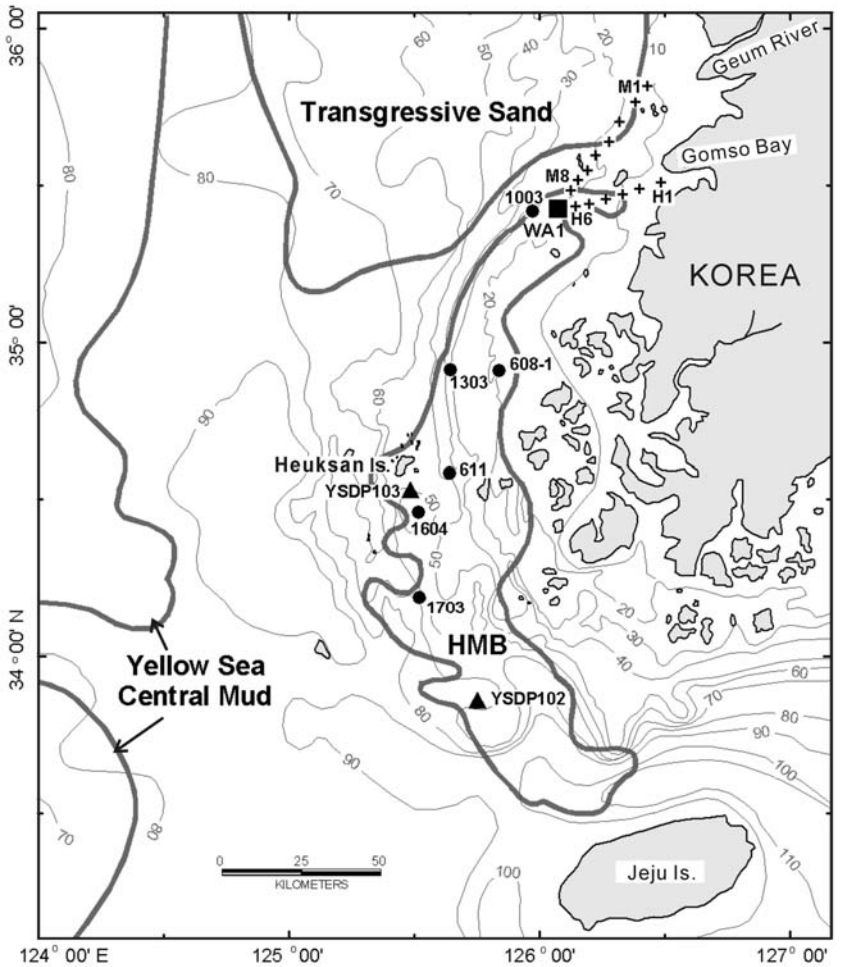

Fig. 7. Map of the Heuksan mud belt (HMB) and its vicinities in the southeastern Yellow Sea, showing locations of hydrodynamic measurements. Square marks anchored station WA1 and is situated at the join of two transects (H and M). Drilled cores (filled triangles) and piston cores (dots) are described in Chang et al. (1996) and Lee et al. (1987), respectively. After Lee and Chu (2001).

environments possibly with disastrous results. Yearly measurements of nearshore suspended sediment concentrations and tidal-flat sedimentation rates in front of the Daeho dyke on the mid-west coast indicate that most of the coastal sediments bypass the dyke rather than enter the reclaimed bay and the nearby tidal flats are subject to continuous erosion (Lee et al., 1999).

In the following section, the quantitative results and data regarding sediment transport in the coastal region of Korea are summarized. For the first time, in-situ systematic measurements of suspended sediments and currents have been conducted offshore seasonally (Lee and Chu, 2001). The detected seasonal difference in suspended sediments has shed light on the origin of the HMB. Another noble feature of the recent studies is the development and use of sophisticated, self-contained measuring instruments (Lee and Jo, 2003; Lee et al., 2004). These are capable of automatically recording a suite of basic hydrodynamic parameters necessary for the quantitative evaluation of sediment transport. The duration of deployment of these instruments on tidal flats can be continued for more than 15 days, i.e., a spring-neap tidal cycle. The time-series data obtained have provided new information on details of waves and currents forcing sediment transport in macrotidal beaches as well as typical tidal flats.

4.2. Heuksan Mud Belt

The Heuksan mud belt (HMB) dominates the southeastern Yellow Sea and poses a sedimentological riddle in regard to its dimensions and possible sources (Fig. 7). The HMB takes a giant bow-like form, 2050 km wide, 200 km long and up to 60 m thick. Two different sources of the HMB have been suggested: the west coast of Korea and the offshore region to the west. The former is represented by the Geum River (Chough et al., 2000) and the latter by the Changjiang or Huanghe rivers (Park et al., 2000). Lee and Chu (2001) have attempted to acquire a more direct, hydrodynamic indication that the Geum-River is a likely source by performing suspended-matter measurements at an anchored station and along some pre-determined transects over the HMB (Fig. 8). The results are briefly described below.

The summer-time measurements (30–31 August 1997) for a tidal cycle show that 20 m of the water column at station WA1 were well stratified in terms of both temperature and salinity, which ranged between 22 and 26°C and between

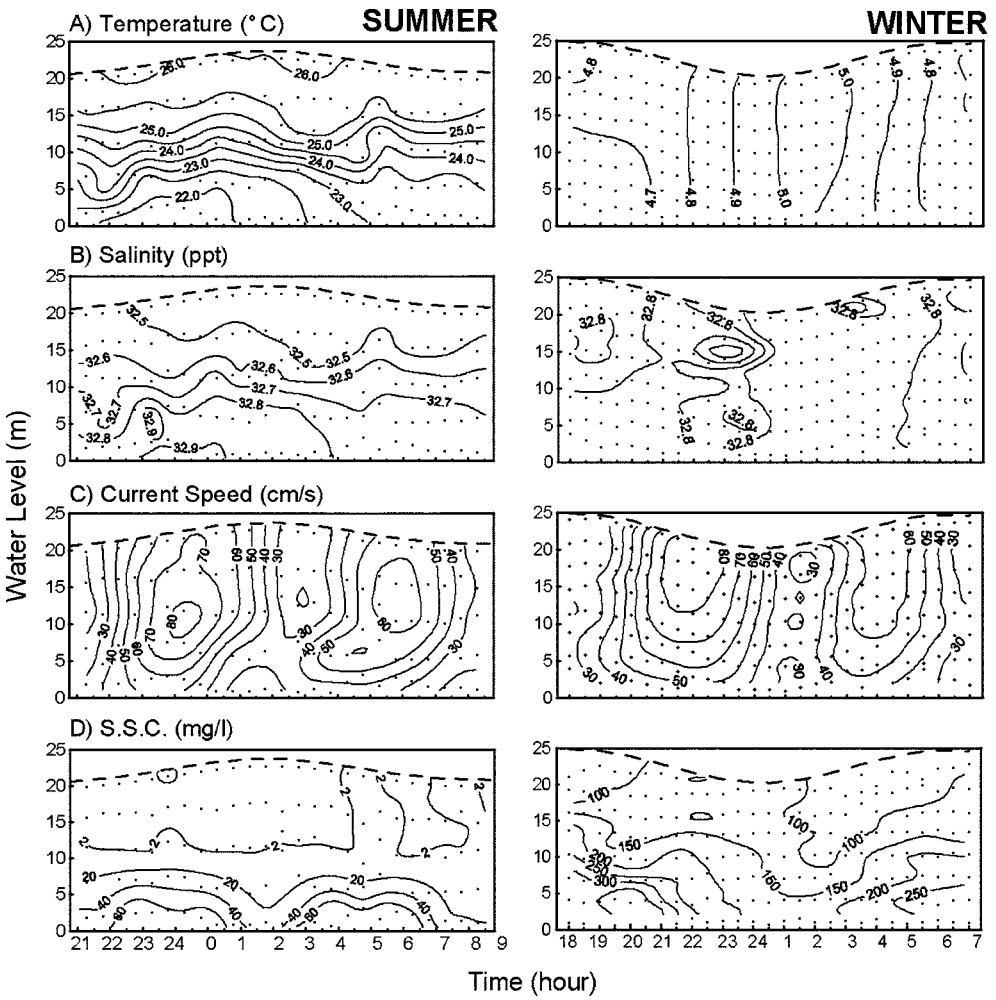

Fig. 8. Time-series (12.5 h) hydrodynamic measurements at station WA1 during summer (30–31 August 1997) and winter (16–17 February 1998). For location of the station, see Figure 7. Times are local. After Lee and Chu (2001).

32.5 and 32.9 ppt, respectively (Fig. 8A, B). Tidal currents were rectilinear with a NE–SW major axis and somewhat flood-dominated with maximum speeds of 0.8 m/s as compared with 0.6 m/s of ebb currents (Fig. 8C). The distribution of suspended sediment concentrations (SSC), in the range of 1–3 mg/l, suggests that the seabed mud could be resuspended by tidal currents alone (Fig. 8D). The winter regime of suspended sediments, 16–17 February 1998, was completely different. The water was totally mixed such that the temperature was in the narrow range of 4.7–5.0°C, whilst the salinity was uniform at 32.8 ppt regardless of water depth (Fig. 8A, B). Tidal currents also varied radically, displaying an obvious ebb-dominance which is opposite to the flood-dominant phase during summer (Fig. 8C). The surficial ebb currents had a maximum speed of 0.93 m/s, whereas the flood currents had a maximum of 0.75 m/s. Accordingly, the SSC were much higher, exceeding 350 mg/l near the seabed and up to 100 mg/l at the surface, during most of the tidal cycle (Fig. 8D).

This strong contrast in all measured parameters can be attributed to the addition of northerly or northwesterly wind waves to the intrinsically flood-dominant tidal regime over the study area during winter: the ebb currents reinforced by wind-generated components overcame the flood currents. The elevated energy level could also induce more vigorous agitation at the seabed resulting in highly turbid water columns. Such an interaction between the muddy seabed of the HMB and overlying energetic waters can be readily testified by the abrupt increase in the SSC at the northern tip of the HMB (Fig. 9). Enhanced shear stress at the seabed should create a lateral lutocline in the water column across the boundary between the HMB and the nearshore muddy sands or sands (Fig. 7). A simple evaluation of the SSC flux during the survey illustrates that the wintertime southward flux amounted to 0.7 kg/ms, roughly an order of magnitude higher than the northward flux of 0.1 kg/ms for the summer season. Therefore, the hydrodynamic results strongly suggest that the HMB is intimately coupled with the Geum River derived suspended sediments. Based on these measurements with an aid of previous studies, a schematic diagram can be

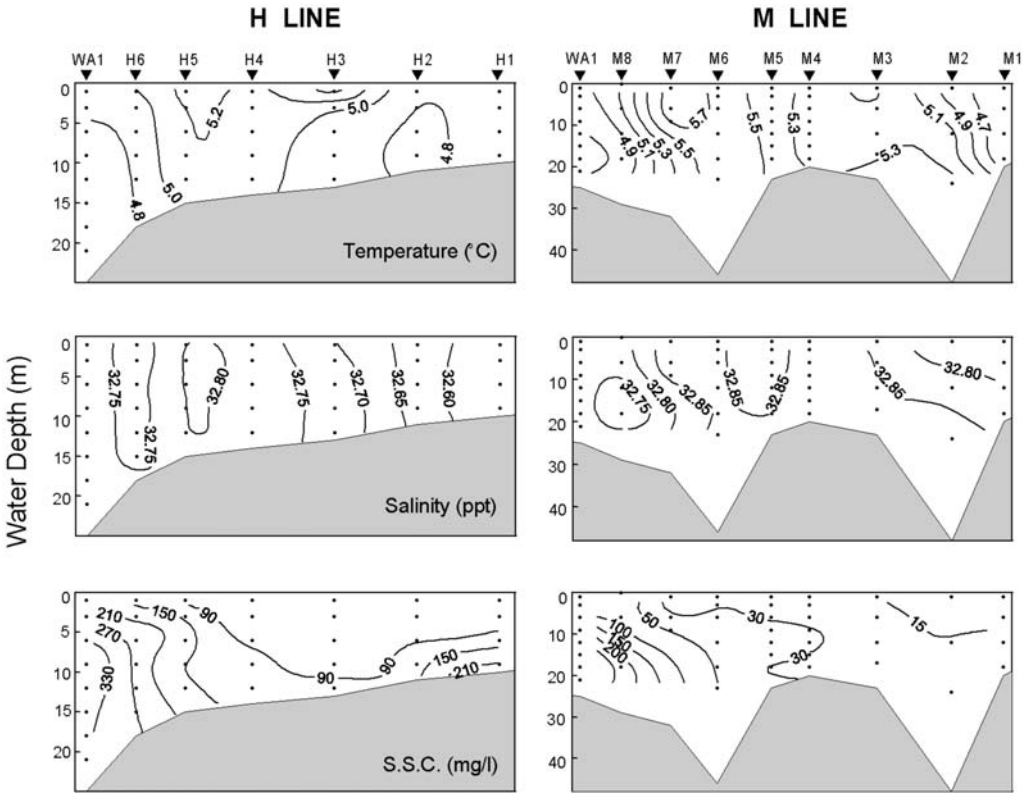

Fig. 9. Cross sections of temperature, salinity and suspended sediment concentration (SSC) along two transects (H and M lines) measured during 14–17 February 1998. For location of the transects, see Figure 7. After Lee and Chu (2001).

drawn which delineates the dispersal of suspended sediments originating from the Geum River over the HMB and possibly toward the southern coast of Korea (Fig. 10).

5. TIDAL FLATS

The eastern Yellow Sea is characterized by embayments with macrotidal flats, a typical ria-type coast. Various intertidal flats such as embayed, estuarine, semi-enclosed and open-coast tidal flats drape the western coast of the Korean Peninsula. With as much as 10 m of extreme macrotidal range, the extensive tidal flats are recognized worldwide as rivaling those of the North Sea. Although the coastal classification schemes of Hayes (1979) and Boyd et al. (1992) indicate several transitional settings between wave- and tide-dominated coastal environments (Fig. 11), most studies have focused on the two end-member settings, namely sheltered tidal flats and exposed beaches and shorefaces. In contrast, non-barred, open-coast tidal flats have been less studied despite their widespread occurrence, especially along the coasts of East Asia (Reineck and Cheng, 1978; Mukherjee et al., 1987; Chun et al., 2000; Li et al., 2000; Yang and Chun, 2001; Yang et al., 2004).

Tidal flats are tide-dominated environments with a gentle slope, little wave influence and well-developed tidal creeks (Reineck and Singh, 1980; Klein, 1985; Dalrymple, 1992), whereas beaches and shorefaces have relatively steep slope and experience strong wave action (Davis, 1985; Walker and Plint, 1992). As a result, these two environments are considered to be distinct. Tidal flat deposits are represented by muddy heterolithic facies, including flaser, wavy and lenticular bedding. Beach and shoreface deposits are wave and storm-generated, and include hummocky cross stratification (HCS) and swaley cross stratification (SCS). Indeed, these two environments are almost invariably considered in separate chapters in textbooks (e.g., Reineck and Singh, 1980; Davis, 1985; Walker and James, 1992; Reading, 1996).

5.1. Environmental Setting

The tidal flats of the western Korean Peninsula are mostly 4–10 km wide and face directly onto the sea, which mostly correspond to open-coast type, except for typical embayed muddy or estuarine tidal flats. They are generally bordered on its landward side by rocky coastal cliffs or by artificial dykes that have been constructed to reclaim tidal marshes. These dykes inhibit the input of terrigenous sediments. Tides are semi-diurnal (diurnal inequality of about 1 m) with a mean spring range of 4.3–9.1 m. The maximum tidal-current velocity is mostly 0.46–1.95 m/s during spring tides and 0.36–2.21 m/s during neap tides except for some tidal channels with unusually high speed. The current speeds generally

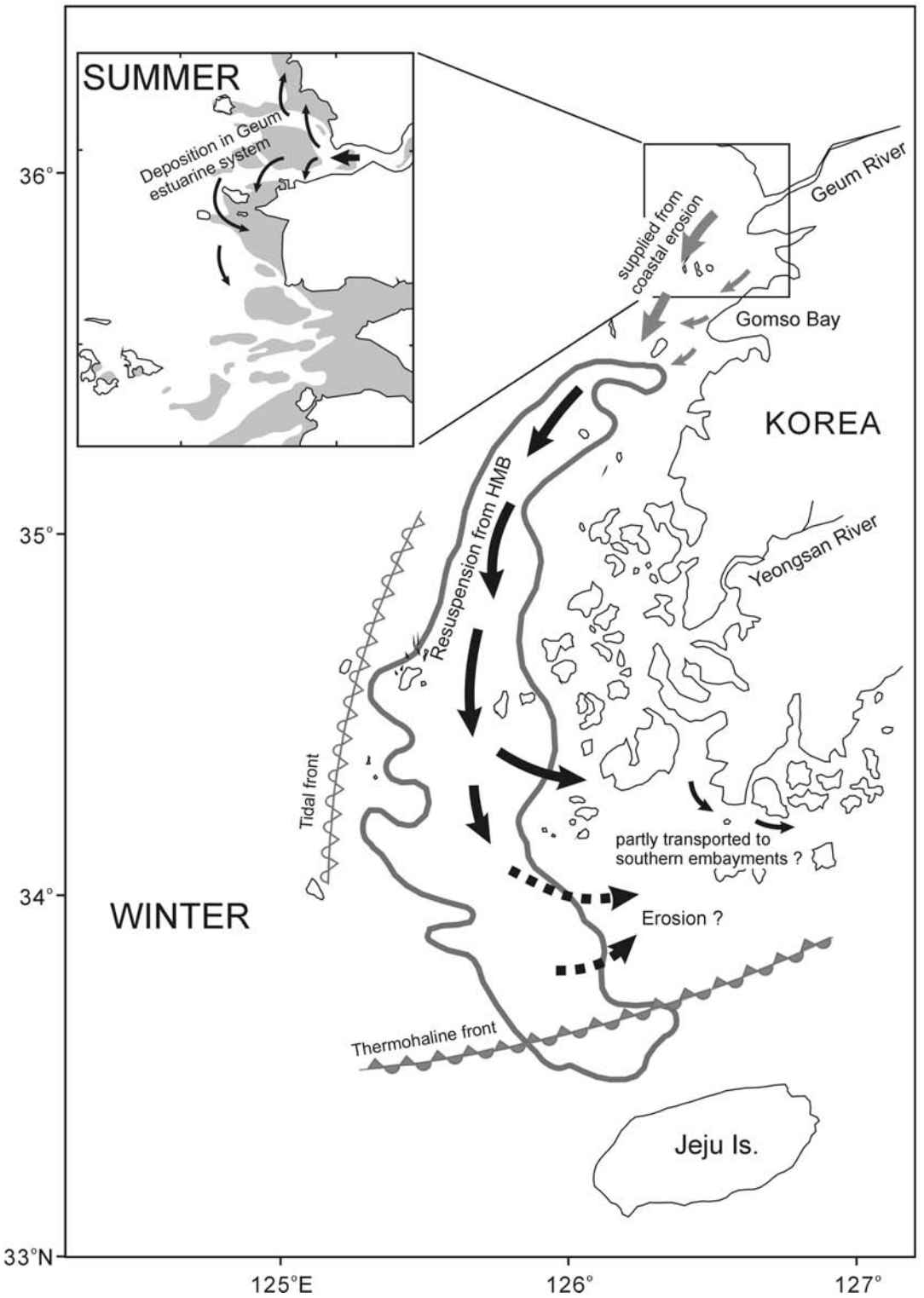

Fig. 10. Schematic diagram illustrating seasonal dispersal of suspended sediments derived from the Geum River onto the HMB. After Lee and Chu (2001).

depend strongly on the magnitude and direction of winds.

The winds in the coastal area show a pronounced seasonality associated with monsoon. During winter, winds blow mainly onshore from northwest and north with a mean speed of ca. 5–6 m/s. In summer, by contrast, they are from the south, in an obliquely offshore direction, with a mean speed of 2–3 m/s (Korea Meteorological Administration, 1997, 1998). Storms (defined as >13.9 m/s in wind speed)

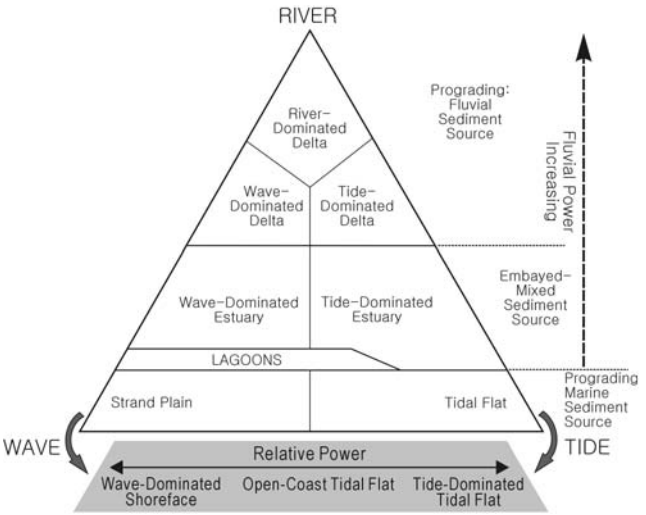

Fig. 11. Classification of clastic coastal environments. It should be noted that sandy, open-coast tidal flats are intermediate between the wave- and tide-dominated end members of the coastal spectrum.

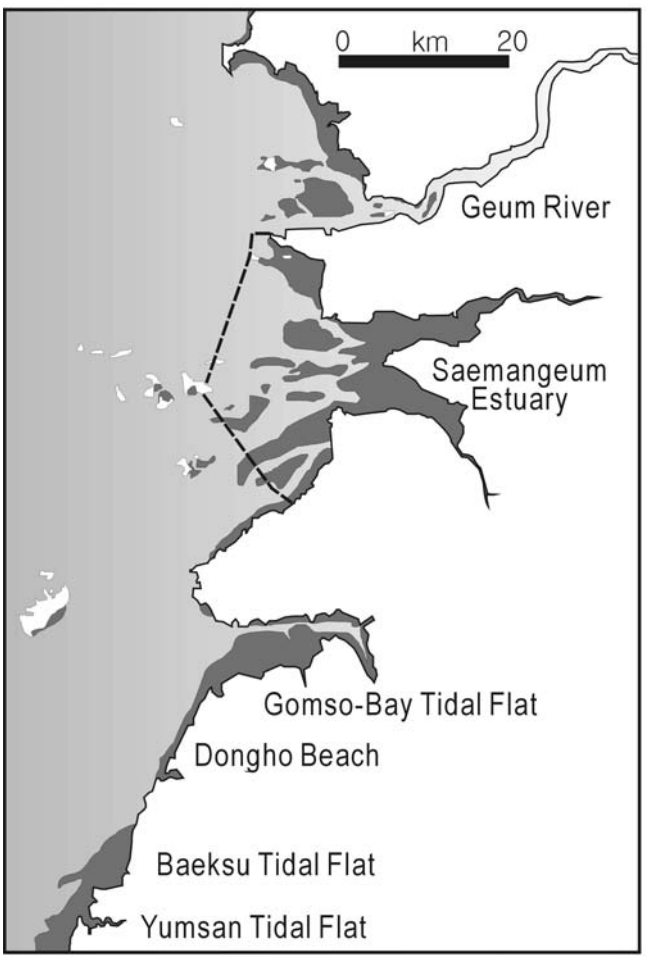

Fig. 12. Open-coast tidal flats (Yumsan, Baeksu, Dongho Beach and Gomso Bay) and estuarine tidal flats (Geum River mouth and Saemangeum estuary) along the southwestern coast of the Korean Peninsula.

also display a pronounced seasonality, occurring less than 2–3 days/month during summer, but more than 9 days/month during winter, when waves with heights of 1.5–2.0 m are common (Table 1). Typhoons (>17 m/s in wind speed) occur mainly during summer with an average of 1–3 times each year. Although some typhoons can produce waves up to 5 m high, the summer season is generally characterized by weak coastal waves with significant heights of 0.5–1.0 m (Korea Meteorological Administration, 1997, 1998; National Fisheries Research and Development Institute, 1997, 1998). In winter, however, onshore-directed winds generate significant wave height of 1.5–2.0 m on the tidal flat. Some intertidal swash bars and/or cheniers form in the upper intertidal flat, which are 100 to 300 m wide and 0.5 to 1.5 m high and migrate landward at various rates. These bars migrate mostly by storms and typhoons.

5.2. Surface Sedimentation and Preservation Potential

5.2.1. Seasonal model of surface sediment distribution on open-coast tidal flats

Although there are various types of tidal flats on the western coast of Korea, detailed studies of the seasonal changes in surface sediment distribution have scarcely been made. Most tidal flats show evident seasonal variations. Based on sedimentological data obtained from the open-coast tidal flats (Baeksu, Yumsan and Gomso Bay) (Fig. 12) for the past 5 years (1998–2002), surface sediment distributions are outlined. Surface sediments in most intertidal flats can be classified into three types according to the sand/mud ratio: sand facies (sand, more than 70%), mixed facies (sand, 40–70%) and mud facies (sand, less than 40%). The clay component in the surface sediments is characteristically very low throughout the year.

In open-coast tidal flats (Fig. 12), most inner flats of mud facies (mostly silt sediments) are restricted to a narrow zone within 200–500 m of the shore. In the case of the embayed tidal flat, Gomso Bay, the inner half of the bay-head flat

Table 1. Summary of wind data for the western coast of the Korean Peninsula. Storms and typhoons are defined as periods with wind speeds of >13.9 m/s and >17 m/s, respectively. Only 17% of typhoons directly impact the west coast of Korea (Korea Meteorological Administration, 1997, 1998). Less intense, winter storms cause more wave energy.

	JAN.	FEB.	MAR.	APR.	MAY	JUN.	JUL.	AUG.	SEP.	OCT.	NOV.	DEC.	Total
Occurrence of typhoons (1951–1998)	0.5	0.2	0.5	0.7	0.9	1.8	4.0	5.7	5.0	4.1	2.6	1.3	27.3/yr
Effective typhoons (1904–1999)	-	-	-	-	0.01	0.18	0.88	1.2	0.78	0.08	-	-	3.13/yr
Occurrence of storm wind (1997–1998)	10	6	6	4	2	2	3	2	6	6	7	9	63/yr

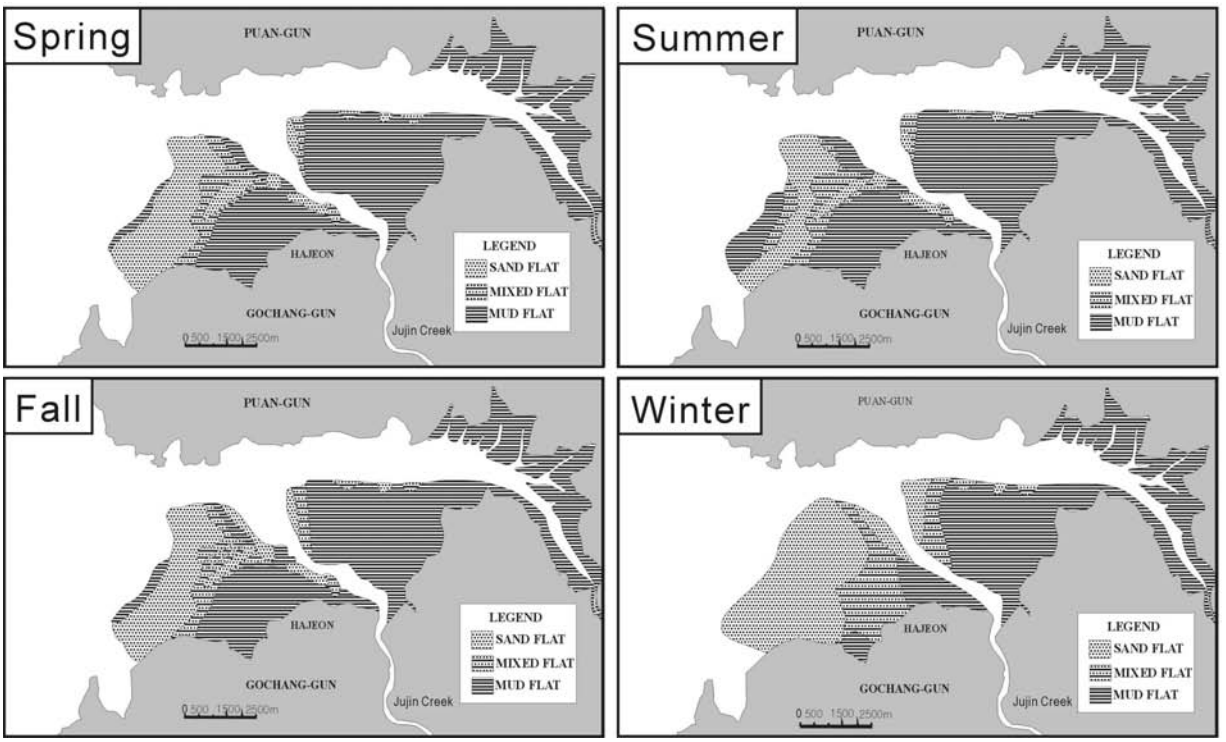

Fig. 13. Seasonal model of surface-sediment distribution (sedimentary facies) in the open-coast intertidal flat of Gomso Bay.

lacks seasonal changes in surface sediment (Fig. 13). Tidal beach forms in the upper shore area of sandy tidal flats (sandy inner flat) such as the Yumsan (Fig. 14), Dongho and Gamami beaches (Fig. 12). The inner-flat surface is generally covered with silty mud regardless of seasonal changes in dynamic conditions. The inner-flat zone is sheltered from wave energy, which is dissipated by the shallow tidal flat surface. Intricate tidal creeks form only in this region. *Sueda Japonica* (Halophytes) and some cheniers occur. The cheniers are variable in size (0.1–2 km long and 20–40 m wide), and are relatively small compared with well-known cheniers worldwide (Woodroffe et al., 1983; Chappell and Grindrod, 1984). They are most probably of storm origin and migrate during storms (Lee et al., 1994; Yang, 2000). The outer flat shows a distinctive seasonal variation in surface sediment distribution.

The models showing the seasonal change of surface sedimentation distribution have been made in the Gomso (Fig. 13), Yumsan (Fig. 14) and Baeksu (Fig. 15) open-coast intertidal flats. Most open-coast intertidal flats in the southwestern coast of the Korean Peninsula show a similar pattern in seasonal change of surface sediment distribution, although it is variable according to their coastal geomorphology, tidal range and sediment supply, as typified by the Baeksu tidal flat (Figs. 12 and 15).

5.2.1.1. Spring

In the spring season, the Baeksu intertidal flat can be divided into two distinctive zones beyond the relatively stable inner flat: sand-facies (0.2–1.3 km in width) and mixed-facies (>1.3 km in width) zones (Fig. 15). Such zonation occurs also in the Yumsan flat, except for the lower mud flat which is relatively consistent through the year (Fig. 14). In the Gomso Bay, the distribution of surface sediment is zonal, which is characterized by a narrow mud-flat zone in the lowermost flat (Fig. 13). Sand content generally decreases toward the subtidal zone with an increasing mud content. Sand grains consist dominantly of very fine sand, and muds are composed mostly of coarse to medium silt. Sand content ranges from 70–85% nearshore to 40–60% offshore.

5.2.1.2. Summer

Along the Baeksu coast, surface sediments in the early summer dominantly exhibit mud facies in the lower flat and mixed facies in the middle flat, respectively (Fig. 15). Sand facies occur only in the upper flat (Fig. 15). With time, most of intertidal flat is draped with thick mud deposits (5–30 cm thick). However, sand contents in the upper middle and lower upper flats (between 0.4 and 0.9 km from the shore) are high, similar to those of spring. In the Yumsan coast, most intertidal flat is covered with mud facies with some patches of mixed-flat facies in the lower tidal flat (Fig. 14). Surface sediment distribution in the Gomso-Bay tidal flat is relatively complex, but the banded pattern is maintained for spring to fall seasons (Fig. 13).

Along the Baeksu coast, the inner-flat region extends slightly offshore during summer. Sand content decreases offshore with an increase in mud. These textural character-

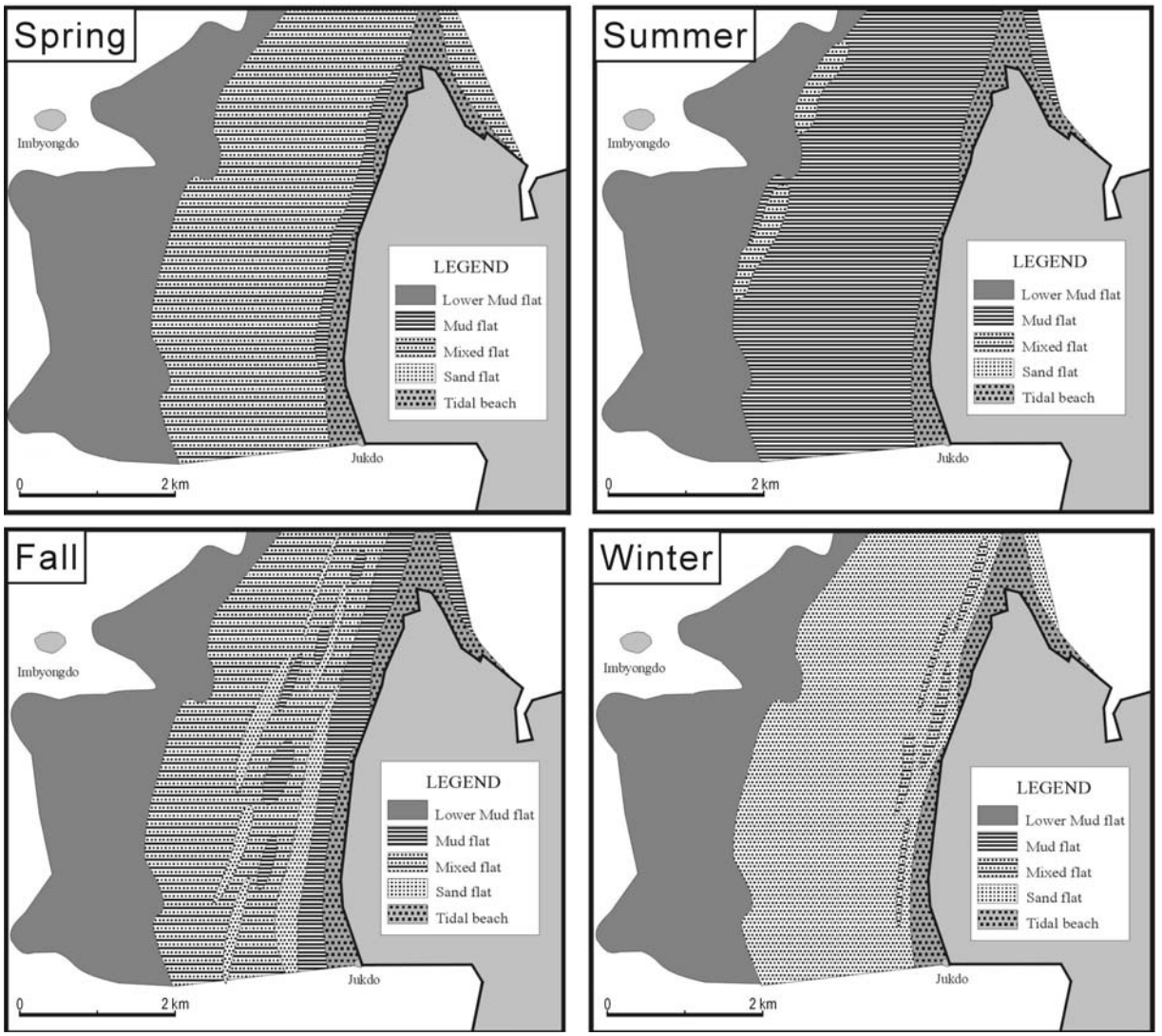

Fig. 14. Seasonal model of surface-sediment distribution (sedimentary facies) in the open-coast Yumsan intertidal flat.

istics would reflect relatively weak energy conditions, resulting from subdued wave effect and relatively rapid settling of fine-grained particles by temperature enhancement (Kröel and Flemming, 1998). During the summer, tidal-flat sedimentation is dominantly influenced by tidal currents with minor wave action. Furthermore, the maximum solar insolation facilitates rapid drying and consolidation of fine-grained sediments. Heterolithic stratification (including lenticular and tidal bedding) and homogeneous mud are the dominant types.

5.2.1.3. Fall

In the Baeksu and Yumsan tidal flats, the mud sediments deposited in summer experience severe erosion from early fall, probably caused by increased wave attack. Erosion takes place firstly in the upper flat and progresses into the middle flat, resulting in a textural change into sand facies (Figs. 14 and 15). The sand deposits typically show large amounts of mud fraction. Shallow tidal creeks and mud patches form on the sandy tidal-flat surface. Mud deposits in the lower and lower-middle flats remain uneroded and show a relative higher content of clay fraction than in other seasons. The high contents of mud fraction in the surface sediments suggest that some parts of eroded fine sediments are re-supplied through the ephemeral tidal creeks (Fig. 16). By the end of the fall season, most of the summer mud has been eroded, leaving only small, isolated mud patches (Fig. 16). The remaining tidal-flat surface is covered by fine to very fine sand. Mud balls are produced by erosion of the summer mud and are abundant at this time of the year.

5.2.1.4. Winter

The surface sediments on the open-coast tidal flats during winter comprise ca. 3.5ø in size except for the inner flat. Sand fractions in most flats are more than 80% but decrease offshore with increasing mud contents. These grain-size distributions suggest that strong wave action would prevent

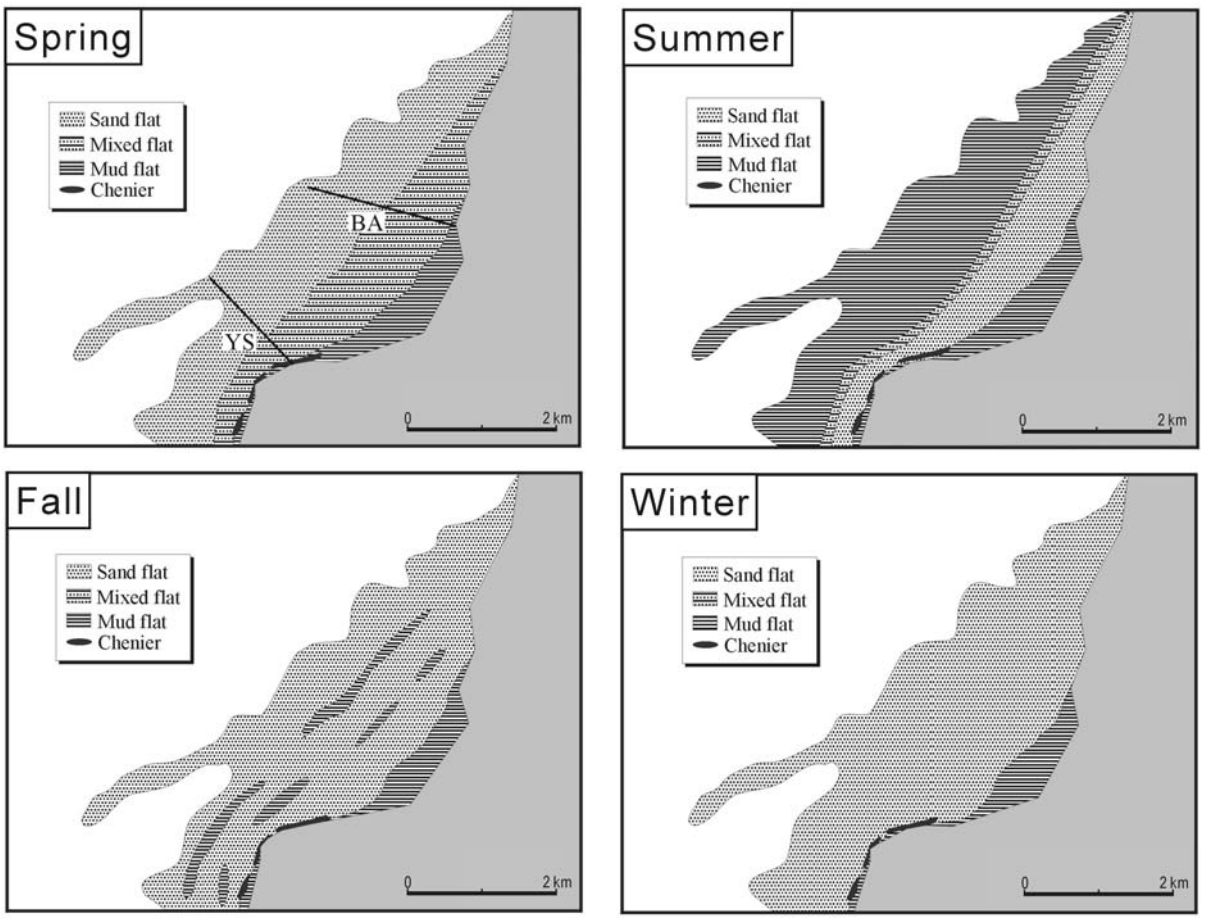

Fig. 15. Seasonal model of surface-sediment distribution (sedimentary facies) in the open-coast Baeksu intertidal flat.

suspended particles from settling on the upper flat. The extent of inner-flat mud sediments is reduced by expansion of the sand flat, probably due to bottom reworking by strong waves. Intense storm waves occur more than 9 days/month, resulting in the development of wave-generated parallel lamination, HCS/SCS-like wavy stratification and climbing wave-ripple lamination across the tidal flat (Fig. 17). The HCSs are notable for their short wavelength (30–50 cm), compared with those reported from the offshore and shoreface deposits. Late-stage runoff current ripples are common, but these current-generated structures are easily reworked by storms; preserved sedimentary structures are mostly wave-generated. Bioturbation is extremely rare, except in the uppermost tidal flat where the wave energy is minimal. Surface sediments consist dominantly of well-sorted fine to very fine sand with minor silt. Mud pebbles are the only remnants of the summer mud layer. The preserved sedimentary structures closely resemble shoreface deposits.

5.2.2. Other characteristics and preservation potential

Regardless of the seasonal change, surface sediments on the open-coast intertidal flats in the southwestern Korea reveal a seaward-fining trend, unlike those in other tidal flats (Reineck and Singh, 1980; Klein, 1985). It is unclear how the seaward-fining trend develops on the intertidal flat, although a combination of seasonal changes (wave vs. tidal energies) may play a role.

The prevalence of strong northerly (obliquely onshore) winds decreases through the spring and the intervals of calm weather increase in number and duration. Wave-generated structures are produced during the storms, whereas muddy sediments consisting mainly of silt are deposited during the quiet periods when tidal processes dominate. Therefore, the spring deposits are characterized by mixed facies that are coarser-grained.

Most thick, fine-grained deposits formed during summer are not well preserved, and are easily eroded by strong waves during winter. The upper part deposited in summer (mud-flat facies, MF in Fig. 17) is completely eroded in winter, resulting in the dominance of upper-flow-regime plane bedded (PL in Fig. 17) and hummocky cross-stratified (HCS in Fig. 17) sand facies in preserved sections, except those of the inner flat areas. These sand facies are very similar to those in shoreface environments, so distinguishing open-coast intertidal flats from shoreface environments can be difficult, especially in ancient deposits.

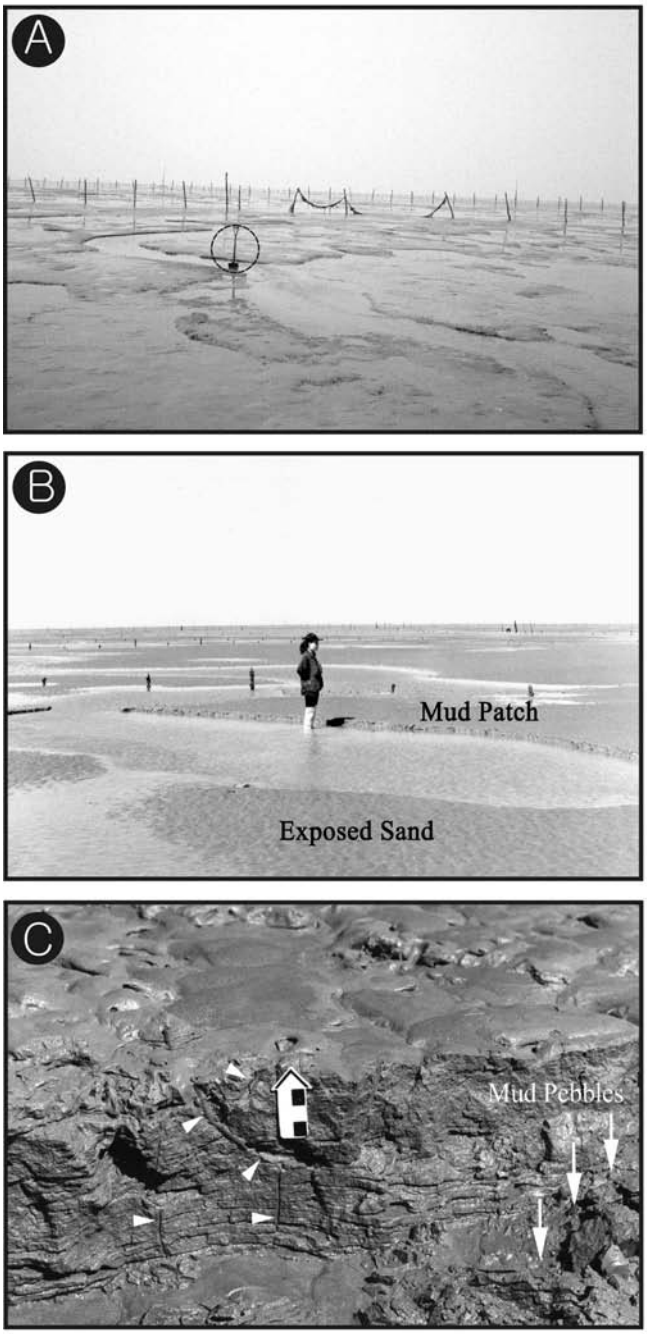

Fig. 16. Surface features of the Baeksu intertidal flat in the fall season. (A) Ephemeral tidal creeks form by erosion of the mud layer due to increasing wind waves. (B) Exposed sand flat and mud patches. (C) Mud pebbles form by breaking of mud patches due to attacks of strong waves. These pebbles are often preserved in sub-bottom layers under the conditions of rapid sedimentation (Yang and Chun, 2001). Triangles indicate burrows; large arrows for mud pebbles. Scale is 4 cm long.

5.3. Models for Prograding vs. Retrograding Tidal-flat Deposits with Sea-level Rise

Progradational, fining-upward facies successions are typical of both modern and ancient embayed and estuarine intertidal deposits, well documented from the tidal flats of the North Sea and Bay of Fundy. On the North Sea coast, broad, gently dipping tidal flats generally consist of shore-parallel subtidal, intertidal and supratidal subzones (Reineck, 1972; DeJong, 1977; Reineck and Singh, 1980; Klein, 1985). Although relative sea level in the North Sea rose rapidly during the early to mid Holocene (>10 mm/yr, prior to about 6 ka) and subsequently fell during the mid to late Holocene (~1 mm/yr) (Van de Plassche and Roep, 1989; Beets et al., 1992; Van der Spek and Beets, 1992), the tidal flats are generally characterized by coastal progradation due to high sediment input (Klein, 1977, 1985). Continuous progradation has generated a fining-upward tidal-flat succession (Fig. 18). This succession consists of a dominantly sandy subtidal zone of channel-fill, point bar and shoal sediments; mixed sand and mud intertidal-flat deposits; and muddy high-tidal-flat and salt-marsh deposits (Klein, 1977; Reineck, 1972). A decrease in grain size can also be seen within the individual subfacies.

A progradational tidal-flat succession also developed in the macrotidal Cobequid Bay-Salmon River estuary in the Bay of Fundy during the Holocene. The deposits in the inner estuary consist of an axial belt of sands flanked by mud flat and salt marsh (Dalrymple et al., 1990). Despite a relatively rapid rise of sea level over the last 4000 years (more than 1 mm/yr; Scott and Greenberg, 1983), the tidal flats in the Bay of Fundy have also built a prograding fining-upward succession because of high sediment input (e.g., $1.15–9.25\times10^6$ m^3/yr; Amos and Long, 1980). Progradation has produced a 20-m-thick, fining-upward succession (Dalrymple et al., 1990) (Fig. 18) with a base that is marked by a gravel lag which formed in the subtidal zone. Sands overlying the lag fine upward from coarse sand at the bottom of deeper channels to the medium sand of bar crests, and then to the fine sand of the sand flat. These sands are, in turn, overlain by the increasingly muddy sediments of the mixed flat, mud flat and salt marsh.

Retrogradational, coarsening-upward tidal-flat successions have been less well documented (e.g., Reineck, 1972; Yeo and Risk, 1981; Frey et al., 1989). Figure 18 shows a generalized model for a retrogradational tidal-flat succession in a storm-influenced, macrotidal setting, based on analyses of vibracores in the tidal flat of Gomso Bay. It comprises a coarsening-upward succession of three principal depositional environments that recorded a retrogradational trend from mud at the base to sand at the top. This lithological trend is exactly opposite to that of the general facies models for prograding tidal flats.

The depositional responses of the Jade Bay (North Sea), Bay of Fundy and Gomso Bay tidal flats to Holocene sea-level rise appear to be influenced mainly by interaction of accommodation and sediment supply (cf. Posamentier et al., 1988; Van Wagoner et al., 1990; Schlager, 1993). Although the rate of relative sea-level rise during the mid to late

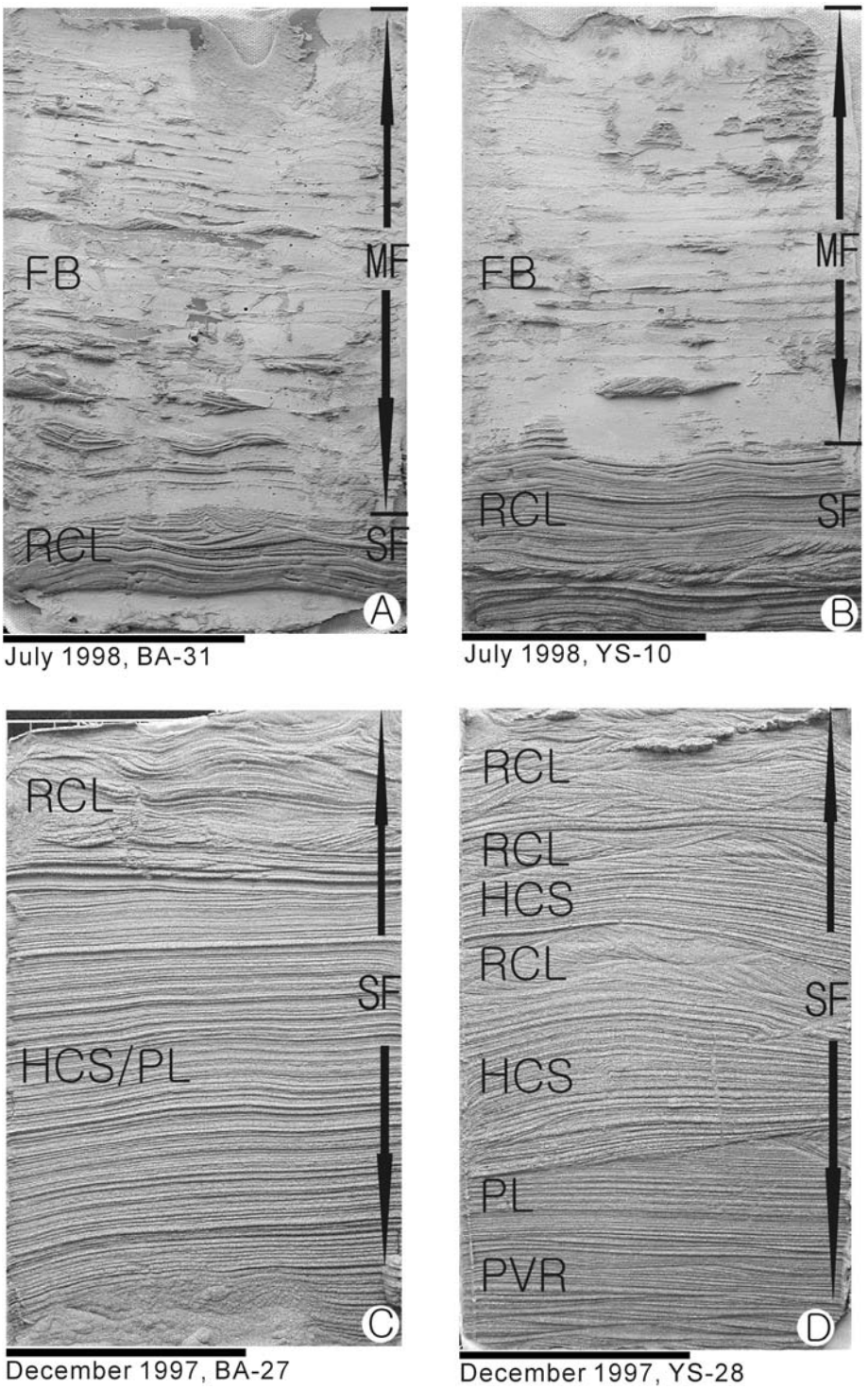

Fig. 17. Cancore peels in the summer (A and B) and winter (C and D) in the Baeksu intertidal flat. After Yang and Chun (2001). Note that most sediments consist of mud-flat facies (FB, flaser bedding) in summer, whereas wave-generated structures are conspicuous in winter. Peels of C and D (winter) consist mainly of stratified and slightly inclined stratified sand-flat facies. MF, Mud-flat facies; SF, sand-flat facies; HCS, hummocky cross lamination; PL, parallel lamination; RCL, ripple cross lamination; PVR, post-vortex ripple. Horizontal bar is 10 cm long.

Holocene is similar in these areas (Amos, 1978; Scott and Greenberg, 1983; Amos and Zaitlin, 1985; Van de Plassche and Roep, 1989; Beets et al., 1992; Van der Spek and Beets, 1992; Korea Ocean Research and Development Institute, 1994; Kim et al., 1999) the rate of accumulation was quite different. The mean Holocene accumulation rate in intertidal flats was much lower in Gomso Bay (0.2–2.0 mm/yr) than in the North Sea (3–10 mm/yr: Reineck, 1963; McCave, 1970; Eisma, 1981) and Bay of Fundy (5–50 mm/yr: Amos and Long, 1980; Dalrymple et al., 1990, 1991). Such a low accumulation rate is most likely responsible for the retrogradational pattern in the Gomso tidal deposits during the mid to late Holocene transgression (Fig. 19).

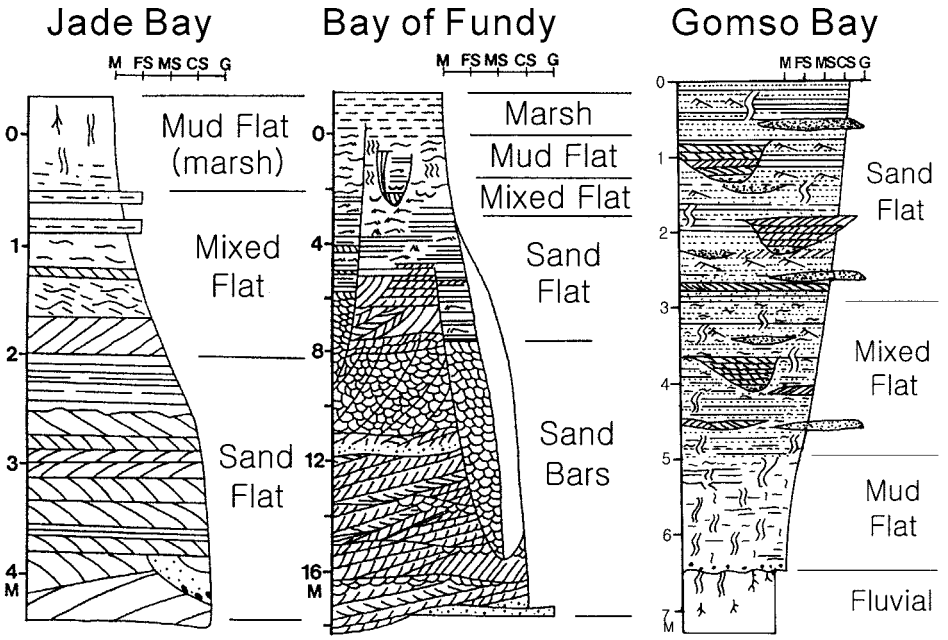

Fig. 18. Facies models for tidal flats of the North Sea (Jade Bay) and Bay of Fundy, showing fining-upward succession by coastal progradation (modified from Klein, 1977 and Dalrymple et al., 1990), and facies model for tidal flats of Gomso Bay, showing coarsening-upward succession by coastal retrogradation with sea-level rise.

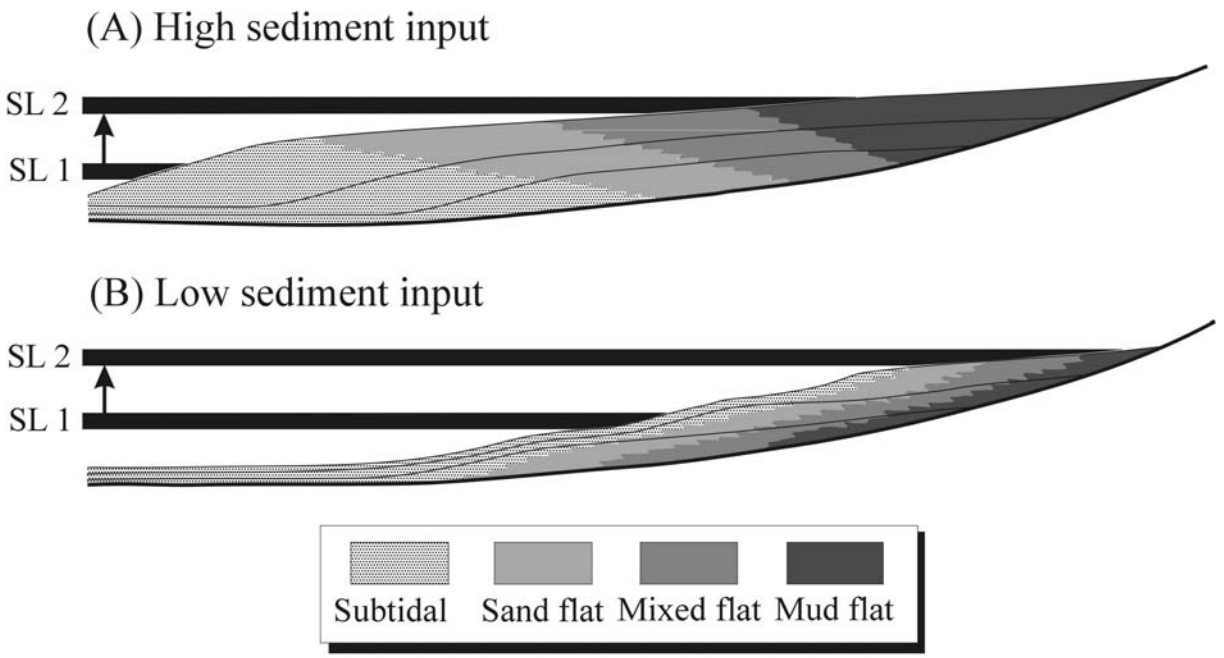

Fig. 19. Schematic cross sections showing the evolution of tidal-flat successions during sea-level rise. (A) Classic model for North Sea and Bay of Fundy in which progradation occurs during sea-level rise due to high sediment input. (B) Model for the southwestern open coast of Korea. Retrogradation occurs during sea-level rise due to low sediment input. After Kim et al. (1999).

5.4. Sedimentological and Stratigraphic Implications

The retrogradational, coarsening-upward succession in storm-influenced, macrotidal flats on the western coast of the Korean Peninsula also differs from the progradational, coarsening-upward successions in high-energy shoreface environments, especially associated with macrotidal beach environments such as in New South Wales and Queensland, Australia (Wright and Short, 1984; Short, 1991). Although these progradational macrotidal beach-shoreface deposits show a similar coarsening-upward trend, they consist entirely of sands, usually from fine sand at the base to medium to coarse sand at the top. This is partly because the macrotidal beach environments are always strongly affected by wave action, whereas the open-coast tidal flats with seasonal change of surface sediment are only intermittently (or seasonally) influenced by storm waves. One key element to help distinguish the two successions in the rock record may

therefore be the presence or absence of interlayered (or remnant) mud deposits and some bi-directional structures in the succession. Yang et al. (2003a, 2004) observed two types of storm beds in the Korean open-coast tidal flats: rising-tide and falling-tide successions. The increasing wavelength of wave ripples within a storm succession of intertidal deposits would indicate an increase in wave-orbital diameter due to increase in water depth during a storm. The succession can be accumulated during flood tide, i.e., rising-tide storm succession. The other storm bed begins with an erosional surface locally overlain by mud pebbles or shell fragments, and is followed by parallel lamination or HCS. This succession is commonly formed during the waning stage of a storm. However, it would represent the falling-tide succession. Although the first succession is not well preserved (ca. 10% of all observed storm beds), it could be a useful tool for distinguishing wave-dominated tidal flats from shoreface deposit in the ancient records.

The fining-upward tidal-flat successions in the North Sea and the Bay of Fundy conform to the definition of parasequences. Parasequences are generally characterized by progradational and shoaling-upward associations of sedimentary facies, bounded by marine flooding surfaces that represent abrupt increases in water depth (Van Wagoner et al., 1990). However, the Holocene coarsening-upward tidal deposits in Gomso Bay suggest retrogradational deposition during Holocene sea-level rise. This is out of accord with the classic concept of sequence stratigraphy in that vertical facies associations indicative of a gradual increase in water depth have not been observed within a parasequence (Van Wagoner et al., 1990). The transgressive macrotidal deposits above the flooding surface in Gomso Bay should, however, be considered as the base of the ongoing, or probably overlying, retrograding parasequence, as described in the wave-dominated shoreface succession by Arnott (1995).

5.5. Hydrodynamic Monitoring of Tidal-flat Sediments

Tidal flats on the west coast of the Korean Peninsula act as a principal repository for littoral sediments carried by macrotidal currents. They may trap incoming sediments as preserved part of an aggradational/progradational sequence mostly under fair-weather conditions, or release some of the uppermost layer particularly during energetic events such as typhoons and winter storms. Traditional sedimentological studies have unraveled that depositional processes of fine-grained sediments on the tidal flats usually undergo seasonal variations (Ryu, 2003; Ryu et al., 2004). Such variations are well expressed by the distribution of textural characteristics and accumulation rates measured during multi-annual field experiments. As a result, the tidal flats can be simply divided into two types: open and sheltered against winter winds. The Daeho tidal flats and the Baeksu tidal flats may represent the open type which characteristically faces the Yellow Sea to the west, being subject to a seasonal mud-cycle of summertime deposition and wintertime erosion (Lee et al., 1999; Chun et al., 2000). The sheltered type is frequently found within bays/embayments that can be exemplified by the Garolim, Muan and Hampyeong bays (Lee et al., 2002; Ryu, 2003; Ryu et al., 2004).

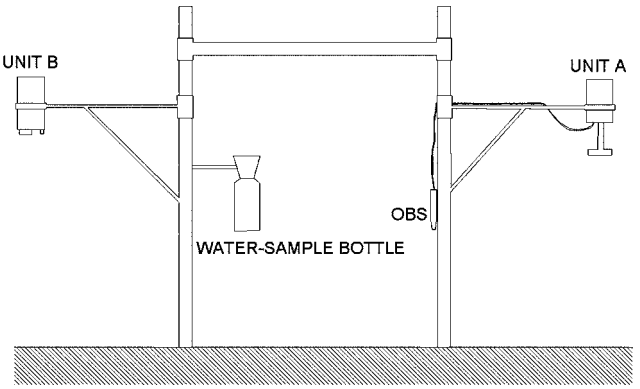

Fig. 20. The TISDOS frame showing principal measuring equipment including units A and B, an OBS and a water-sample plastic bottle. Units A and B each contain a data logger and autonomously operate, for two-fold measurements of the current and pressure and the suspended sediment concentrations and bed level, respectively. After Lee et al. (2004).

A quantitative study of the sediment transport on tidal flats has been made using a self-recording instrument, named Tidal Sediment Dynamics Observational System (TISDOS). Developed by the coastal sedimentary dynamics research team of the KORDI (Lee et al., 2002), TISDOS is an instrument that autonomously measures a series of hydrodynamic parameters including water depth, wave height, current velocity, suspended sediment concentrations (SSC) and bed elevation (Fig. 20). The 10-minute average values for water depth and wave height are derived from the pressure data of a Digiquartz pressure, whereas an acoustic Doppler current sensor (DCS3620, Aanderaa Instruments) provides the 30-s (or 1-min) averages of current velocities. Changes in bed elevation are recorded with a 50/200 kHz dual frequency altimeter every 10 minutes. An optical backscatterance sensor (OBS) records suspended sediment concentrations. The TISDOS, turned on when a salt switch senses sea water, can be deployed on tidal flats for more than 15 days. Further details of the TISDOS can be seen elsewhere (Lee et al., 2002, 2004). Some examples are given of the use and result of the TISDOS deployment on the tidal flats (and beaches) of the Garolim and Hampyeong bays and Imja Island.

5.5.1. Garolim Bay

Garolim Bay has been extensively studied with respect to both the sedimentary processes and hydrodynamic characters (Song et al., 1983; Lee et al., 2002). The bay is semi-enclosed with a narrow entrance (about 2 km across) and an

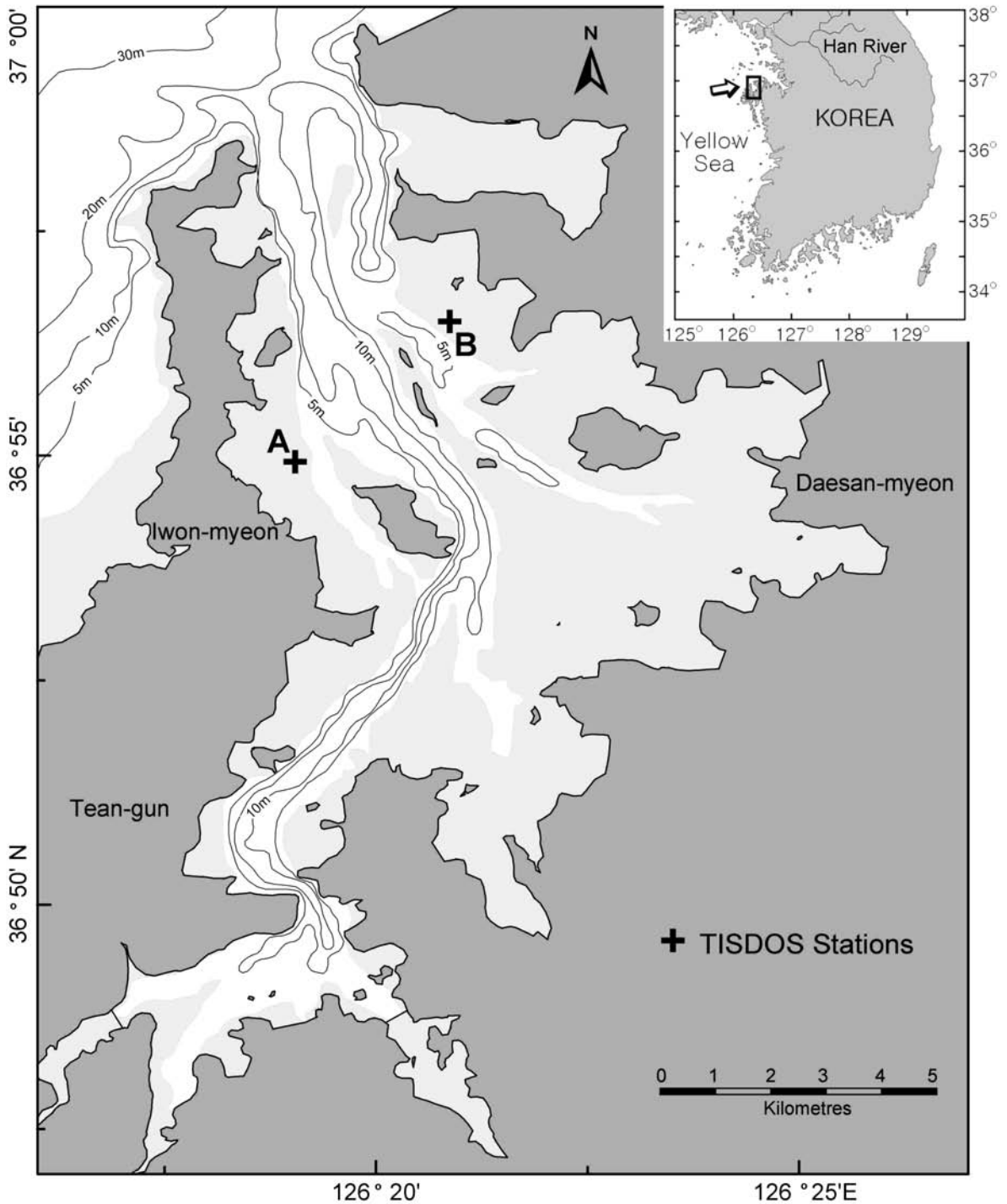

Fig. 21. Map of Garolim Bay showing two locations of the TISDOS deployments. After Lee et al. (2004).

axis approximately 20 km long and trending NW-SE (Fig. 21). A prominent tidal channel at the entrance bifurcates into the bay head, separated by a large tidal sand ridge. Tidal flats along the periphery of the bay are much wider in the east than in the west (Fig. 21). The spatial distribution of surface sediments shows that sand dominates over the tidal sand ridge, whereas mud prevails on the tidal flats. The surface sand on the sand ridge moves toward the bay head according to interpretations of sand wave geometry (Lee et al., 2002). The current measurements using an Acoustic Doppler Profiler (ADP, SonTek) across the bay mouth indicate that most water and suspended matter enter the bay through the eastern half of the bay mouth resulting in development of wider tidal flats on the eastern side of the bay than on the western counterpart (Lee et al., 2002).

The TISDOS was deployed at two stations on tidal flats

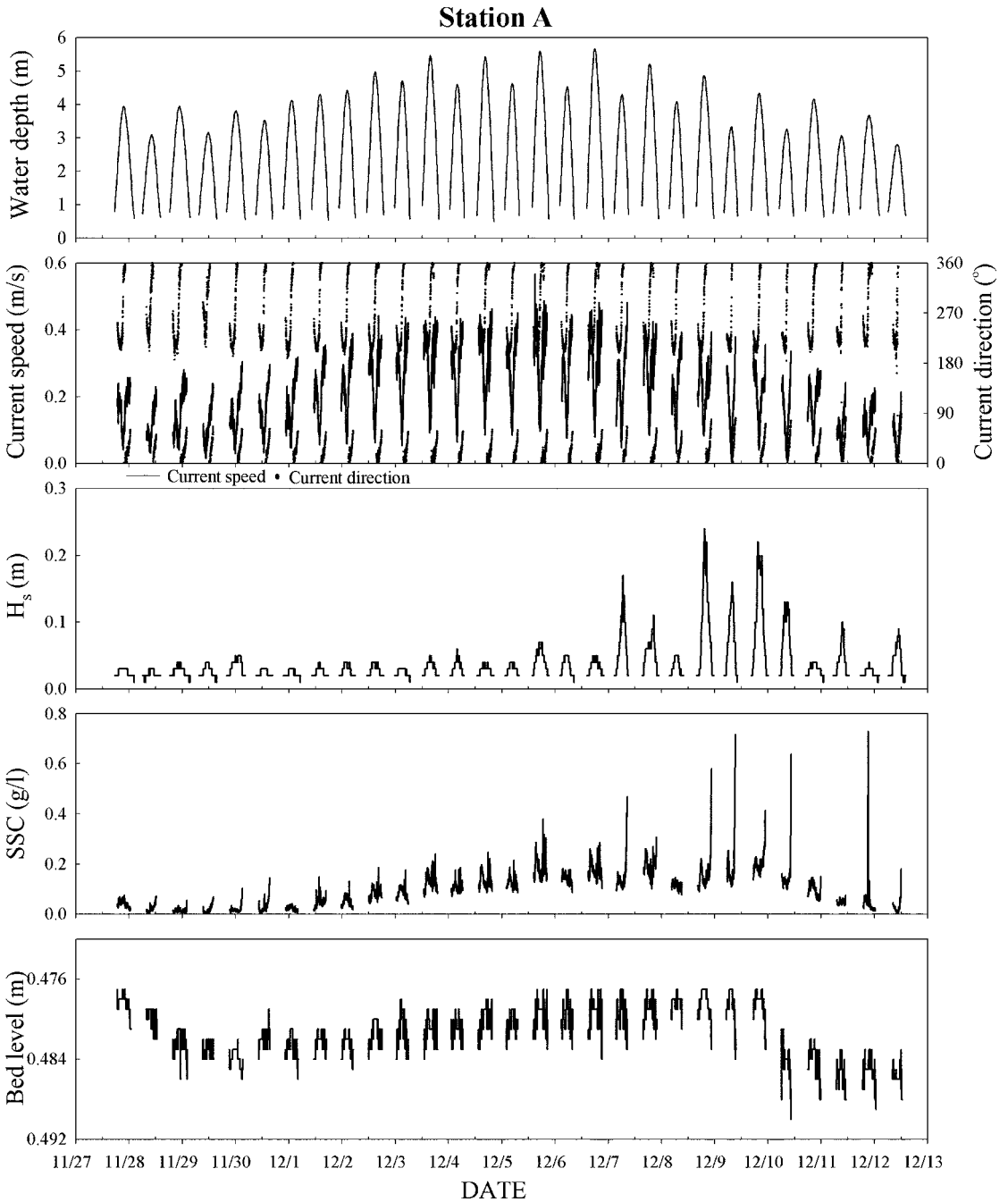

Fig. 22. Time-series of water depth, current speed and direction, wave height (H_s), suspended sediment concentrations (SSC), and bed level from a TISDOS at station A over a spring-neap period from 27 November to 12 December 2002. Bottom sediment is sandy silt (40.5% sand, 49.2% silt, 10.3% clay, mean size 0.03 mm). For location, see Figure 21. After Lee and Jo (2003).

(Fig. 21). The stations were located to represent the western mud flats and eastern sand flats during the winter seasons of the year 2002, even though the two measurement times were almost one year apart (early and late 2002). The profiles of time-series data are shown for stations A and B in Figures 22 and 23, respectively. Although the two stations are governed by the tide which commonly shows two distinct temporal scales, semi-lunar and semi-diurnal, their tidal asymmetry is quite different from each other. In the eastern tidal flat (station B), tide is flood-dominant with a maximum velocity of 0.8 m/s near the low waterline at spring. The tidal currents are strongly rectilinear, mostly in the direction of NW−SE, with flood currents toward SE (Fig. 22). In contrast, station A exhibits ebb-dominance in tidal currents with a maximum of 0.4 m/s and a clockwise rotation from south at flood to north during ebb (Fig. 23). High waves were detected on both stations during the measurements (Figs. 22 and 23). The maximum values of the

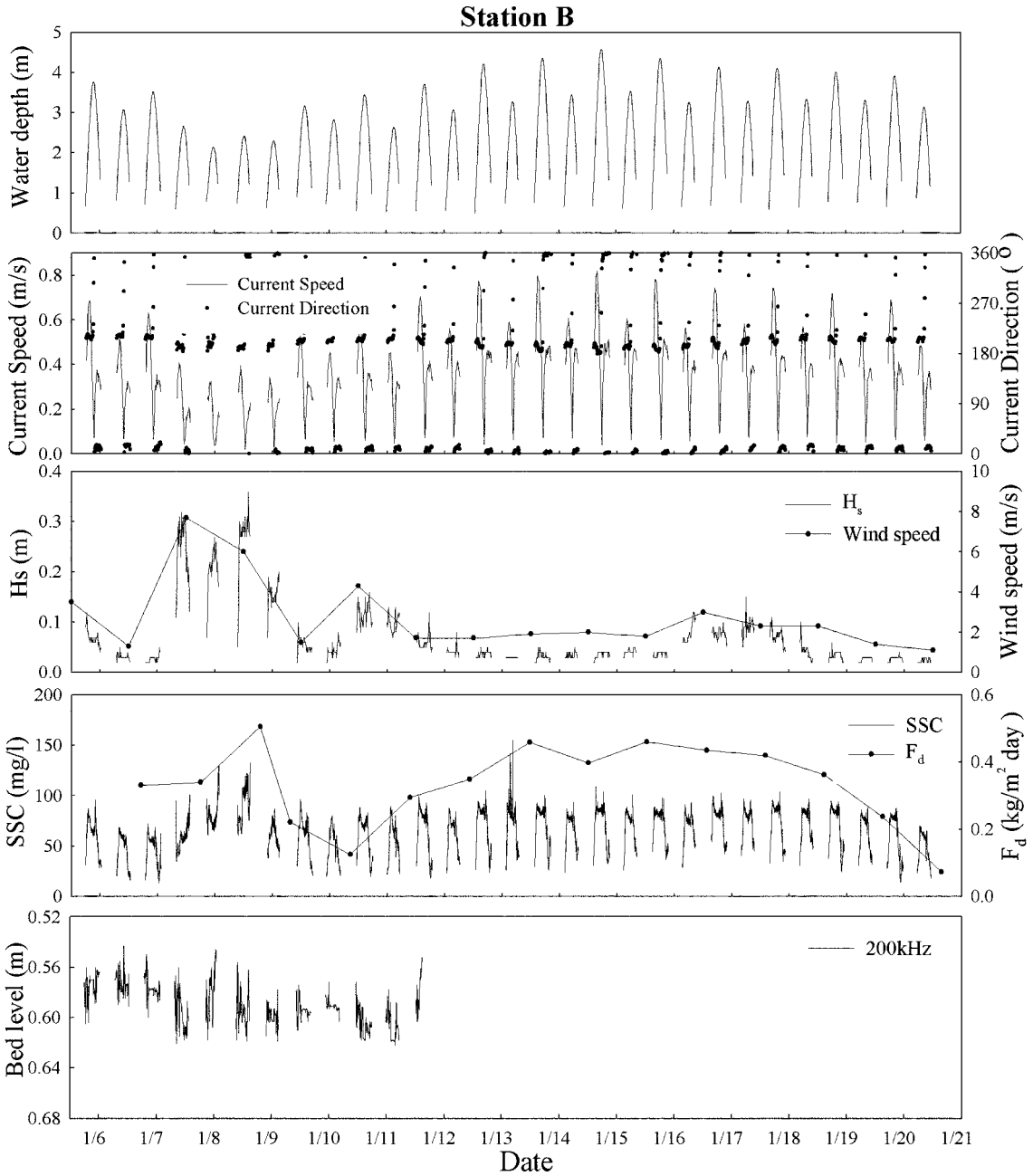

Fig. 23. Time-series of water depth, current speed and direction, wave height, suspended sediment concentrations, daily vertical flux of suspended sediments (F_d), and bed level from a TISDOS at station B over a spring-neap period from 5 to 20 January 2002. Bottom sediment comprises 99% sand with a mean grain size of 0.51 mm. For location, see Figure 21. After Lee et al. (2004).

significant wave height ranged between 0.2–0.3 and 0.3–0.4 m, respectively, on stations A and B. When waves were high, the SSC tended to increase, especially at ebb, to 700 and 130 mg/l at stations A and B, respectively (Figs. 22 and 23). The fair-weather SSC were more or less correlated with tidal current intensities, in the range of 30–250 and 30–80 mg/l at stations A and B, respectively (Figs. 22 and 23). For station B, the bed level was recorded for the first 6 days only, whereas the data set of bed level at station A was complete. It is noticeable that high waves caused the seabed to be eroded through resuspension at the muddy station A, whereas they produced undulation of the seabed through bedform migrations at the sandy station B (Figs. 22 and 23).

The transport rates of bedload and suspended load were calculated following Li and Amos (2001). In order to examine effects of waves and tidal asymmetry on sediment transport, two intervals of the time-series data from station B were selected to represent current-only and combined-current-and-wave cases (Figs. 24 and 25). On January 5–6,

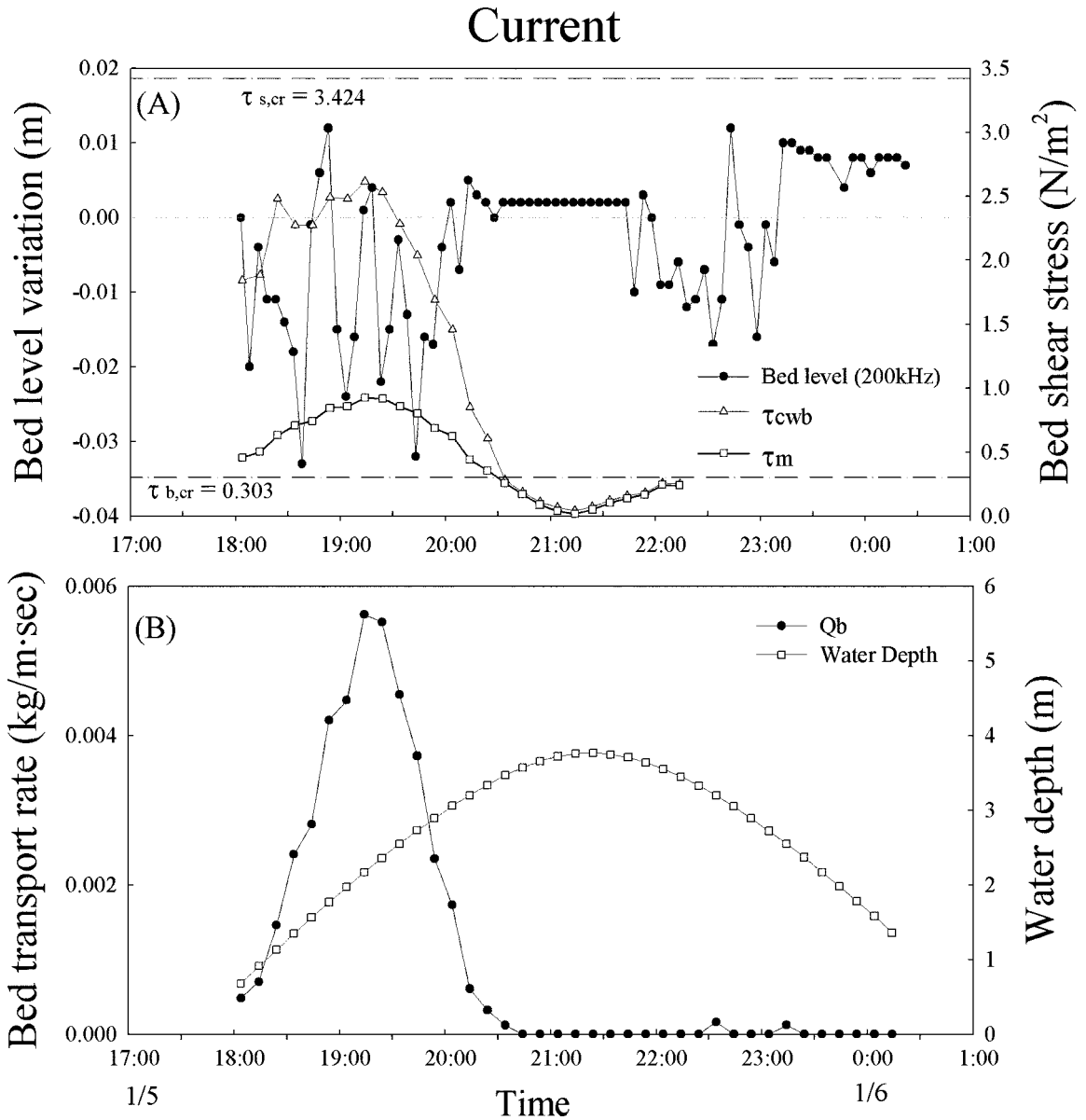

Fig. 24. Typical one-tidal-cycle profiles for fair weather conditions (5 January 2002) at station B showing (A) bed level variation and bed shear stress, and (B) water depth and bed transport rate (Q_b). All of the parameters were calculated using the program of Li and Amos (2001) except for average combined wave-current shear stress (τ_m), which was determined using methods given by Soulsby (1997). Wave height at this time remained lower than 5 cm even though maximum flooding currents were stronger than 0.6 m/s. $\tau_{s,cr}$, critical shear stress for suspension transport; $\tau_{b,cr}$, critical shear stress for bed transport; τ_{cwb}, bedload combined shear stress.

waves were less than 0.15 m high and the flooding currents of transitional tide reached 0.76 m/s with a tidal range of 3.8 m (Fig. 24). In this case, the substantial bed transport rate is calculated during flood tide only, with a maximum of about 0.006 kg/ms, whereas no suspension transport of coarse sands (median, 0.51 mm) is evaluated throughout the tidal cycle (Fig. 24). Waves during the January 7 tidal cycle, representative of the combined-current-and-wave case, were the highest (0.36 m) during the measurements, while the neap current speeds were next to the weakest with a maximum of 0.40 m/s under a tidal range of 2.7 m (Fig. 25). Calculations indicate that the flood currents, aided by waves, could overcome the threshold for bedload transport in spite of being less energetic than the counterpart of the current-only case. In this context, suspension transport as well as bedload transport is computed to take place during the flood (Fig. 25). However, the estimated bedload and suspended load transport rates are small, the former being approximately one fifth of that of the current-only case. The suspended flux at 0.5 m above the seabed, based on the OBS and current data, was directed toward the bay head at station B, but oppositely toward the bay mouth at station A.

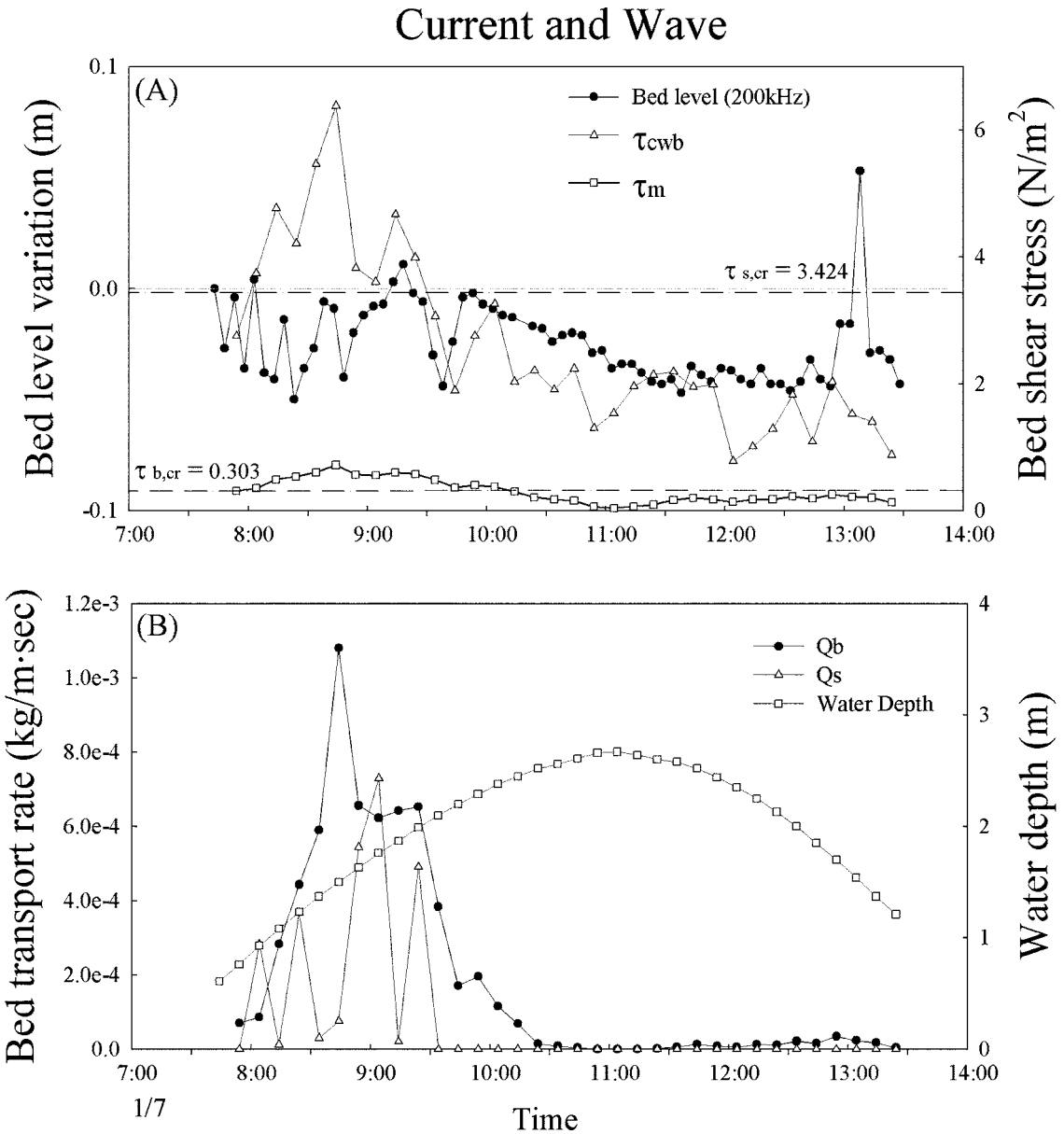

Fig. 25. Typical one-tidal-cycle profiles for large wave conditions (7 January 2002) at station B showing (A) bed level variation and be d shear stress, and (B) water depth, bed transport rate (Q_b) and suspended transport rate (Q_s). All of the parameters were calculated using the program of Li and Amos (2001) except for average combined wave-current shear stress (τ_m), which was determined using methods given by Soulsby (1997). The symbols $\tau_{s,cr}$, $\tau_{b,cr}$ and τ_{cwb} are as explained in Figure 24.

5.5.2. Hampyeong Bay

Hampyeong Bay has a similar form to that of Garolim Bay, elongated NW-SE with a maximum width of 8.5 km and a length of 17 km (Fig. 26). The bay mouth is narrow, 1 km wide, with a maximum water depth of about 23 m. A large tidal channel occupies the center of the bay with some branches originating from the western tidal flats (Fig. 26). However, Hampyeong Bay is much different in geological setting from Garolim Bay. Even though the entire shoreline of the bay is fringed with tidal flats, the surface sediments of the tidal flats differ from one place to another; muds dominate the both sides of the bay, whereas the innermost tidal flats are covered with gravelly muddy sand (Ryu, 2003). The bay-head shoreline of weathered soils is subject to continual retreats by cliff erosion caused by combined waves and tidal currents mainly during winter and early spring. Four-year measurements of accumulation rates on the tidal flats also demonstrate that their surfaces, except for the western soft, watery muds inaccessible, have undergone continuous erosion, although with somewhat seasonal variations (Ryu, 2003). The rather monotonous seabed of the central channel consists of gravelly sandy mud without any tidal sand ridge as seen in Garolim Bay. On the other hand, the relatively wide tidal flats in the bay head left after cliff

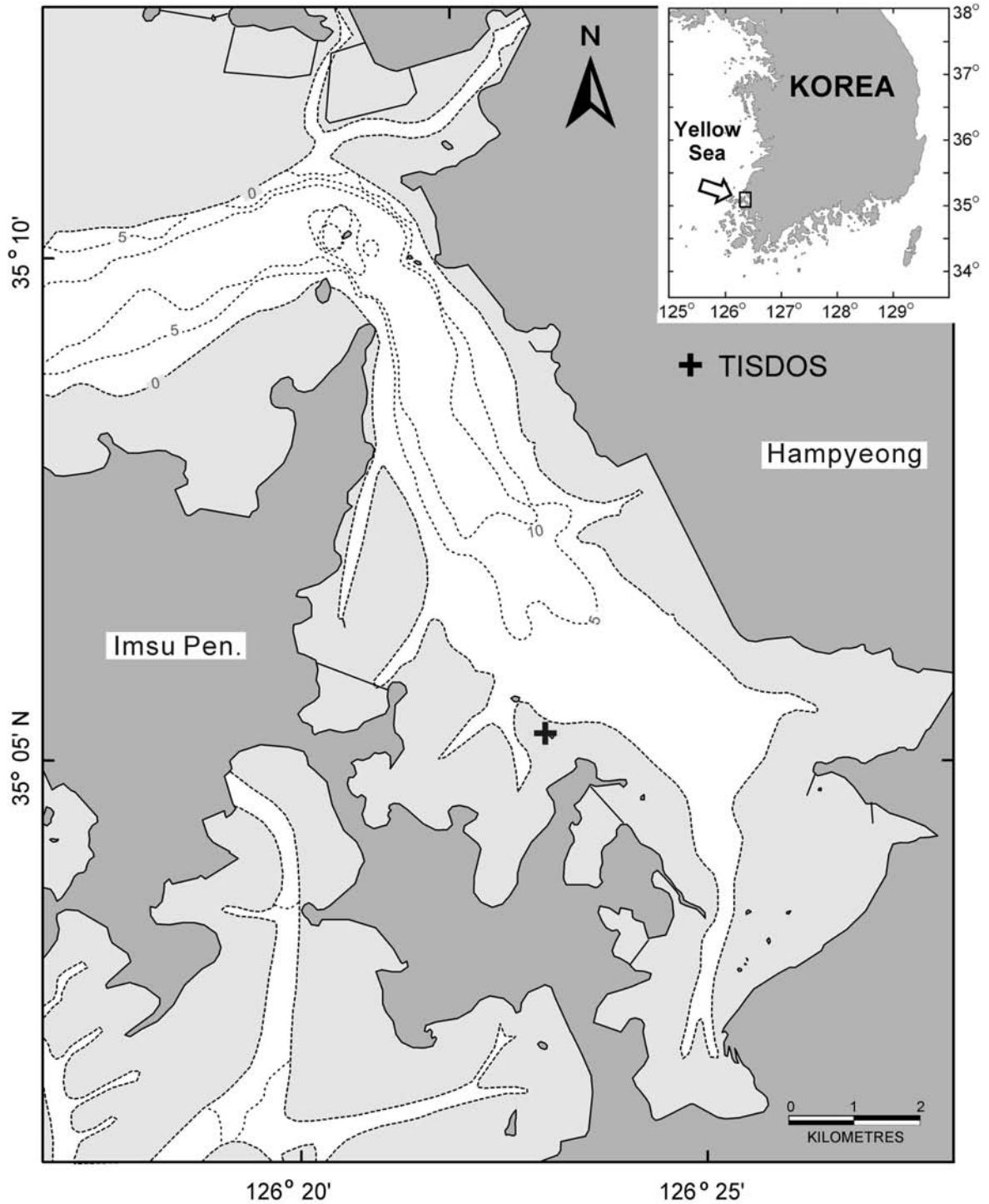

Fig. 26. Map of Hampyeong Bay showing the location of the TISDOS deployment. Contours in meters.

retreats contain a number of isolated sand bars. The TISDOS was deployed on a site near the shoreline fringed by soft, highly watery muddy tidal flats during the period between 24 October and 13 September 2003 (Fig. 26). Although these tidal flats were considered to be depositional, extreme difficulties of access onto the wet muds had hampered any measurements including accumulation rates. The hydrodynamic data from the TISDOS began to unveil the behavior of suspended sediments in response to the local tidal regime and waves on the tidal flats unexplored so far in Hampyeong Bay.

The variation in water depth clearly shows semi-diurnal characteristics as well as a spring-neap cycle (Fig. 27). The maximum tidal range at the station was more than 3 m

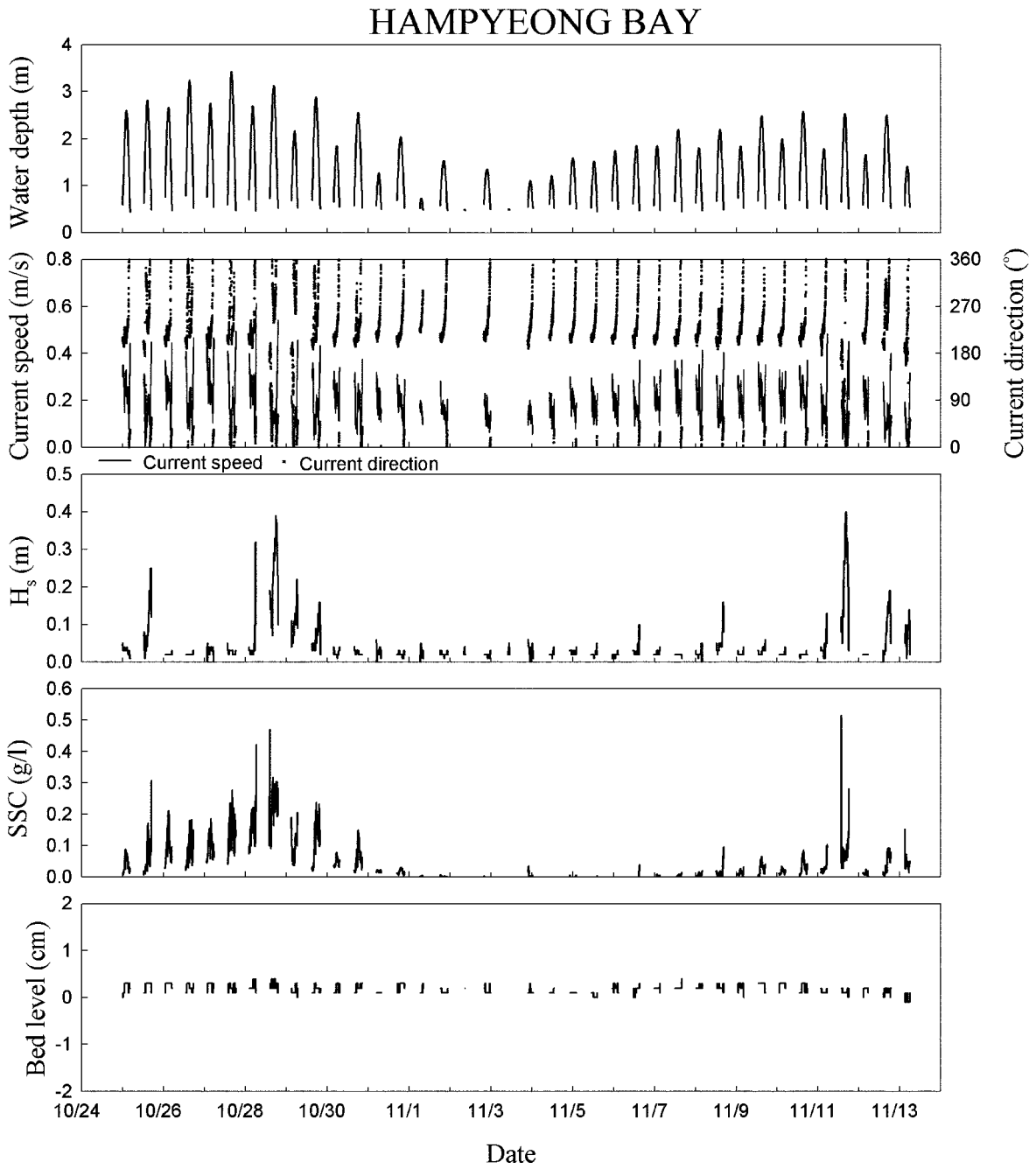

Fig. 27. Time-series of water depth, current speed and direction, wave height (H_s), suspended sediment concentrations (SSC), and bed level from a tidal-flat station of TISDOS, Hampyeong Bay over a spring-neap period from 24 October to 13 November 2003. Bottom sediment is sandy silt (40.5% sand, 49.2% silt, 10.3% clay, mean size 0.03 mm). For location, see Figure 26.

despite short distances from the shoreline (Fig. 27). During the measurements, two intervals of high waves (significant wave height up to 0.5 m) were encountered. The SSC peaked at 500 mg/l when waves were highest, but normally ranged between 50 and 200 mg/l at spring and between nearly nil and 100 mg/l at intermediate tides (Fig. 27). The presence of peaks in the SSC during each of the tidal cycles except for the neap phase indicates that the muddy seabed could be resuspended by tidal currents alone. However, the variation in bed level seems to be insensitive to the resuspensional processes, suggesting that the thickness of the surface layer once eroded was below the resolution of the altimeter (about 2 mm).

5.5.3. Imja tidal beach

Imja Island belongs to the archipelago studding the southwestern coastal region of Korea (Fig. 28). Off the island, sands are abundant mainly in the form of large sand ridges

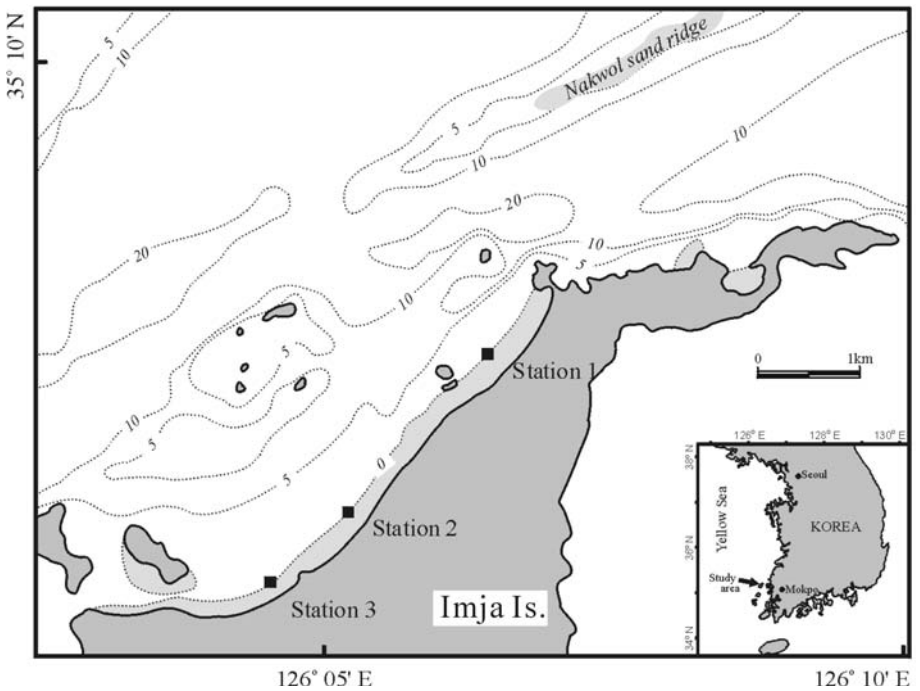

Fig. 28. Map of macrotidal beaches in Imja Island showing location of three stations of TISDOS. Contours in meters.

including Nakwol sand ridge (Fig. 28). There have been few studies on the origin of the sands and it is unknown whether these are transgressive deposits or modern sediments derived from the present-day coastline, particularly from the Yeongsan River. A stretch of macrotidal sand beaches is well developed on the northwestern coast of the island (Fig. 28). To explore hydrodynamic characteristics of the sand transport during fair weather, three TISDOS stations were set up near the low water line of the beach during the period of 24 June–11 July 2003 (Fig. 28).

The tide was in the range of 2.0–3.5 m with both semi-diurnal and semi-lunar inequalities at station 1 (Fig. 29). In general, ebb currents are stronger than flood currents, with a maximum of about 0.25 m/s in spring tidal cycles. However, waves occurring during the windy days (25 and 28 June) escalated the measured velocities up to 0.65 m/s

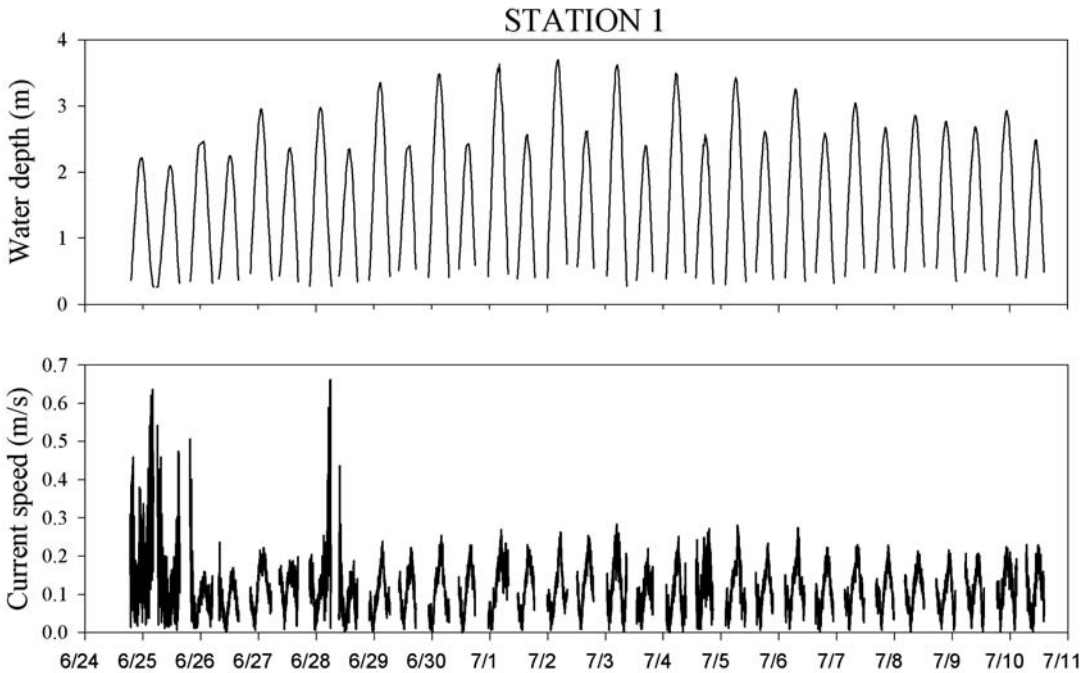

Fig. 29. Time-series of water depth and current speed at station 1 on the macrotidal beach of Imja Island during 24 June to 10 July 2003 . For location of station 1, see Figure 28.

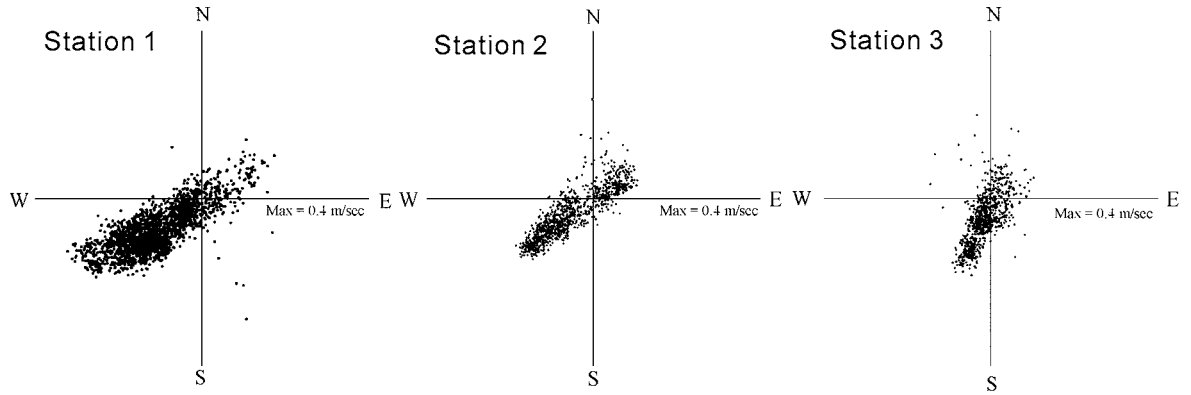

Fig. 30. Vector diagrams of tidal currents at stations 1 to 3 on the macrotidal beach of Imja Island. Note that current directions are similar to one another but speeds tend to increase from station 1 to station 3. For location of stations, see Figure 28.

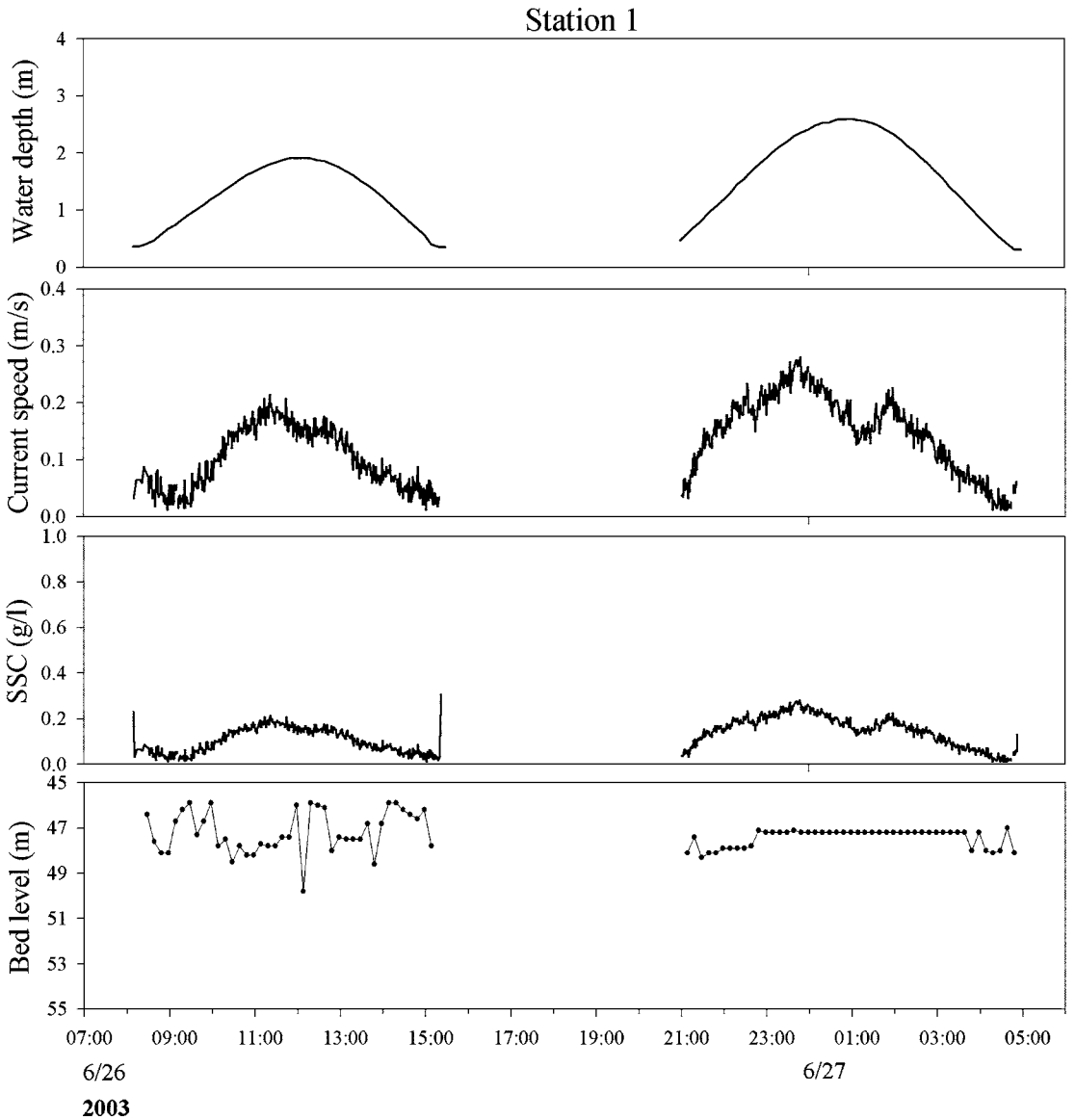

Fig. 31. Time-series of water depth, current speed, suspended sediment concentrations (SSC) and bed level at station 1 on the macrotidal beach of Imja Island during 26–27 June when waves were virtually absent. For location of station 1, see Figure 28.

caused mainly by wave breaking on the beach (Fig. 29). The tidal-current vectors clearly show ebb-dominance at all stations with the almost same major tidal axis trending NE–SW (ebb to SW) and a gradual decrease in magnitude from station 1 to station 3 (Fig. 30). This means that sands reaching the beach from the north are likely to accumulate on the beach sector between stations 1 and 3. Figures 31 to 33 show variable parameters measured at each station during 26–27 June when waves were nearly absent. The SSC ranged between 0.1 and 0.4 g/l and tended to increase substantially near the end of ebb phases. The bed level fluctuated noticeably during the smaller one of twice daily tidal cycles, whereas it remained flat through the larger tidal cycle. The fluctuating seabed reflects migration of ripples whereas the flat seabed suggests upper-flow-regime environments.

6. HOLOCENE RELATIVE SEA-LEVEL CHANGES

The Holocene relative sea-level curves of the Yellow Sea have been derived from the Chinese and Korean coasts (Bloom and Park, 1985; Pirazzoli, 1991, Kim et al., 1999; Chough et al., 2000). The sea-level curves along the Chinese coast suggest highly variable position, depending on time and locality (Fig. 34). The general pattern shows a rapid rise in sea level from −40 m (about 10 ka) to −10 m (about 7 ka) with varying transgression rate. This was followed by a gradual rise to the present level with minor oscillations (Yang and Xie, 1984; Feng and Wang, 1986; Pirazzoli, 1991) (Fig. 34). A refined sea-level curve was reconstructed from the Yangtze delta plain based on corrected data of long-term subsidence and tidal ranges (Chen

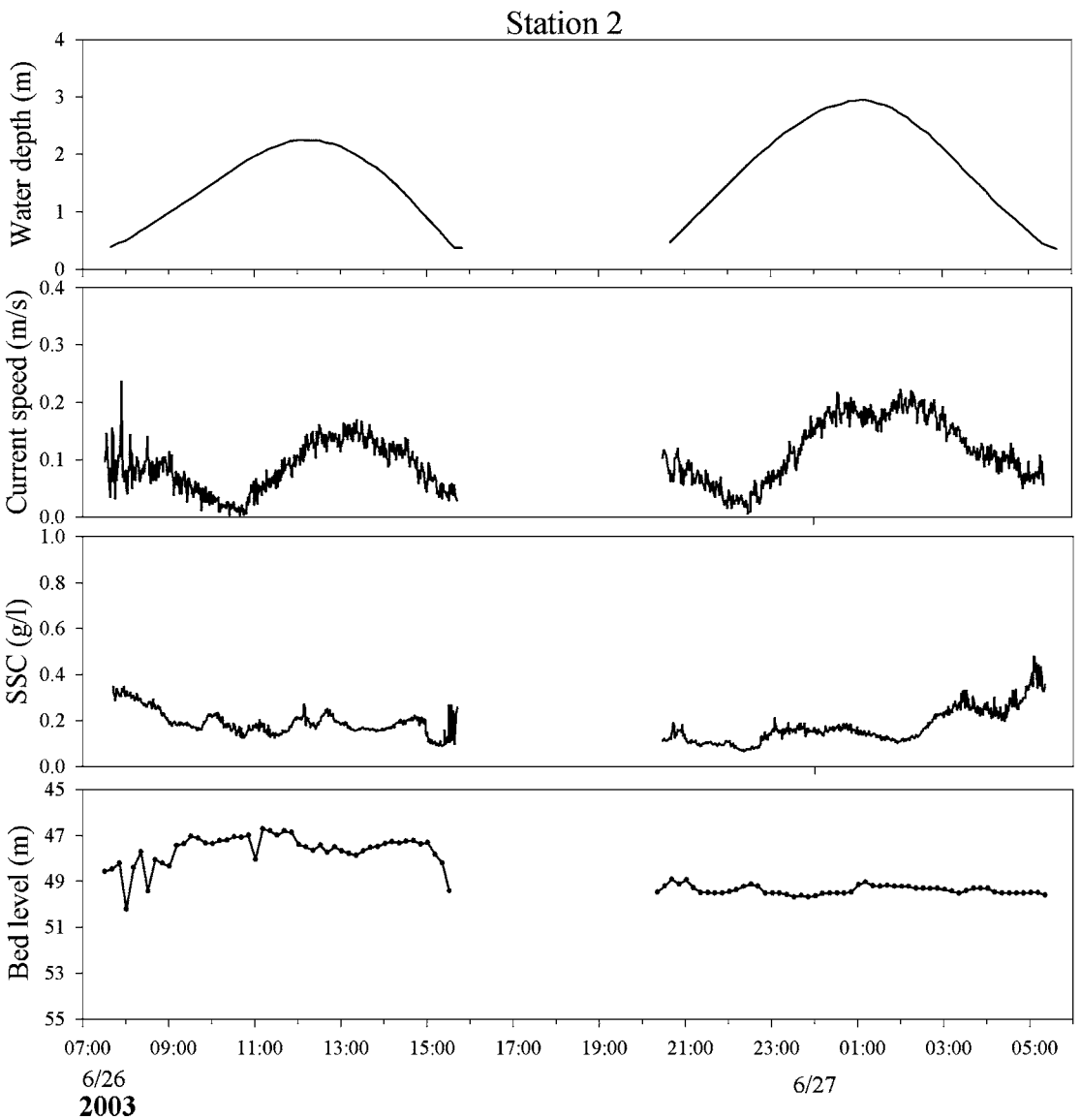

Fig. 32. Time-series of water depth, current speed, SSC and bed level at station 2 on the macrotidal beach of Imja Island during 26–27 June when waves were virtually absent. For location of station 2, see Figure 28.

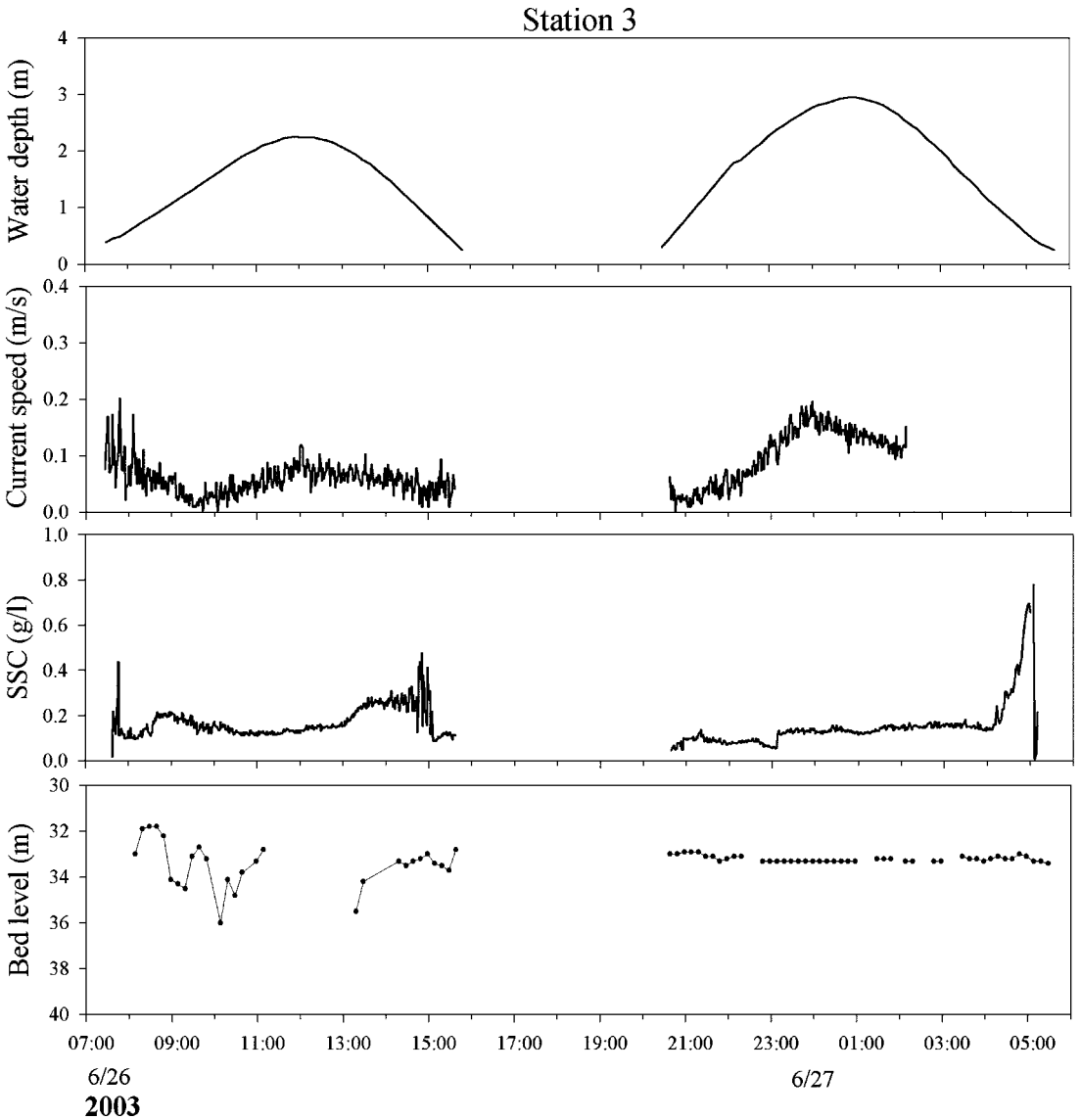

Fig. 33. Time-series of water depth, current speed, SSC and bed level at station 3 on the macrotidal beach of Imja Island during 26–27 June when waves were virtually absent. For location of station 3, see Figure 28.

and Stanley, 1998; Zong, 2004) (Fig. 35A). It shows an early period of rapid, continuous rise up to about 7 ka and a slow rise during highstand (since about 7 ka). It is generally apparent that the mid Holocene highstand started at −4 m mean sea level.

For the Korean coast, a sea-level curve constructed by Bloom and Park (1985) displays a gradual rise from −8 m mean high water level around 8.5 ka to −2 m around 5 ka and a gradual rise thereafter. Figure 35B shows Holocene relative sea-level curve based on an integration of additional radiocarbon dates obtained from plant remains, peat and shells of Gomso Bay and other coastal areas (Table 2). The paleo-mean sea level (MSL) was determined using the assumption that tidal range and frequency and bathymetric slopes in each area have changed little during the mid to late Holocene. It was also assumed that the distribution of sub-environments within the tidal flat has been controlled primarily local water level (Table 3), which is similar to the assumptions applied to Gomso Bay (Fig. 36). The paleo-MSL was estimated according to the vertical relationship between sediment type in which a dated sample accumulated and its occurrence range (Table 4). The reconstructed Holocene sea level generally shows a relatively rapid rise up to about 7 ka, followed by a gradual rise without discernable fluctuation (Fig. 35B). The sea level reached −5 m around 7 ka and approached its present level at about 3 ka. The reconstructed sea-level curve is similar to those given by Kim et al. (1999) and of the Yangtze delta plain (Fig. 35A, B).

Based on shallow-marine, inter-tidal and submerged terrestrial data from the East China Sea, Yellow Sea and Sunda shelf, Liu and Milliman (2004) suggested a step-wise Holocene sea-level curve for the western Pacific coast

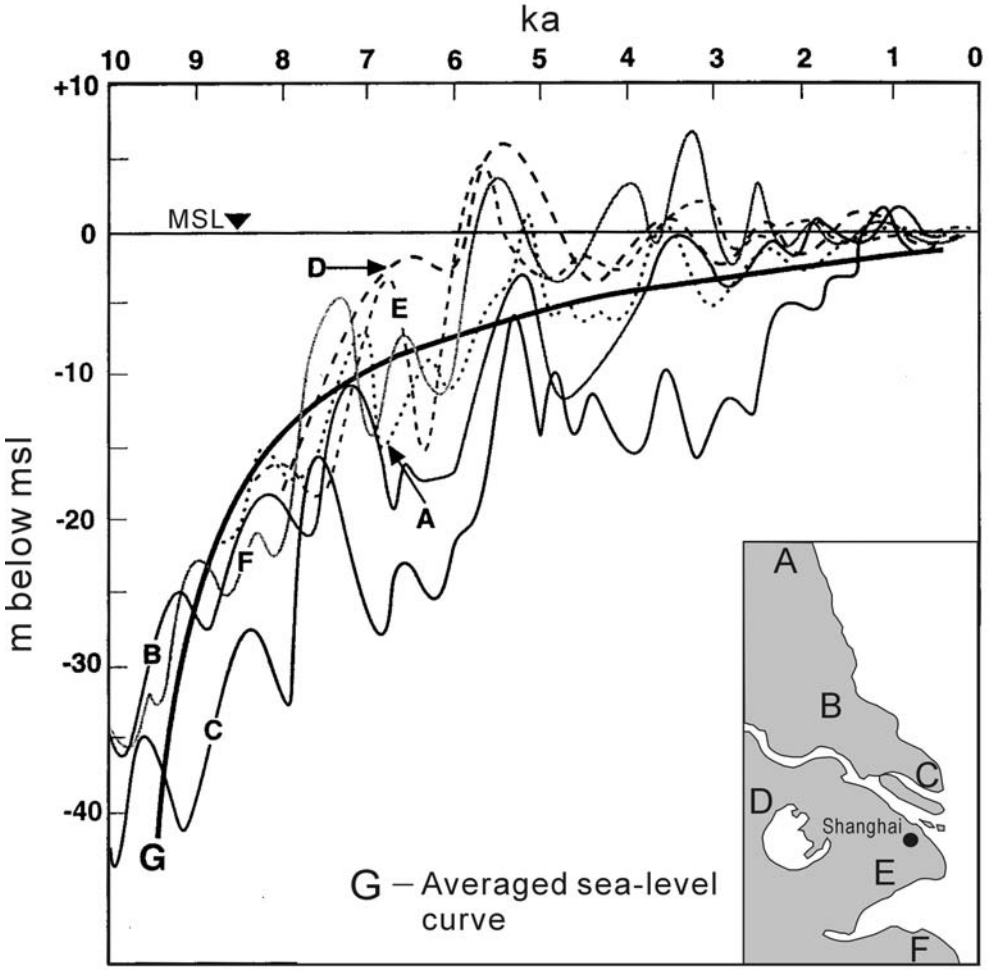

Fig. 34. Reconstructed Holocene relative sea-level curves from Yangtze delta plain (after Chen and Stanley, 1998).

showing a series of rapid flooding events (as fast as 80 mm/yr), separated by long-term slow rises (2–10 mm/yr) (Fig. 37). Based on radiocarbon dating on benthic foraminifera, Kim and Kennett (1998) reported that the Holocene marine transgression started in the central Yellow Sea at about 11.3 ka and approached the present lower tidal flat level at about 7.5 ka. The sedimentary records in the inner-middle shelf areas suggest that the post-glacial transgression was dominated by a series of spasmodic sea-level rises.

7. HIGH-RESOLUTION SEISMIC DATA

7.1. Echo Types

Large amounts of closely spaced (2.2–4.4 km interval) high-resolution subbottom profiles (Chirp, 2–7 kHz) were obtained in the eastern part of the Yellow Sea south of 38°N by the Korea National Oceanographic Research Institute (Fig. 2). On the basis of seafloor morphology, surface bedforms and subbottom acoustic characteristics, eleven echo types have been identified (Chough et al., 2002; Kim, 2003; Shinn, 2003; Shinn et al., 2004). The echo types are classified into three major classes according to the seafloor topography: flat echoes (echo types 1-1, 1-2, 1-3 and 1-4), mound echoes (echo types 2-1, 2-2, 2-3, 2-4 and 2-5) and irregular gullied echoes (echo types 3-1 and 3-2) (Table 5).

Echo type 1-1 consists of relatively flat, sharp bottom echoes with either no or few subbottom reflectors (Fig. 38A). It generally covers the inner-shelf to nearshore area where sandy sediments predominate. Echo type 1-2 is characterized by flat seafloor with moderate to well developed subbottom reflectors (Fig. 38B). The deeper sound penetration suggests that the surface comprises relatively fine-grained sediments (e.g., Damuth and Hayes, 1977).

Echo type 1-3 represents acoustically transparent units of good lateral continuity. Echo type 1-3a is a sheet of uniform thickness (3–5 m) and type 1-3b is a wedge with a few vague interlayers (<7 m thick) (Fig. 38C). Echo type 1-3b overlies echo type 1-3a and progressively thins toward the south and east. Echo type 1-3a comprises sandy muds with very thin sand layers in the uppermost part, interpreted as a transgressive sediment sheet underlain by a ravinement surface (Lee and Yoon, 1997). The upper transparent unit, echo type 1-3b, is made up of watery (>50% in water con-

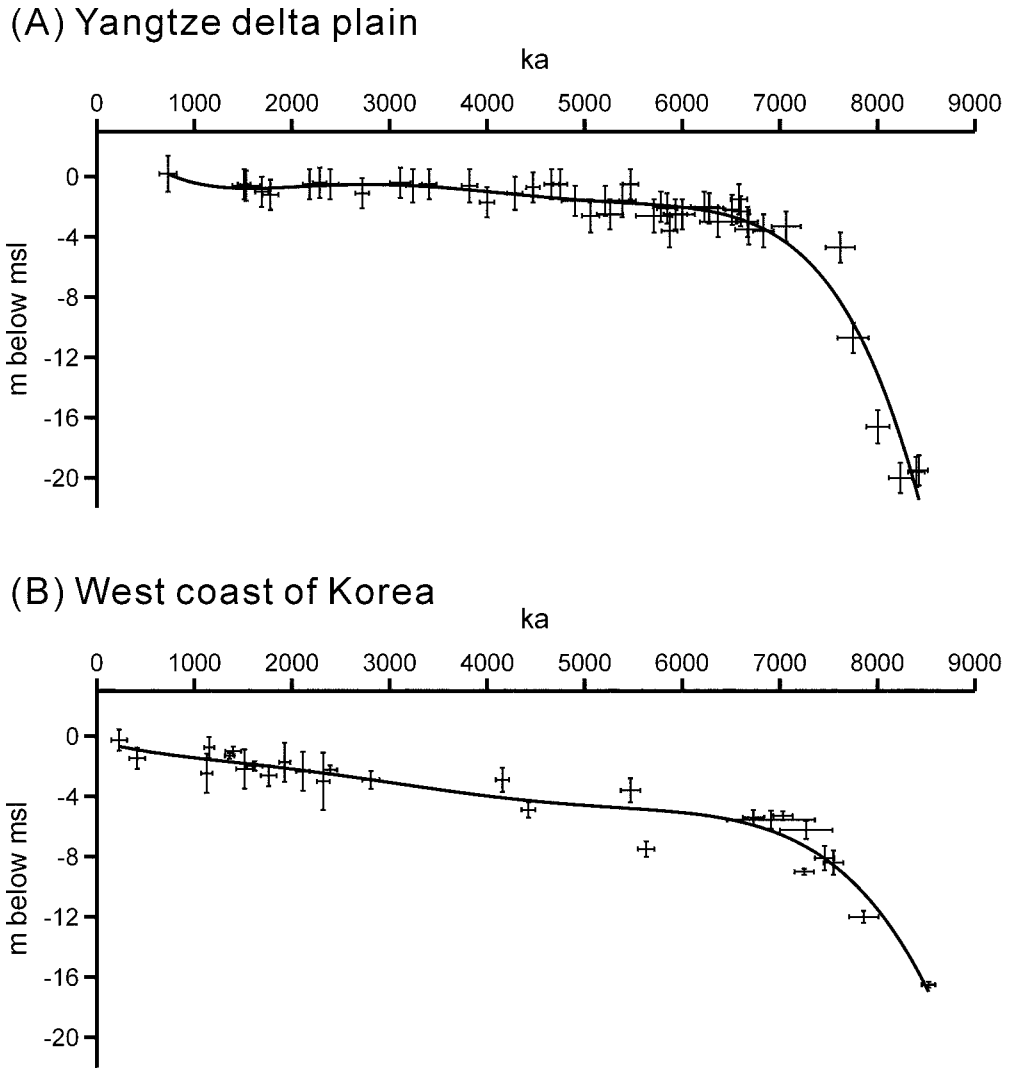

Fig. 35. Holocene relative sea-level curves based on radiocarbon dates and estimated paleo-mean sea level in the Yangtze delta plain (A) (after Zong, 2004) and the western coast of Korea (B).

tent) clayey muds (Butenko et al., 1983; Lee and Yoon, 1997). The clay composition with high smectite content, diagnostic of Huanghe River sediments, suggests that this echo type represents Huanghe River-derived mud (Milliman et al., 1985; Lee and Chough, 1989; Alexander et al., 1991; Park and Khim, 1992).

Echo type 1-4 is characterized by flat seafloor covered with regularly spaced wavy bedforms (Fig. 38D). These bedforms are 3–10 m high, 150–500 m wide and either asymmetrical or symmetrical in cross section. The morphological characteristics of the wavy bedforms, i.e., wavelength, height and cross-sectional shape, suggest that these bedforms are large-scale subaqueous dunes formed under the influence of tidal currents (Allen, 1980; Stride et al., 1982; Ashley, 1991).

Echo type 2-1 represents gently mounded seafloor with sharp, smooth surface (Fig. 38E). The mounds are 15–25 m in height and generally more than 3 km in width, and show a slope gradient of less than 1°. Echo type 2-1 characterizes the transverse cross section of an elongate sediment body whose dimension and relationship with regional currents are suggestive of tidal ridges (Houbolt, 1968; Belderson et al., 1982; Johnson and Baldwin, 1996). The rounded profile and smooth surface probably indicate a temporarily dormant stage of the mounds (e.g., Yang, 1989). The lack of internal reflections is most likely due to veneering of coarse-grained sediments on the mound surface (Bahng et al., 1994; Jung et al., 1998).

Echo type 2-2 mimics echo type 2-1 in geometry and acoustic characters, except for wavy bedforms on the surface (Fig. 38F). The broader and flat-topped mounds are often entirely covered by regularly spaced and similar sized bedforms of symmetrical shape. The wavy bedforms on the mound surface can be interpreted as large-scale subaqueous dunes superposed on the ridge (Allen, 1980; Ashley, 1991).

Echo type 2-3 exhibits a subdued, broader cross-sectional

Table 2. Holocene relative sea-level index samples from the west coast of Korea.

No.	Location	Laboratory code	Dated materials	Sediment type	Altitude from present msl (m)	Radiocarbon date (yr BP)	Eastimated paleo-msl (m)	Source of data
1	Gomso Bay	HJ-03, 0.82	*Crassostrea*	mud flat	0.07	1925±58	−1.73±1.3	Kim et al. (1999)
2	Gomso Bay	HJ-23, 1.14	*Crassostrea gigas*	mixed flat	−2.08	1515±86	−2.18±1.3	
3	Gomso Bay	HJ-31, 1.30	*Crassostrea gigas*	mixed flat	−2.37	1128±58	−2.47±1.3	
4	Gomso Bay	HJ-35, 1.63	*Meretrix*	sand flat	−2.75	1152±51	−0.75±0.7	
5	Gomso Bay	HJ-43, 0.60	*Dosinia japonica*	sand flat	−2.27	229±81	−0.27±0.7	
6	Gomso Bay	HJ-43, 1.80	*Crassostrea gigas*	sand flat	−3.47	414±81	−1.47±0.7	
7	Gomso Bay	HJ-43, 2.95	*Crassostrea gigas*	sand flat	−4.62	1762±80	−2.62±0.7	
8	Gomso Bay	SW-07, 5.79	Plant remains	mud flat	−3.49	7032±98	−5.29±0.3	
9	Gomso Bay	SW-09, 1.68	*Crassostrea gigas*	mud flat	−0.18	1619±81	−1.98±0.3	
10	Pyeongtaek	Pyeongtaek-1	Peat		1	4157±67	−2.9±0.8	
11	Pyeongtaek	Pyeongtaek-2	Peat		0.3	5470±100	−3.6±0.8	
12	Daecheon	Daecheon-1	Peat		−3.63	7270±270	−6.23±0.6	
13	Daecheon	Daecheon-2	Peat		−2.96	6910±450	−5.56±0.6	
14	Gomso Bay	SW-09-070	Plant remains	mud flat	0.8	1398±81	−1.0±0.3	Chang & Choi (2001)
15	Yeongkwang	D-12-205	Unidentified shell	mixed flat	−2.33	2112±69	−2.33±1.3	
16	Yeongkwang	J-01-265	*Meretrix*	mud flat	−0.64	2392±70	−2.24±0.3	
17	Yeongkwang	J-29-340	*Crassostrea gigas*	sand flat	−4.81	2809±88	−2.91±0.6	
18	Namyang Bay	NY-4	Oyster	mixed flat	−3	2321±65	−3.0±1.9	Lim (2001)
19	Namyang Bay	NY-5	Plant remains	mud flat	−4.9	5630±85	−7.5±0.5	
20	Cheonsu Bay	CS-K1	Plant remains	mud flat	−10.4	7860±150	−12.0±0.4	
21	Haenam Bay	HN-TS1	Oyster	mud flat	−0.3	1362±48	−1.3±0.2	
22	Haenam Bay	HN-BH5	Plant remains	mud flat	−8	7250±100	−9±0.2	
23	Haenam Bay	HN-BH1	Plant remains	mud flat	−15.5	8524±69	−16.5±0.2	
24	Asan Bay	DH4-1-2	Gastropoda	mud flat	−2.3	4423±71	−4.9±0.5	Kim & Kennett (1998)
25	Asan Bay	DH4-1-3	Oyster	mud flat	−2.8	6730±110	−5.4±0.5	
26	Asan Bay	DH4-1-4	Peat	mud flat	−4.2	7460±100	−8.1±0.8	
27	Asan Bay	DH4-1-5	Peat	mud flat	−4.5	7550±100	−8.4±0.8	

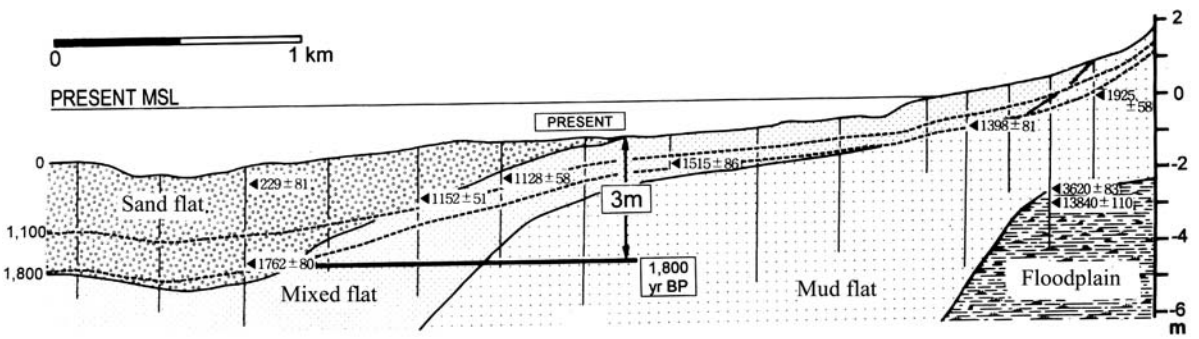

Fig. 36. Simplified stratigraphic cross section of the Gomso tidal flat, showing retrograding, coarsening-upward Holocene marine succession underlain unconformably by nonmarine deposits. ^{14}C dates are used to plot two isochrones, representing the paleo-bay floor at 1.1 and 1.8 ka. Solid vertical lines represent vibracores. Numbers beside arrow heads depict radiocarbon dates (yr BP) on shells and plant remains. After Kim et al. (1999).

shape and smooth surface (Fig. 38G). The wavy bedforms, smaller than those of echo type 2-2, occupy only a small portion of the mounds, and are often transitional to digitized surface or small-scale hyperbolae. The subdued ridge profile and poorly developed bedforms indicate that the echo type 2-3 represents ridges mostly in a stagnant state. The acoustically transparent wedges on the flanks suggest a sporadic deposition of fine-grained material (e.g., Stride et al., 1982; Berné et al., 1998; Reynaud et al., 1999).

Echo type 2-4 denotes the large-scale, bank-like seafloor topography (up to 40 m thick), in which inclined internal reflectors form a prominent prograding configuration. Indi-

Table 3. Reference water table from local tide gauges.

	Gomso Bay[1)]	Pyeongtaek coast[2)]	Daecheon coast[3)]	Yeongk-wang coast[4)]	Namyang Bay[2)]	Cheonsu Bay[5)]	Haenam Bay[6)]	Asan Bay[2)]
Highest high water (HHW)	3.69	4.86	3.35	3.25	4.86	3.45	2.23	4.86
Mean spring high water (MSHW)	3.05	4.16	2.77	2.67	4.16	2.90	1.67	4.16
Mean high water (MHW)	2.27	3.13	2.01	2.00	3.13	2.09	1.24	3.13
Mean neap high water (MNHW)	1.49	2.10	1.24	1.34	2.10	1.27	0.80	2.10
Mean sea level (MSL)	0.10	0.13	0.06	0.02	0.13	−0.04	−0.11	0.13
Mean neap low water (MNLW)	−1.29	−1.85	−1.12	−1.30	−1.85	−1.35	−1.02	−1.85
Mean low water (MLW)	−2.07	−2.88	−1.89	−1.97	−2.88	−2.17	−1.45	−2.88
Mean spring low water (MSLW)	−2.85	−3.91	−2.65	−2.63	−3.91	−2.08	−1.89	−3.91
Lowest low water (LLW)	−3.48	−4.61	−3.23	−3.22	−4.61	−3.53	−2.45	−4.61

[1)]National Geographic Institute (1981), [2)]National Geographic Institute (1978), [3)]National Geographic Institute (1980)
[4)]National Geographic Institute (1983), [5)]National Geographic Institute (1979), [6)]National Geographic Institute (1982)

Table 4. Sediment types and their occurrence range.

Sediment type	Occurrence range
Brackish peat	MHW-HHW
Plant remains	MHW-HHW
Shells in mud flat	MHW-MNHW
Shells in mixed flat	MNHW-MNLW
Shells in sand flat	MNLW-MSLW

vidual internal reflectors are highly backscattering and have a good lateral continuity (Fig. 38H). The deep-drill core data raised from this type demonstrate that sediments of echo type 2-4 consist predominantly of muds with silt laminae (Chang et al., 1996; Jin, 2001). The internal organization and areal distribution of echo type 2-4 suggest that it represents a mud bank (Heuksan mud belt) formed by residual transport of suspended sediments derived from the Geum River and other sources (Jin and Chough, 1998; Park et al., 2000; Lee and Chu, 2001).

Echo type 2-5 is identified by a flat-topped mound with prograding clinoforms (Fig. 38I). The low-angle inclined clinoforms (<0.13°) prograde both southeastward and northeastward onto a flat erosional surface. Echo type 2-5 exhibits slightly mounded seafloor (4–10 m high and 10–15 km wide). The surface is laterally exposed to the flat seafloor that forms a step-wise terrace and gently slopes offshore. The

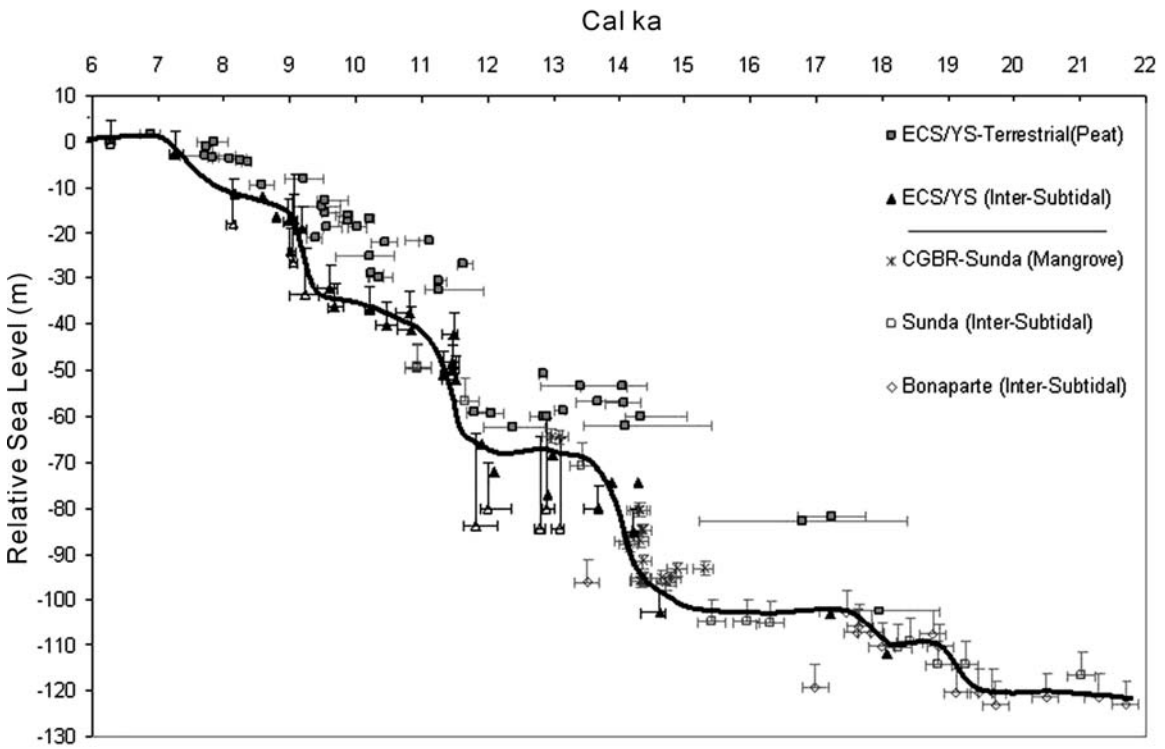

Fig. 37. A sea-level curve showing the western Pacific post-glacial sea-level history suggested by Liu and Milliman (2004).

Table 5. Summary of echo types. After Chough et al. (2002) and Shinn et al. (2004).

Class	Type	Line drawing	Description	Interpretation
1	1-1		Relatively flat sea floor with either no or few subbottom reflectors	Seafloor covered by coarse-grained sediments; relict sands
	1-2		Flat sea floor with moderately to well developed subbottom reflectors	Seafloor covered by relatively fine-grained surface sediments
	1-3	1-3b 1-3a 1-2	Laterally extensive acoustically transparent unit of either sheet (1-3a) or wedge (1-3b) form	Transgressive sediment sheet (1-3a) and Holocene Huanghe-derived muds (1-3b)
	1-4		Flat seafloor covered by regularly spaced, wavy bedforms	Large-scale dunes formed by tidal currents
2	2-1		Mounds with no bedforms; either absent or well developed internal reflectors	Tidal ridges; inactive
	2-2		Mounds covered by wavy bedforms	Tidal ridges with large-scale dunes; actively maintained
	2-3		Mounds accompanying acoustically transparent wedges on the flanks and smaller bedforms on the crest	Tidal ridges, degraded by tidal currents and storms
	2-4		Large-scale mounds with distinct, continuous internal reflectors downlapping onto the substrate	Holocene mud bank
	2-5		Mounds with well-developed clinoforms	Relict subaqueous mud wedge
3	3-1		Regionally flat seafloor incised by shallow troughs	Shallow channel incision by strong tidal currents
	3-2		Sea floors of great topographic relief and deeply incised valleys	Extensive channel erosion or acoustic basement

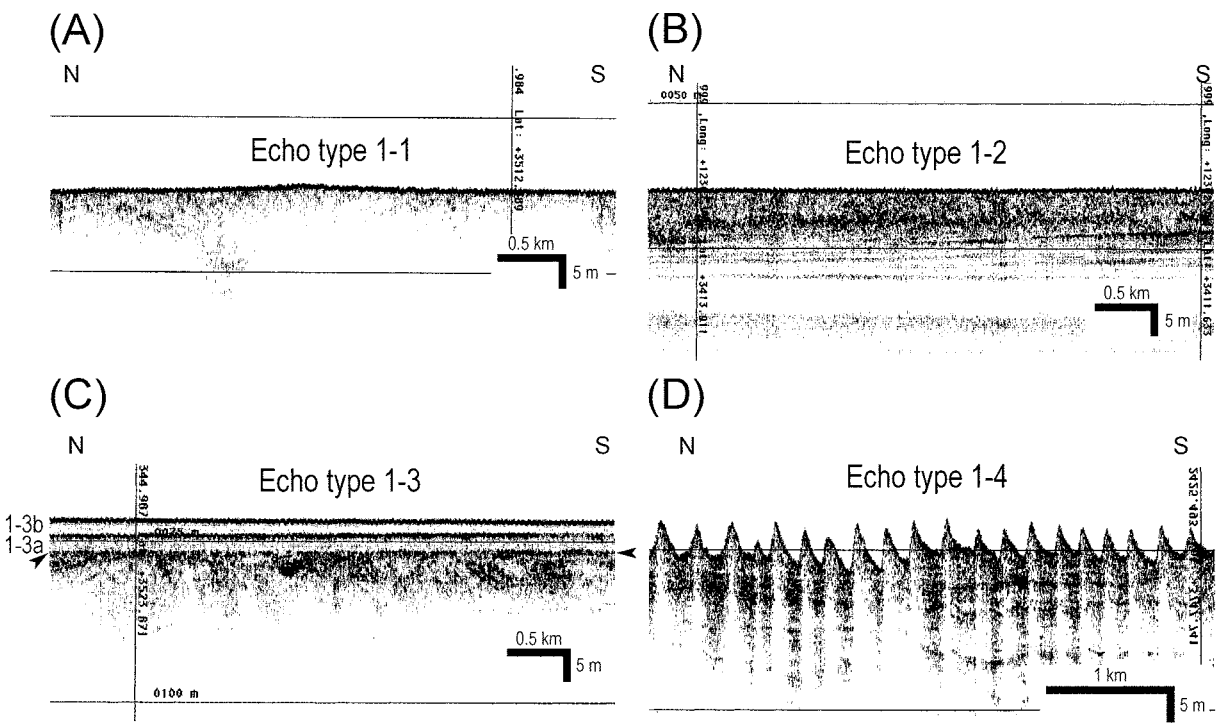

Fig. 38. Chirp (2–7 kHz) seismic profiles. For location of each profile, see Figures 2 and 39. (A) Flat seafloor with no internal reflectors (echo type 1-1). (B) Flat seafloor with moderately to well developed subbottom reflectors (echo type 1-2). (C) Laterally extensi ve acoustically transparent unit of either sheet form (echo type 1-3a) or wedge form (echo type 1-3b). (D) Regionally flat seafloor with regularly spaced, similar-sized, wavy bedforms (echo type 1-4).

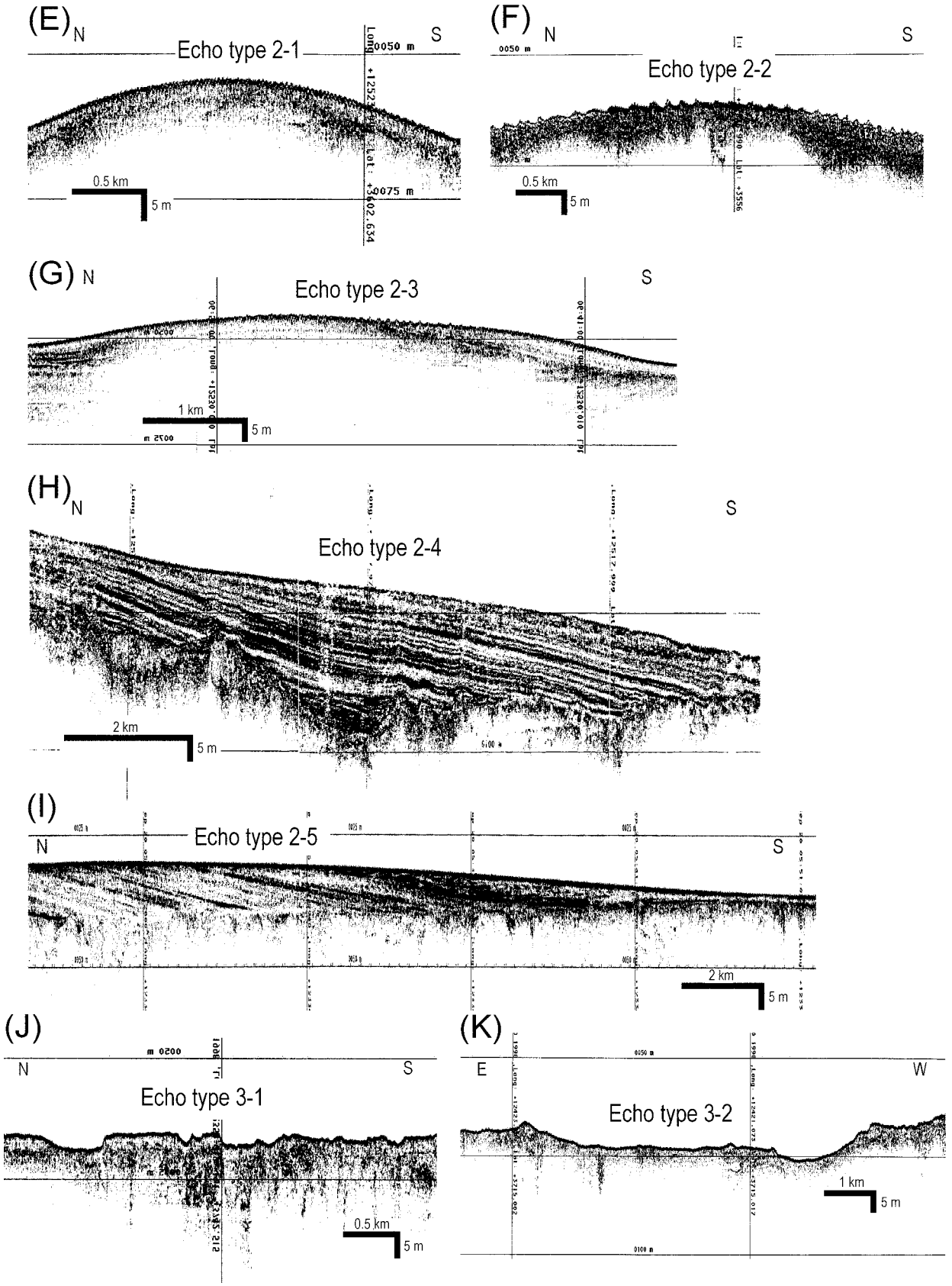

Fig. 38. (continued) (E) Mounds with no bedforms (echo type 2-1). (F) Mounds with wavy bedforms (echo type 2-2). (G) Mounds with acoustically transparent wedge on the flanks and smaller-scale bedforms on the crest (echo type 2-3). (H) Large-scale mounds with parallel-stratified internal reflectors downlapping onto the substrate (echo type 2-4). (I) Mound with clinoforms prograding onto the erosional surface (echo type 2-5). (J) Regionally flat seafloor with small-scale troughs (echo type 3-1). (K) Erosional seafloor of greater topographic relief (echo type 3-2).

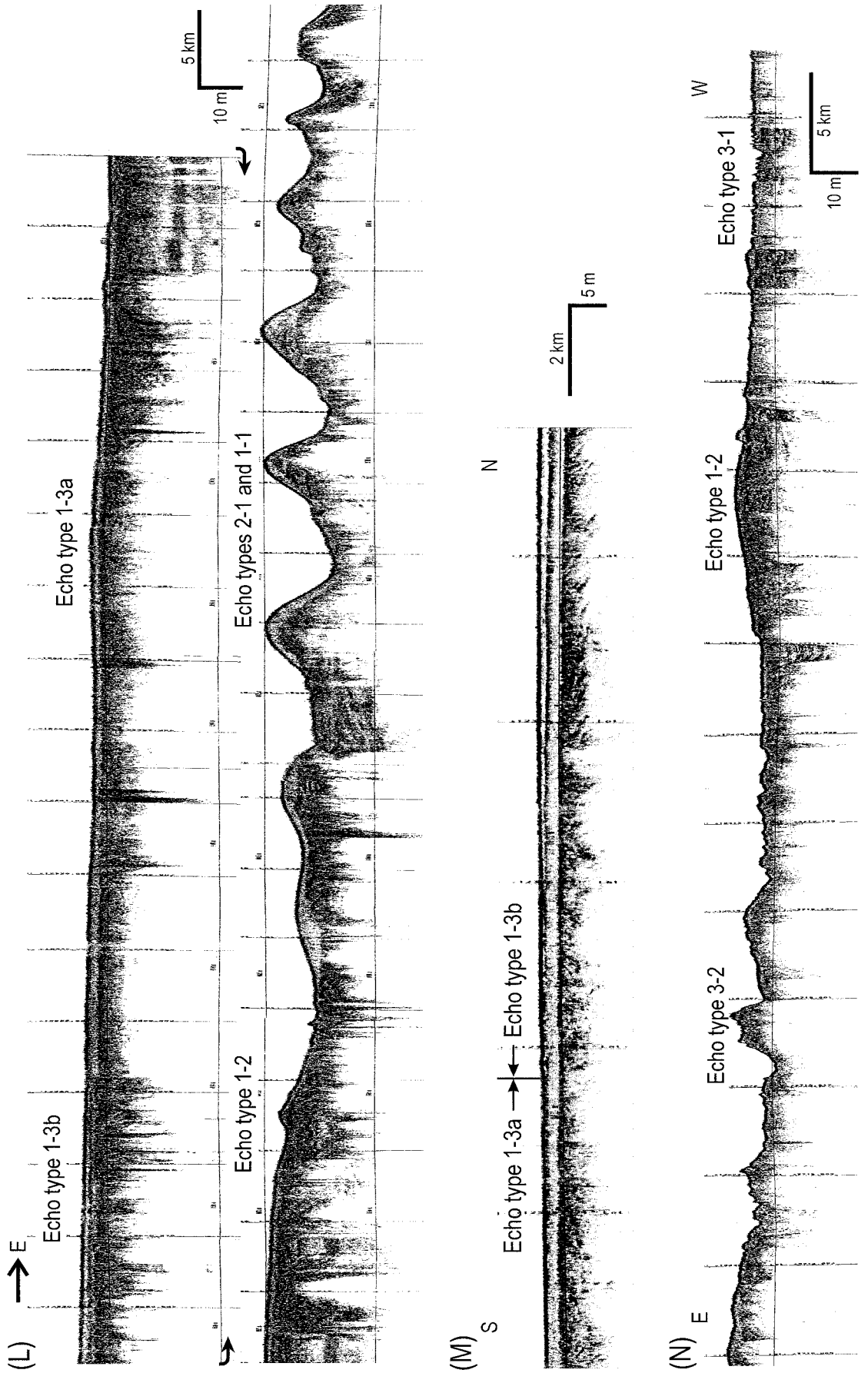

Fig. 38. (continued) (L) Lateral association of echo types across the central-eastern Yellow Sea. Note that the deepened eastern part of the sea is occupied by a series of tidal ridges. (M) Transgressive sediment sheet (echo type 1-3a) overlies extensively flat erosional surface. Note lateral wedging out of superficial prodeltaic mud unit (echo type 1-3b). (N) Eroded seafloor of northern Yellow Sea. Note the areal separation of the western shallow-incised seafloor (echo type 3-1) and the eastern high-relief erosional seafloor (echo type 3-2).

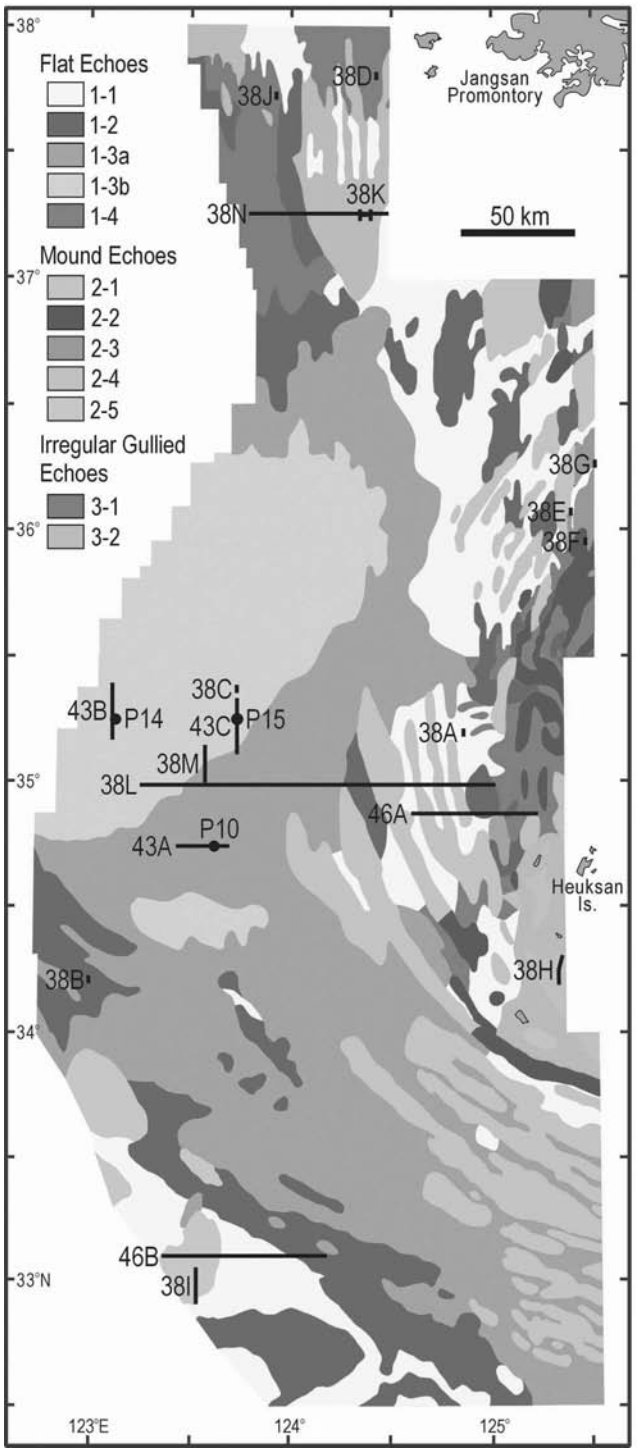

Fig. 39. Distribution of echo types in the eastern part of the Yellow Sea.

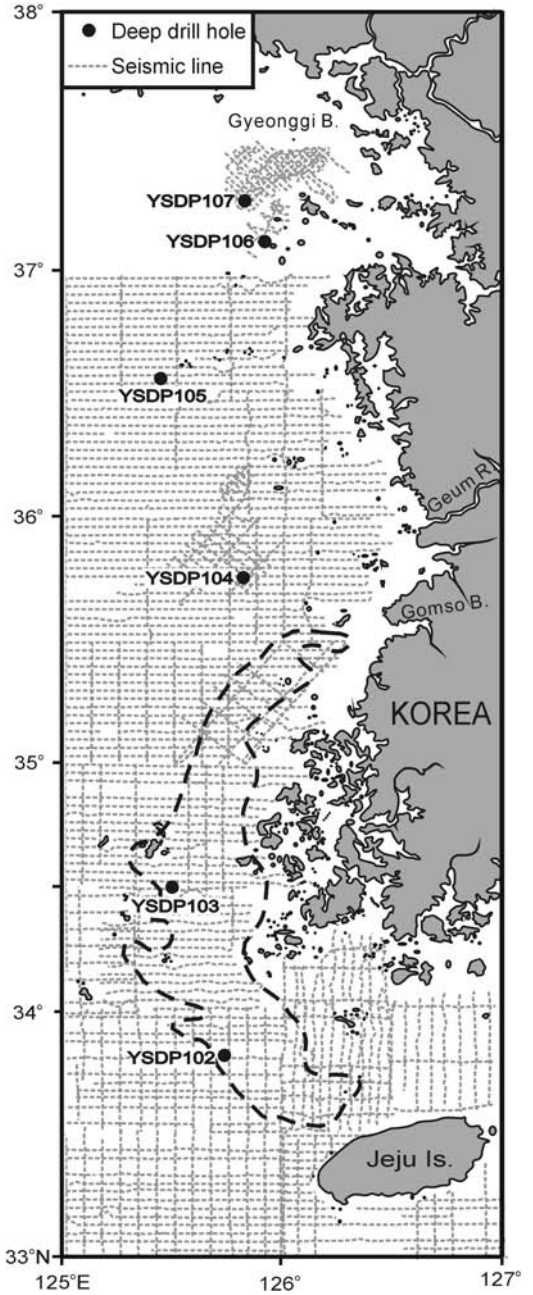

Fig. 40. Location of drill cores. YSDP 102 (33°49.5′N, 125°45.0′E) and 103 (34°29.2′N, 125°29.2′E) were retrieved from the Heuksan mud belt (outlined); YSDP 104 (35°45.7′N, 125°49.8′E) and 105 (36°34.0′N, 125°27.2′E) were from the crest and trough of the sediment ridge; YSDP 106 (37°06.8′N, 125°55.9′E) and 107 (37°16.1′N, 125°49.8′E) from sediment lobes off Gyeonggi Bay.

underlying echo character is acoustically stratified or ill-defined due to shallow penetration of the Chirp signal. Its external shape and stratal pattern suggest that echo type 2-5 is a subaqueous relict wedge that is related to the paleo-Huanghe delta. The prograding clinoform consists of laminated mud (Yoo et al., 2002).

Echo type 3-1 is assigned to the seafloor excavated by troughs of various size (Fig. 38J). The troughs are generally several meters deep and a few hundred meters wide. The small-scale troughs on the seafloor are interpreted as channels. Shallow incision depths, ubiquitous occurrence and the maintenance of flat seafloor topography suggest that the channels most probably formed during the later stage of

sea-level rise and highstand by tidal currents.

Echo type 3-2 collectively refers to the large-scale gullied seafloor and terrains of significant topographic relief (Fig. 38K). The subbottom echoes are relatively poorly developed or very prolonged. The larger valleys are more than 20 m deep and several kilometers wide with steps. The large-scale troughs or depressions with a valley suggest extensive erosion with wave ravinement. The prolonged subbottom echoes with high topographic relief appear to represent exposed basement.

7.2. Distribution of Echo Types

The central part of the Yellow Sea is occupied by acoustically transparent unit (Fig. 39). Echo type 1-3a (transgressive sediment sheet) covers offshore area, overlain by echo type 1-3b (multi-layered mud wedge) that progressively thins south(-east)ward (Fig. 38L, M). Echo type 1-3a gradually changes eastward to echo type 1-1, concurrent with the topographic change to uneven seafloor with markedly reduced sound penetration (Fig. 38L).

The eastern nearshore area (east of 125°) consists of elongated mounds (echo types 2-1, 2-2 and 2-3; tidal ridges) with echo types 1-1 and 1-2 in inter-mound areas (Fig. 39). The tidal ridges (north of 35°45′) are up to 20 m high, a few km wide and 10–50 km long, and are oriented NE-SW (Fig. 39). The region south of 35°45′ is characterized by the subaqueous dune field (echo type 1-4) and tidal ridges with superposed dunes (echo type 2-2). The ridges west of 125°

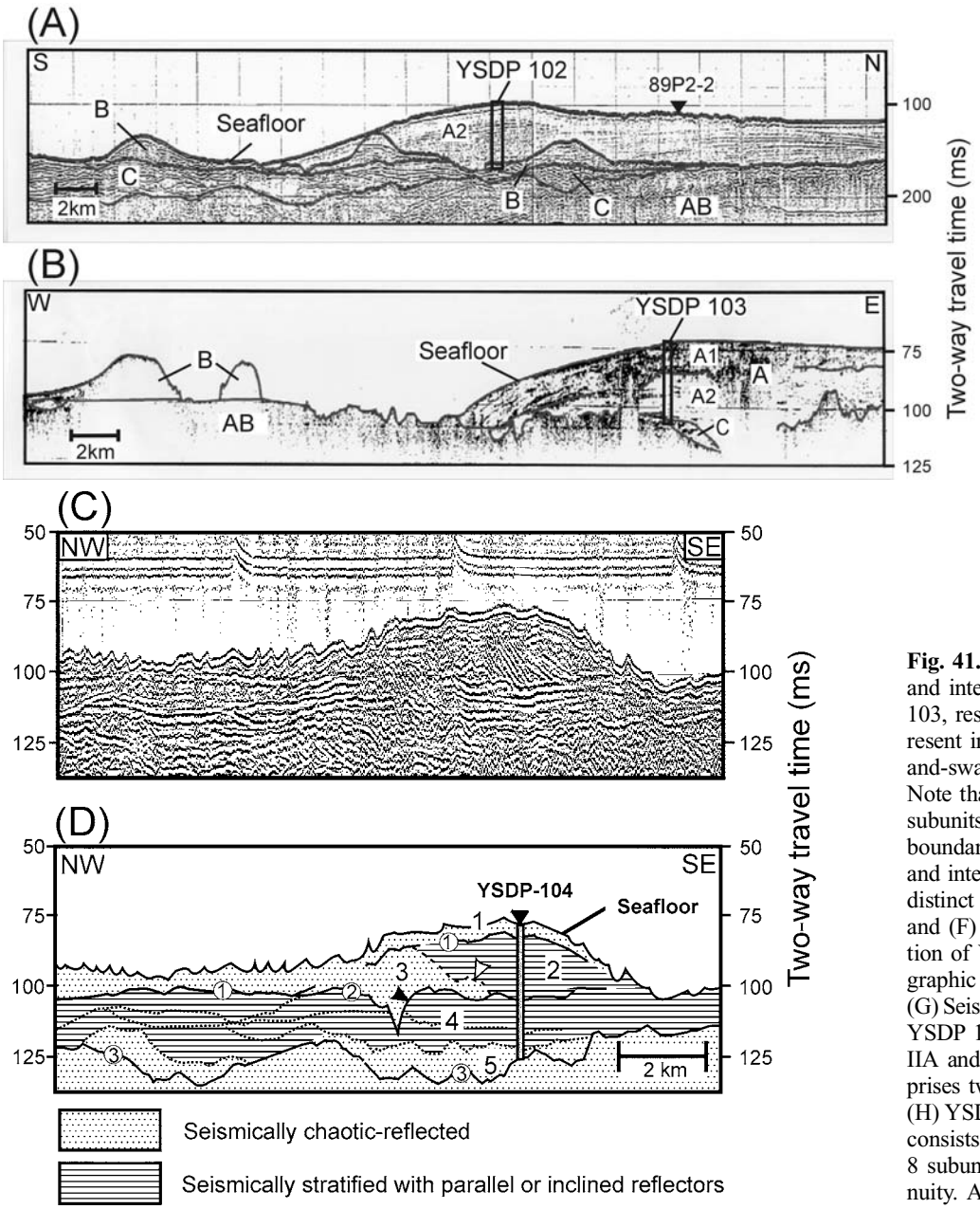

Fig. 41. (A) and (B) Seismic profiles and interpretation of YSDP 102 and 103, respectively. Units C and B represent incised channel fills and ridge-and-swale topography, respectively. Note that Unit A can be divided into subunits A1 and A2 by an erosional boundary. (C) and (D) Seismic profile and interpretation of YSDP 104. Five distinct seismic units are shown. (E) and (F) Airgun profile and interpretation of YSDP 105. Six seismo-stratigraphic units (SU 1-6) are recognized. (G) Seismic profile and interpretation of YSDP 106. Lobe II consists of SUs IIA and IIB. Note that SU IIA comprises two subunits IIA-1 and IIA-2. (H) YSDP 107 drilled on lobe I, which consists of unit IA. Unit IA consists of 8 subunits bounded by local discontinuity. After Jin (2001).

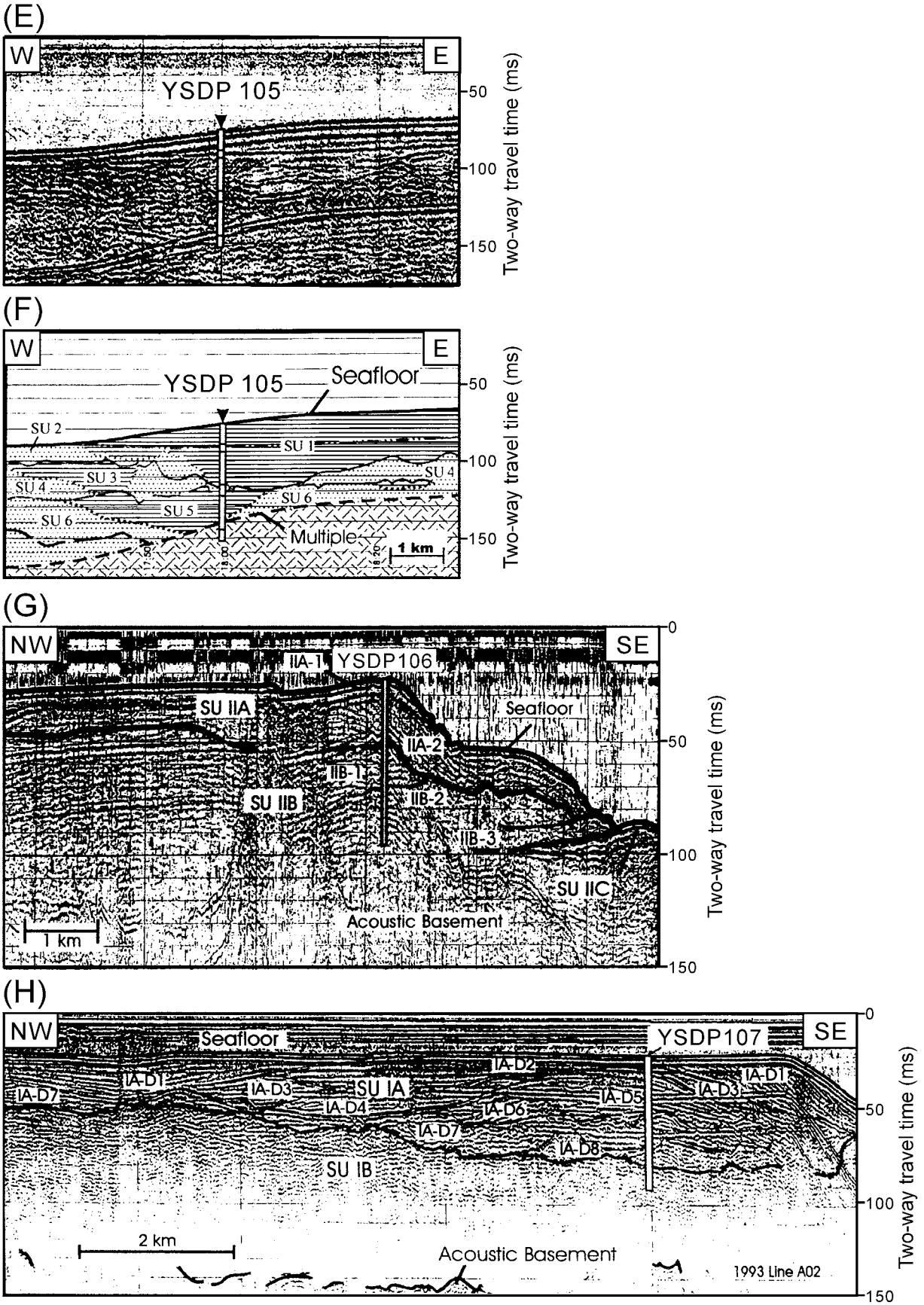

Fig. 41. (continued).

and south of 35°30′ are oriented NW-SE and further offshore. They are 10–30 km wide and 50–150 km long.

The southern nearshore area consists of eroded seafloor (echo type 3-2) and large-scale bank (echo type 2-4) (Fig. 39). Echo type 3-2 is dominant in the area between islands and submerged basement highs. The mapped area of echo type 2-4 corresponds to the western margin of the Heuksan mud belt. Echo type 2-4 covers the southward sloping seafloor with high relief (echo type 3-2) or occurs as small patches in a local depression.

The northern part (north of 37°) is characterized by eroded seafloor (echo types 3-1 and 3-2) with minor occurrence of echo type 1-1, 1-2 and 1-4 (Fig. 39). The western part of the central high area trending N-S (echo type 1-2) is dominated by ubiquitous small-scale shallow channels (echo type 3-1), maintaining a regionally flat topography, whereas the eastern part is dominated by deeper and wider valleys and terrains of significant topographic relief (echo type 3-2) (Figs. 38N and 39). A few elongated windows of echo type 1-1 remain as flat-floored topographic lows in the area of echo type 3-2. A large-scale subaqueous dune field (echo type 1-4) with peaked crests occurs in the northernmost nearshore area.

Off the Jiangsu coast, subaqueous mud wedges (echo type 2-5) are isolated on the flat seafloor at water depth of less than 50 m (Fig. 39). The subaqueous mud wedge generally progrades southeastward. In the northern part, it progrades northeastward. Echo type 1-2 is regionally exposed on the seafloor, overlain eastward by a transparent sheet (echo type 1-3a). Echo type 1-1 mostly occupies the area adjacent to the subaqueous mud wedge.

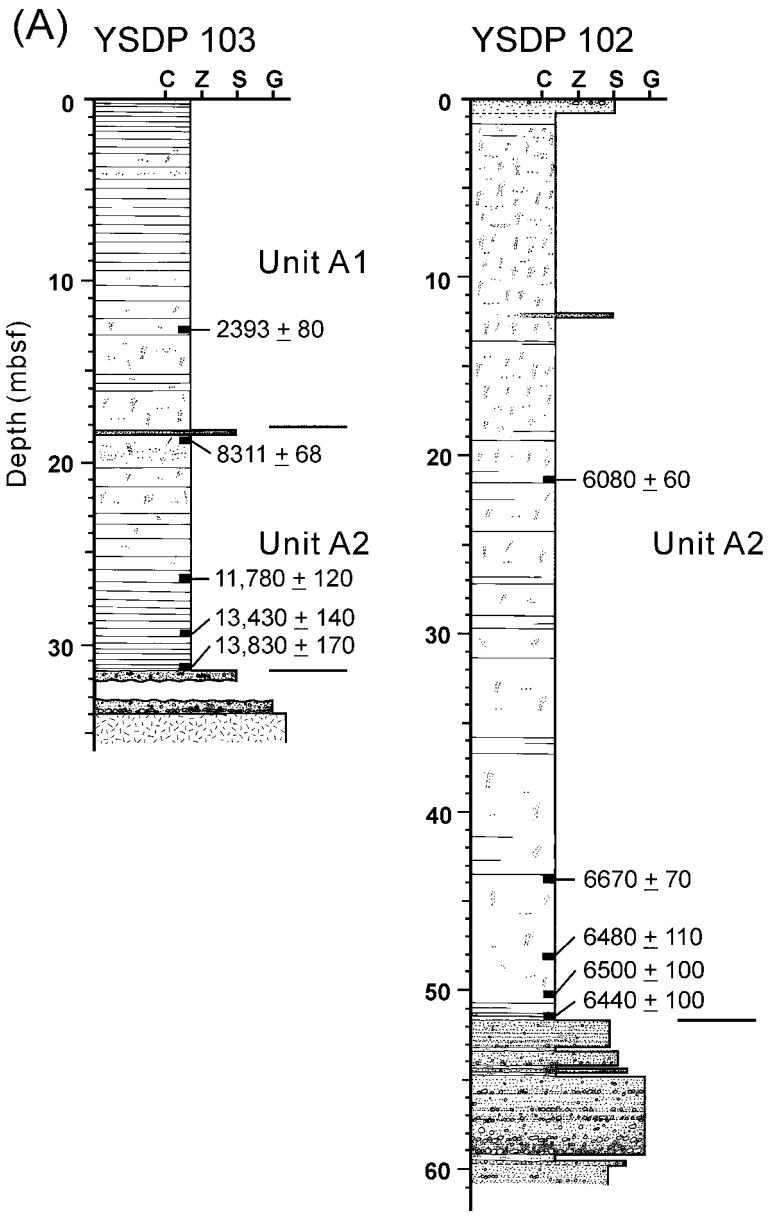

Fig. 42. (A) Radiocarbon dates of drill cores YSDP 102 and 103 with dominant lithofacies consisting of laminated muds in YSDP 103 and bioturbated mud in YSDP 102. C, clay; Z, silt; S, sand; G, gravel. (B) and (C) Descriptions of YSDP 104 and 105, respectively, including texture, sedimentary structures, radiocarbon ages and interpretation of depositional processes, environments and sequences. Seismically chaotic unit consists largely of clast-rich non-marine to paralic sediments, whereas seismically stratified unit mostly comprises tidal fine-grained sediments. LST, lowstand systems tract; TST, transgressive systems tract; HST, highstand systems tract; SB, sequence boundary; TSE, transgressive surface of erosion; TR, tidal ravinement; WR, wave ravinement. (D) and (E) Facies descriptions, radiocarbon ages and interpretation of depositional environments of YSDP 106 and 107, respectively. After Jin (2001).

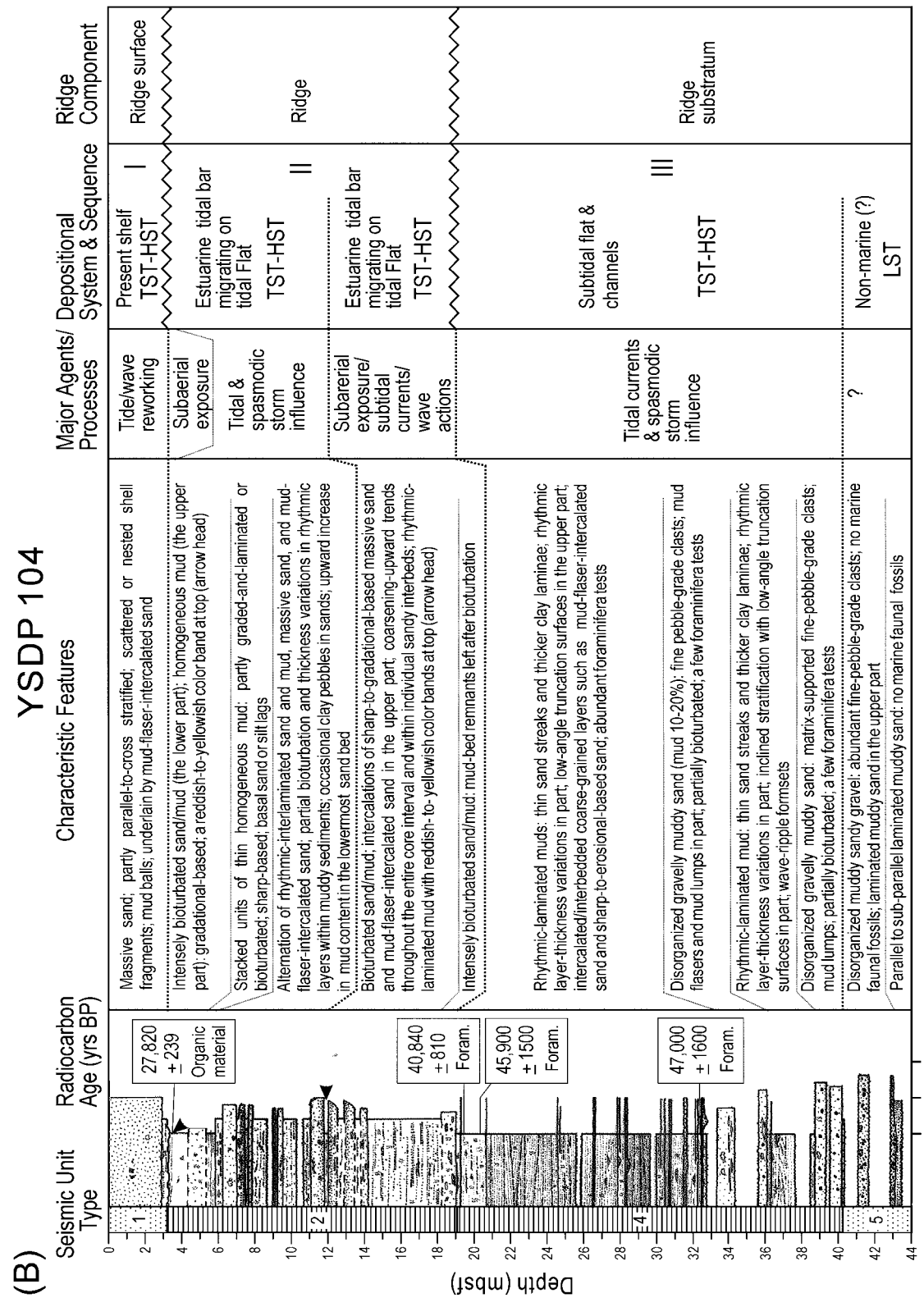

Fig. 42. (continued).

8. DRILL AND PISTON CORES

In order to unravel depositional processes of late Quaternary sediments in the eastern part of the Yellow Sea, six long drill cores (up to 60 m), Yellow Sea drill cores (YSDP) were retrieved by the Korea Institute of Geoscience and Mineral Resources (KIGAM) (Jin, 2001): the Heuksan mud belt (YSDP 102 and 103), the crest and trough of sediment ridges (YSDP 104 and 105) and the sediment lobes off the Gyeonggi Bay (YSDP 106 and 107) (Fig. 40).

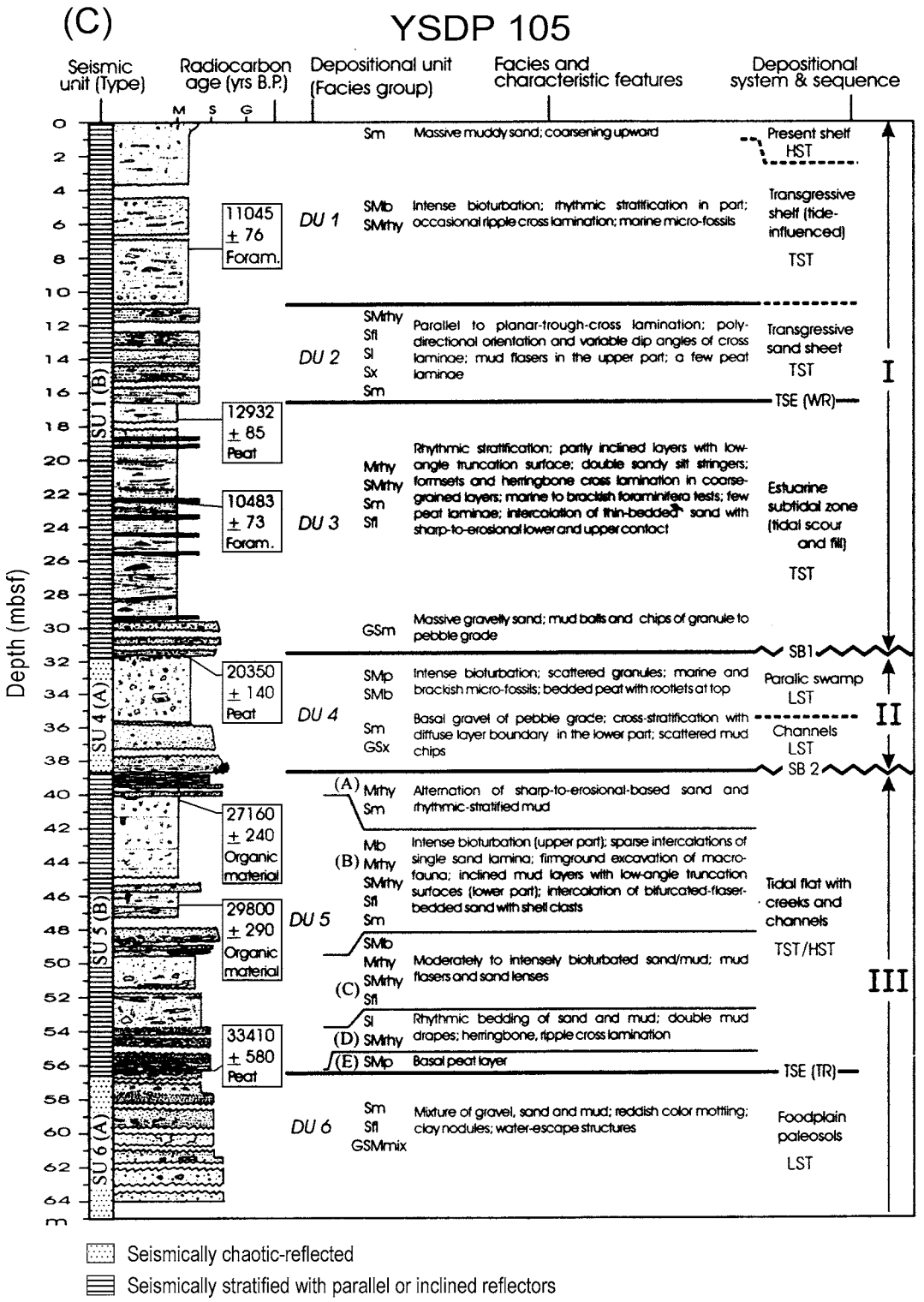

Fig. 42. (continued).

8.1. Drill Cores

YSDP 102 and 103 penetrated three discontinuity-bounded sedimentary units including the Holocene sequence of the Heuksan mud belt (Figs. 40 and 41A, B). The lowermost unit (unit C) consists largely of gravelly sand deposited in the topographic lows and incised valley during the last regression and an early phase of the following transgression (Jin and Chough, 1998). Unit B exhibits ridge-and-swale topography (Fig. 41B) and comprises gravelly sand and

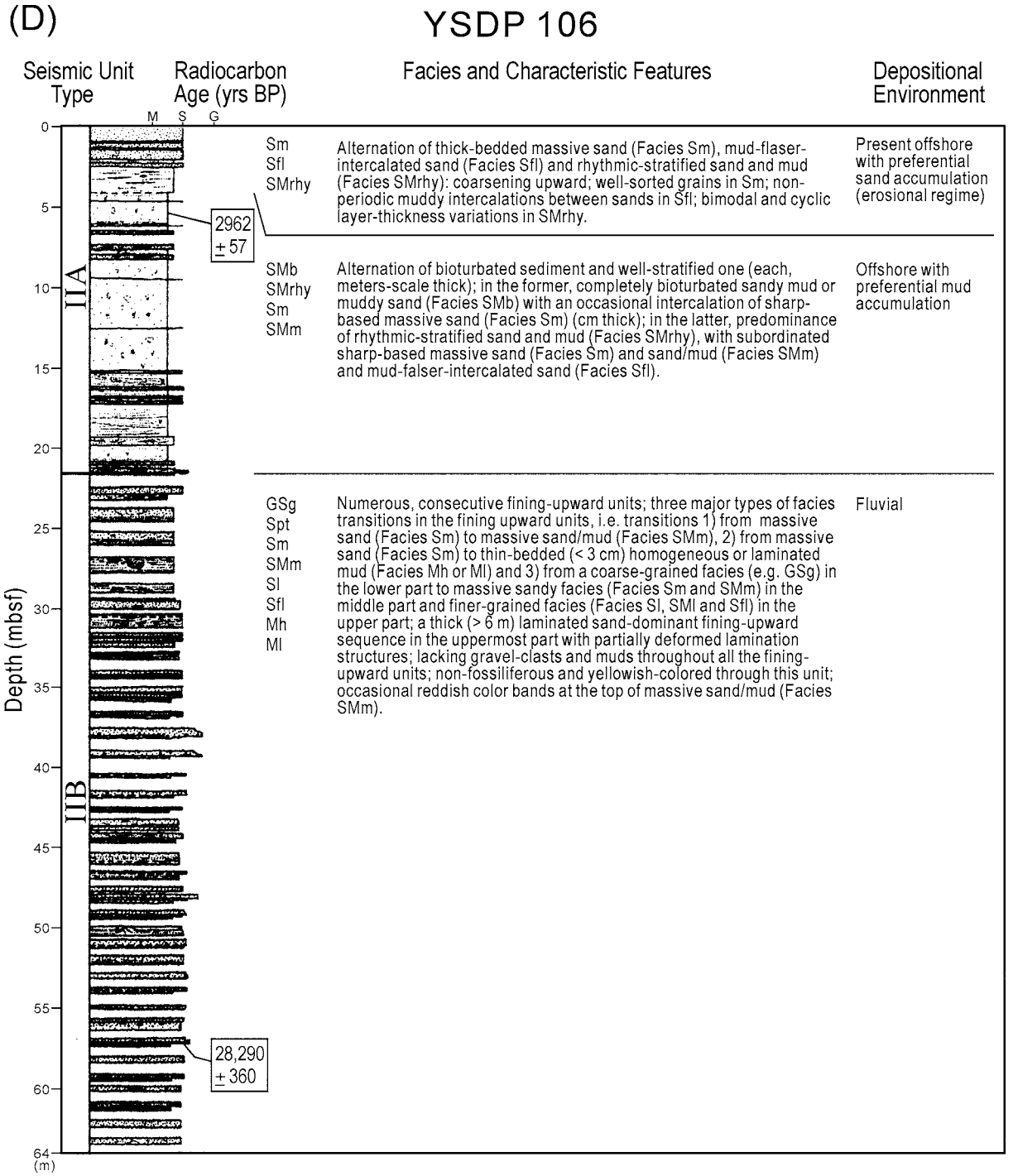

Fig. 42. (continued).

well-sorted massive sand, overlying unit C with a sharp erosional surface, that is, a transgressive surface of erosion (TSE) (Jin and Chough, 1998; Jin, 2001). Unit A consists largely of laminated mud in YSDP 103 and bioturbated mud in YSDP 102 (Fig. 42A), and unconformably overlies units B and C (Jin and Chough, 1998; Jin, 2001). The base of mud deposit (unit A) was dated at about 6 ka in YSDP 102 and 14 ka in YSDP 103, respectively (Fig. 42A). The progradational stratal patterns of unit A in seismic sections are suggestive of southward transport of fine-grained sediment, largely derived from the Geum River, although influenced by oscillatory tidal currents (Jin, 2001).

Drilled on the crest of a sediment ridge, YSDP 104 can be divided into 3 units: ridge substratum, ridge proper and ridge surface (Figs. 41C, D and 42B). The substratum consists of disorganized sandy gravel and laminated muddy

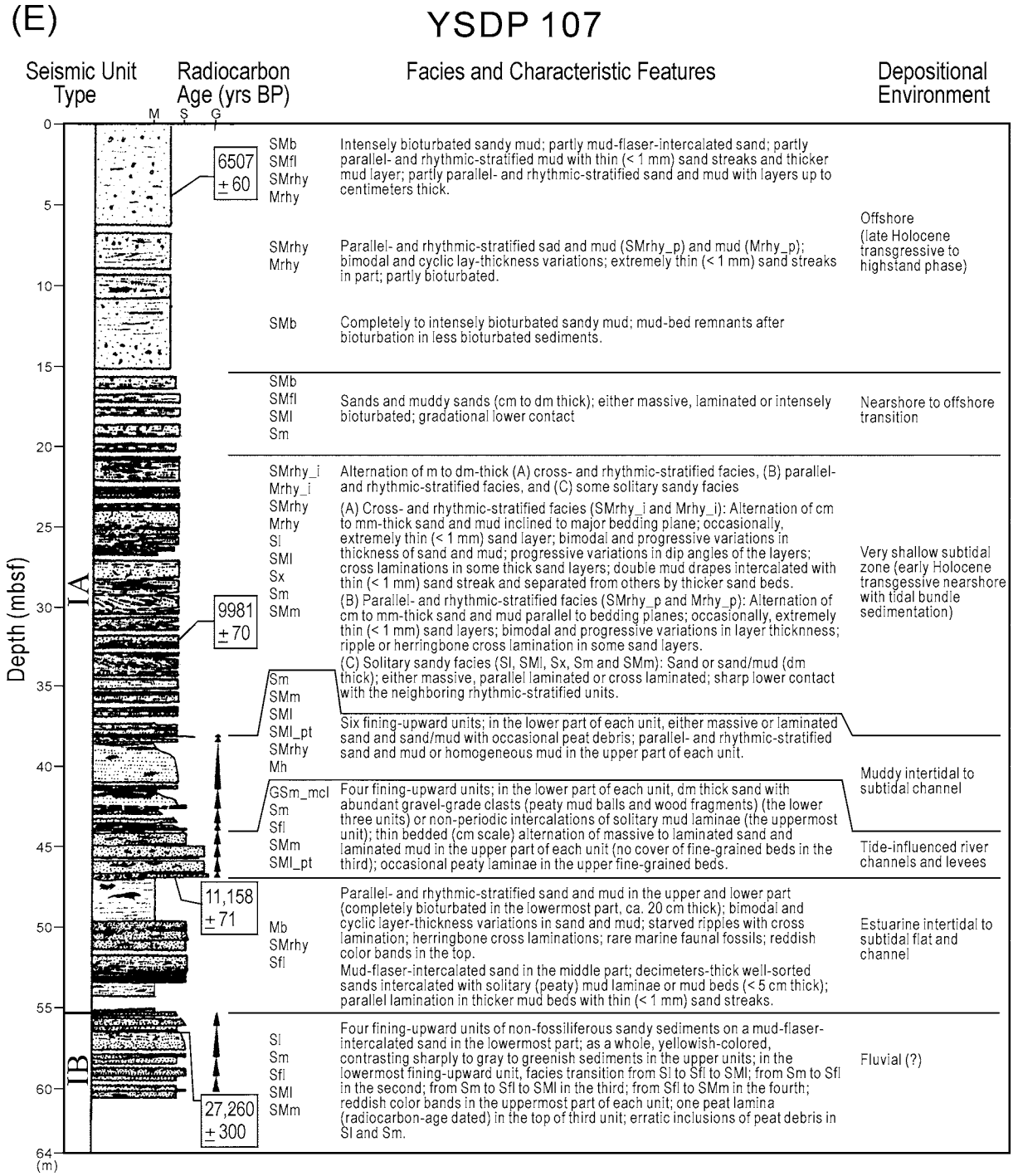

Fig. 42. (continued).

sand, and interlayered rhythmic-laminated mud, indicative of tide-dominated environments (Jin, 2001; Jin and Chough, 2002). The unit is generally older than 4 0ka (Jin and Chough, 2002). The overlying unit (ridge proper) consists of sandy mud with rhythmic interlamination of sand and silt, and subordinate sand and muddy sand with mud chips and mud flasers, which are interpreted as deposits of estuarine environments associated with muddy tidal flats and sandier tidal bars (Jin and Chough, 2002). The ridge surface layer (about 3 m thick) consists of massive sands with scattered shell fragments and immediately overlies a stiff, yellowish mud layer that is also relatively old (about 28 ka at 3.2 m depth). It suggests that the ridge sediments (mainly sands) have been reworked and subsequently covered with sands (cf. Jung et al., 1998).

YSDP 105 (ca. 64 m long) was retrieved from the mid-

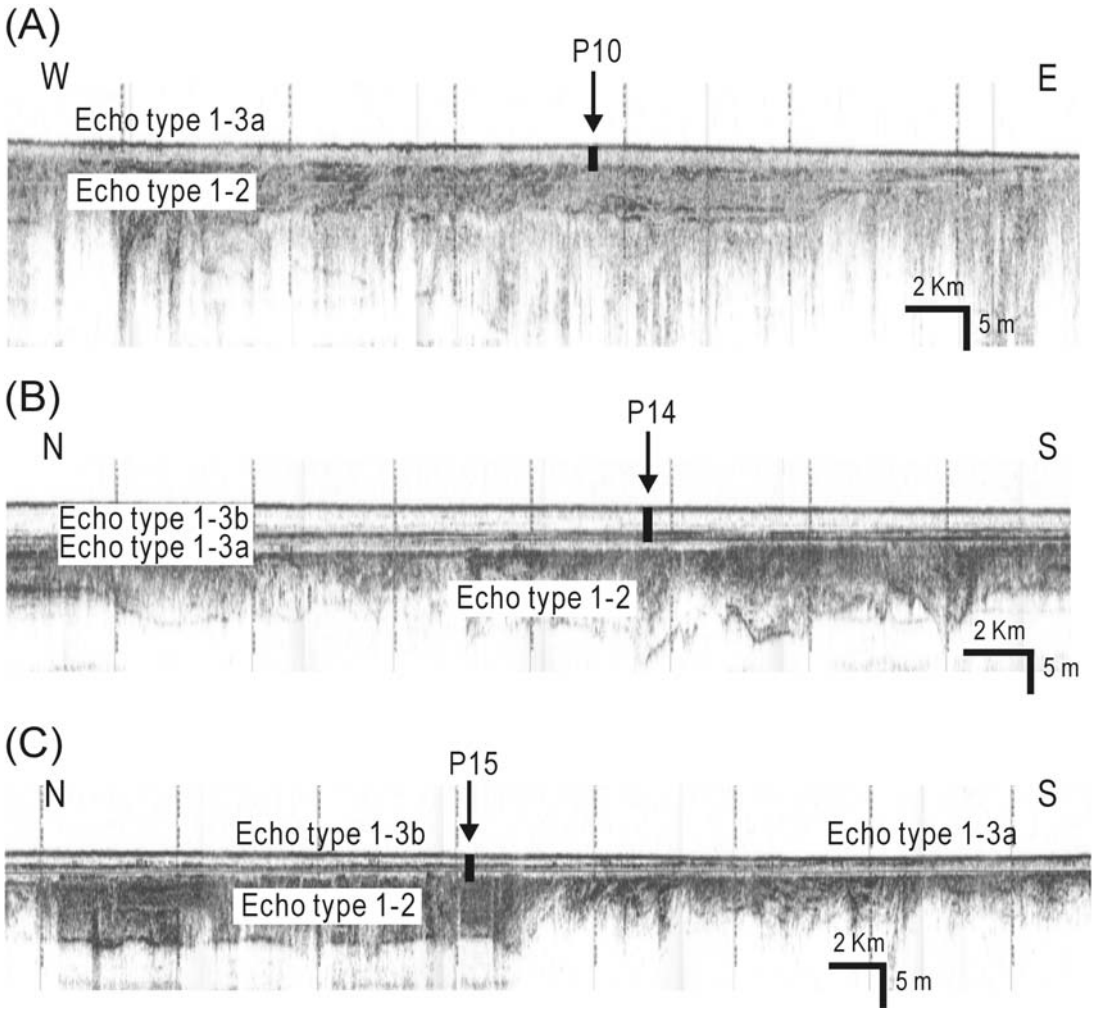

Fig. 43. Acoustic units penetrated by piston cores. For location of each core, see Figures 2 and 39. (A) Core P10 was retrieved from the offshore transgressive sediment sheet (echo type 1-3a) which overlies extensively flat erosional surface. (B) and (C) Two transparent units are separated by a distinct subbottom reflector and cored by P14 and P15. Note that echo type 1-3b laterally wedges. After Shinn et al. (2004).

eastern part of the Yellow Sea (Fig. 40). Based on seismic reflection profiles and lihofacies characters, six depositional units have been identified (Figs. 41F and 42C). The lowermost unit (unit 6) represents floodplain successions mostly comprising mixture of sediments with paleosol fabrics, indicative of subaerial exposure (Jin, 2001; Jin et al., 2002). A peat layer at the top of the unit (57 m below seafloor) represents a transgressive surface of erosion (TSE) and was dated at 33 ka (Fig. 42C) (Jin, 2001). The overlying unit (unit 5) consists of fining-upward tidal flat successions, which is separated by a sequence boundary (SB2) from the overlying unit 4 (Fig. 42C). The sequence boundary is characterized by channel geometry in seismic profiles (Fig. 41F). Unit 4 is interpreted as deposits of tidal inlet/channel and paralic swamp, overlain by tidal ravinement lag deposits and muddy tidal flat successions (unit 3) (Jin et al., 2002). Peat at the base of unit 3 was dated at 20 ka, suggesting that the sequence boundary formed during the period of the last glacial maximum. The ensuing transgression and tidal reworking processes caused deposition of unit 3. The overlying unit 2 consists largely of laminated and massive, well-sorted sand, interpreted as transgressive sand sheet resulting from wave- and storm-generated erosion at retreating shoreface during the Holocene transgression (Jin et al., 2002). The boundary between units 3 and 2 represents a wave ravinement (WR) surface below which peat was dated at about 13 ka (Fig. 42C). The uppermost unit (unit 1) comprises intensely bioturbated silty mud of about 11 ka in age. This unit represents shelf deposits of transgressive phase.

YSDP 106 was retrieved from the seafloor of sediment lobe offshore the Gyeonggi Bay (Figs. 40 and 41G) (Jin, 2001). The lower two-thirds (22–63 m) of the core consists of unfossiliferous reddish to yellowish sands, including laminated and flaser-bedded sands, gravelly and peaty sands, and crudely laminated and homogeneous muds (Fig.

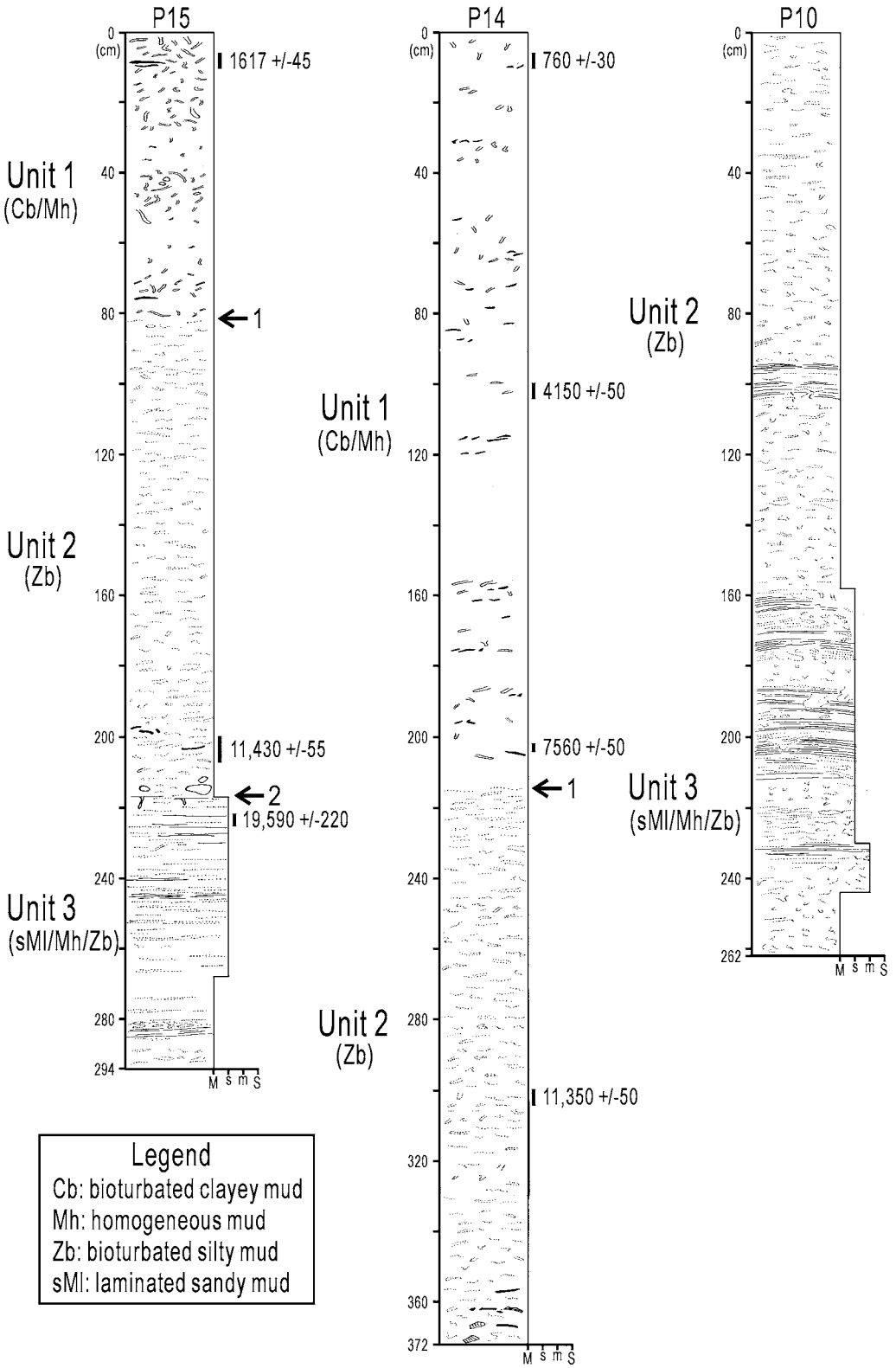

Fig. 44. Simplified lithofacies of piston cores and radiocarbon dates. Arrow 1 indicates the boundary between units 1 and 2. Arrow 2 indicates the basal surface of unit 2. Note radiocarbon age in yrs BP. M, mud; s, sandy mud; m, muddy sand; S, sand. After Shinn et al. (2004).

42D). The reddish sand layers are indicative of subaerial exposure and precipitation of ferruginous materials (Jin, 2001). The fining-upward sand layers probably formed by migration of fluvial channels. A peat layer at about 57 m

depth is dated at about 28 ka, formed prior to the last glacial maximum. The overlying unit (4–22 m) comprises bioturbated and stratified sediment layers with sharp-based massive sand and flaser beds with abundant fossils (Fig. 42D). Foraminiferal tests from the bioturbated mud in the upper part of the unit are dated at about 3 ka (Fig. 42D). The rhythmic beds are indicative of tide-dominated environments during the Holocene.

YSDP 107 was also located on the flat top of sediment lobe where a number of seismic units are identified (Fig. 41H). The cored sediment consists of massive sand/mud, mud-flasers, laminated sand/mud, homogeneous mud, cross-laminated sand/mud, and bioturbated sandy mud (Fig. 42E). The lowermost unit (55–60 m) comprises unfossiliferous yellowish-reddish sand layers with minor amounts of muddy sediments, which is suggestive of subaerial exposure. The overlying unit (47–55 m) consists of bioturbated mud, stratified sand/mud and mud-flaser-intercalated sand that rarely include marine fauna. This unit contains evidence for tidal regime in transgressive estuarine environments (Jin, 2001). The overlying units fine upward, representing a gradual shift in depositional environments from tide-influenced river (44–47 m) to muddy tidal channel (38–44 m). The overlying unit (21–38 m) is characterized by tidal bundles of rhythmic sand and mud with parallel and cross-stratified layers, suggestive of subtidal environments (Jin, 2001). The overlying unit (16–21 m) comprises marine sand and laminated/bioturbated muddy sand layers, which is a transitional facies between the subtidal facies below to the offshore facies above. The uppermost unit (0–16 m) consists largely of bioturbated sandy mud with minor amounts of mud-flaser-intercalated sand and rhythmic sand/mud that contain marine fauna. This unit is suggestive of low-energy conditions influenced by tidal currents. Foraminiferal tests at 4.0 m below the seafloor are dated at about 6.5 ka, which suggests that the unit formed during the Holocene transgressive to highstand phase.

8.2. Piston Cores

Piston cores were obtained from various part of the Yellow Sea (Figs. 2 and 39). Echo types 1-3a and 1-3b are represented by P10, P14 and P15 (Fig. 43). Three lithological units were identified based on grain size and sedimentary structures: units 1, 2 and 3 in descending order (Shinn et al., 2004).

Unit 1 comprises bioturbated clayey mud and indistinctly-interlayered homogeneous mud. This unit is 82 cm thick in core P15 and 215 cm thick in core P14. The clayey mud contains large subvertical or subhorizontal burrows with rims. The intensity of bioturbation is variable throughout the cores. The base of unit 1 is characterized by a gradual change in lithology from silty to clayey mud (Fig. 44).

Unit 2 consists largely of mottled silty mud with lenticular silt lumps, irregular mud drapes and ill-defined burrows (Fig. 44). Rare laminae are present in the middle part of core P10. The boundary between units 2 and 3 shows a sharp transition from laminated sandy mud to bioturbated mud (Fig. 44). In core P15, the lowermost part of unit 2 contains pebble-grade clasts that are composed of semi-consolidated, yellowish muddy sand (Fig. 44).

Unit 3 consists of laminated sandy mud and interlayered bioturbated and homogeneous mud (Fig. 44). Laminated sandy mud is characterized by couplets of silt and clay laminae. The laminated sandy mud layers are variable in thickness from 5 to 80 mm. Low-angle cross-laminated mud is underlain by bioturbated mud in the lower part of core P15.

In the central part of the Yellow Sea, two prominent stratigraphic units are recognized: a transparent sheet (echo type 1-3a) and a transparent wedge (echo type 1-3b) (Fig. 43). Echo type 1-3b corresponds to sedimentary unit 1 and echo type 1-3a to unit 2. The upper part of sedimentary unit 3 is dated at about 19.5 ka. Channel fills and well-developed stratification in echo type 1-2 (unit 3) are suggestive of lowstand deposits of the last glacial maximum (20–18 ka). The erosional surface at the base of echo type 1-3a (unit 2), dated at about 11.5 ka, represents post-glacial transgressive surface of erosion, which is identified as a hiatus between sedimentary units 2 and 3. It is overlain by Huanghe River-derived deltaic mud (echo type 1-3b; unit 1). The deltaic mud is identified as part of the Shandong mud wedge (e.g., Liu et al., 2002).

9. POST-GLACIAL DEPOSITIONAL PROCESSES

In the eastern Yellow Sea, Shinn et al. (2004) identified three high-resolution stratigraphic units: lowstand deltaic/estuarine, transgressive sheet/ridge and highstand mud deposits. Figure 45 outlines the development of the echo types in terms of the rate of sea-level rise, changes in sediment supply and hydrodynamic conditions.

The Yellow Sea was entirely exposed during the last glacial maximum (20–18 ka) when the paleo-shoreline was located at about 120 m below the present sea level (Saito, 1998; Chough et al., 2000). The sea-level lowering caused incision of the pre-Holocene deposits along the central part of the Yellow Sea where well-layered acoustic units and incised-channel fills (echo type 1-2; unit 3) are dominant (Fig. 45A). The incised channels were filled with deltaic/estuarine deposits, separated by an erosional surface from the overlying transgressive deposits. Semi-consolidated, yellowish pebble lags immediately below the transgressive deposits are suggestive of reworking of the underlying pre-Holocene deposits during the early transgressive phase.

The transgressive surface of erosion is marked on seismic records by a flat-lying surface, separating the transparent sheet above (echo type 1-3a) from the lowermost acoustic unit below (echo type 1-2) (Fig. 45B). The transparent unit represents a transgressive sheet of bioturbated silty muds (unit 2). Radiocarbon dating of these sediments indicates

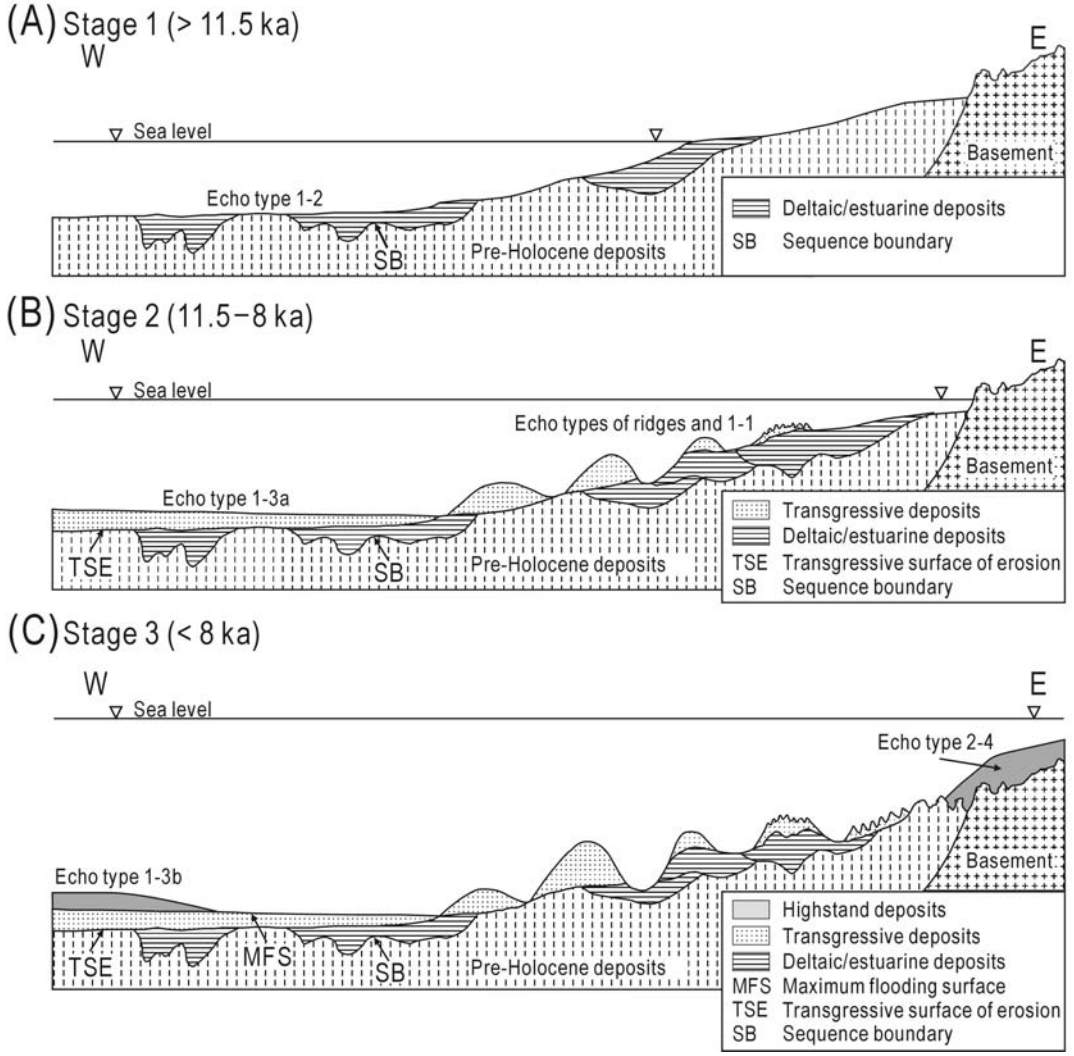

Fig. 45. Schematic diagrams showing echo type development in the central-eastern Yellow Sea. (A) During the last glacial maximum, the eastern Yellow Sea was entirely exposed and pre-Holocene deposits were incised. The basal surface of the incised channel fill represents sequence boundary. (B) During the transgressive period, rapid retreat of shoreface and tidal processes formed tidal ridges and transgressive lag deposits in the inner-shelf area. A transgressive sediment sheet extensively covers the transgressive surface of erosion in the central Yellow Sea. (C) As the rate of sea-level rise decreased, the Huanghe-derived mud unit and the Heuksan mud belt formed in the central Yellow Sea and the southwestern tip of the Korean Peninsula, respectively. After Shinn et al. (2004).

that marine transgression most likely commenced prior to about 11.5 ka in the central Yellow Sea.

In the eastern Yellow Sea, extensive coastal erosion and strong tidal currents caused reworking of pre-Holocene sediments and formed transgressive lags and ridges (echo types 1-1, 2-1, 2-2 and 2-3) in the inner-shelf area (Figs. 39 and 46A). The continuous rise in sea level might have left behind inactive ridges offshore (echo type 2-1), whereas ridges in the nearshore area (echo type 2-2) have undergone active reworking, as evinced by convergence of large-scale dunes on both sides of the ridge by reversing tidal currents. The elongated ridges offshore are oriented subparallel to the direction of regional tidal currents (Figs. 4 and 39). These ridges show seaward-inclined internal reflectors, deposited on relatively flat erosional surface (transgressive surface of erosion). Most ridges in the nearshore area, however, appear to have originated from erosion of substratum, showing undulatory erosional surface (arrows in Fig. 46A). The internal ridge sediments below the erosional surface were dated at 47–28 ka (Jin and Chough, 2002), suggesting that intense tidal reworking processes provided substantial sands suitable for the growth of tidal ridges by erosion of the older pre-Holocene deposits.

Off the Jiangsu coast, extensive lag deposits (echo type 1-1) and isolated sediment bodies (echo type 2-5) were deposited on a flat-lying surface at water depths of 40–50 m (Fig. 46B). The transgressive lag deposits are typical of deposits on ravinement surface formed by the processes of landward movement of shoreface erosion, concurrent with wave and tide activity (e.g., Nummedal and Swift, 1987; Thorne and

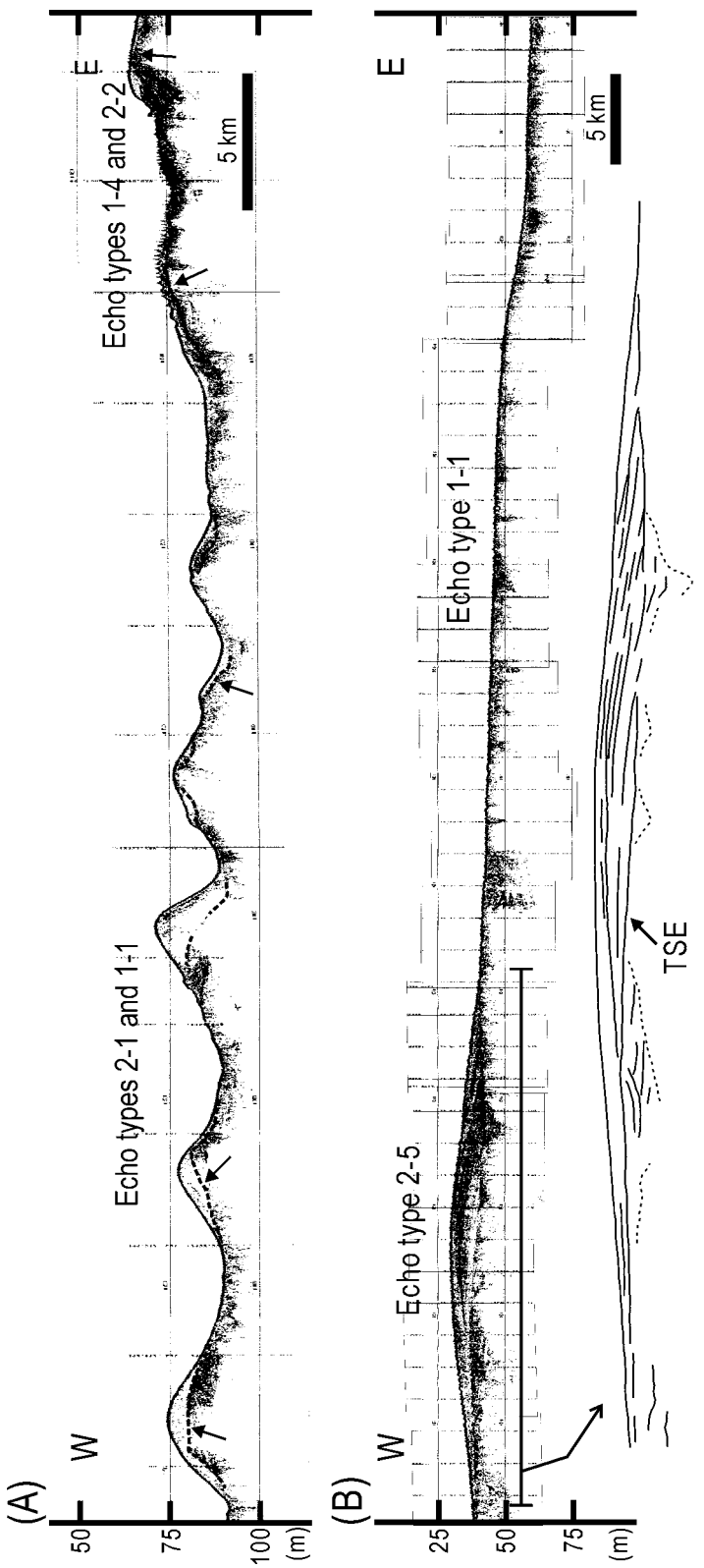

Fig. 46. Typical subbottom profiles showing spatial association of echo types. For location of each profile, see Figures 2 and 39. (A) Subaqueous dunes cover the eastern nearshore area and tidal ridges predominate seaward. Note undulatory erosional surface within the internal ridge sediments. (B) A sedimentary body with seaward prograding clinoforms is underlain by a transgressive surface of erosion (TSE) at water depth between 40 and 50 m. After Shinn et al. (2004).

Swift, 1991). The ravinement surface might have formed at water depths from −60 to −42 m, when a rapid rise in sea level occurred at about 11–10 ka near the Shandong Peninsula (Liu et al., 2002). The isolated sediment body with clinoform geometry is likely interpreted as a relict subaqueous mud wedge, which prograded seaward when the paleo-Huanghe River entered the western part of the Yellow Sea during the period between 9.5 and 7.5 ka (Milliman et al., 1987, 1989). It is conjectured that this mud wedge on the ravinement surface indicates short-period stillstand or fall in sea-level combined with an increase in influx of terrestrial sediments.

The northern part of the Yellow Sea is regionally occupied by eroded seafloor with high topographic relief (Fig. 38N). The transgressive ravinement and tidal processes would be enhanced due to the narrow seaway between the Shandong Peninsula and the Jangsan promontory, which formed eroded seafloor on which very thin Holocene sediments accumulated.

As the rate of sea-level rise decreased, large amounts of mud derived from the Huanghe River were transported to the central Yellow Sea (Fig. 45C). The high proportion of smectite and water content and the seaward thinning geometry of the mud in the central Yellow Sea suggest that echo type 1-3b (unit 1) represents deposition of suspended muds derived from the Huanghe River along the Shandong Peninsula (Milliman et al., 1985; Lee and Chough, 1989; Alexander et al., 1991). A radiocarbon dating in the lower part of the mud wedge indicates that the mud was deposited after about 8 ka. On the other hand, muds of the southward-prograding clinoforms (echo type 2-4) along the southwestern tip of the Korean Peninsula, part of the Heuksan mud belt, were transported by southward-flowing coastal currents during winter (e.g., Jin and Chough, 1998; Lee and Chu, 2001). The elongated morphology of the mud belt resulted from confined sediment dispersal controlled by the physical barriers of tidal and thermohaline fronts (Lee and Chu, 2001). This mud bank locally overlies large-scale dunes (echo type 1-4), which demonstrates that deposition of the mud occurred after the formation of large-scale transgressive dunes, attesting to the facies partitioning controlled by the sea-level rise and sediment dispersal system (Jin and Chough, 1998; Chough et al., 2002).

10. SUMMARY

A synthesis of high-resolution seismic data, surface sediment distribution, piston and drill cores and hydrodynamic measurements of sediment transport in the eastern part of the Yellow Sea reveals that the post-glacial sedimentation was controlled by the rate of sea-level rise, changes in sediment supply and hydrodynamic conditions. During the early transgressive phase (prior to about 11.5 ka), the pre-Holocene deposits experienced intensive reworking. Incised channels were filled with deltaic/estuarine deposits. Subsequent sea-level rise (11.5–8.0 ka) led to deposition of an acoustically transparent sheet of silty muds (echo type 1-3a) on the transgressive surface of erosion in the central-eastern part. Rapid retreat of shoreface and tidal processes formed tidal ridges (echo types 2-1, 2-2 and 2-3) and transgressive lag deposits (echo types 1-1 and 1-2) in the inner-shelf area. The seafloor in the northern Yellow Sea was sculptured by strong tidal currents, resulting in channels and valley-like depressions (echo types 3-1 and 3-2). As the inner-shelf area off the Jiangsu coast was flooded, a seaward prograding wedge (echo type 2-5) formed in the distal part of the paleo-Huanghe delta.

As the rate of sea-level rise decreased (since 8.0 ka), Huanghe River-derived mud (echo type 1-3b) accumulated in the central part. An elongated mud bank formed along the southwestern coast of the Korean Peninsula. Transgressive ridges and large-scale dunes were increasingly affected by tidal currents and waves in the eastern nearshore area (echo types 1-4, 2-2 and 2-3). Off the southwestern Korean Peninsula, fine-grained sediment formed a bank-like feature, the Heuksan mud belt (echo type 2-4), showing southward progradation. The hydrodynamic measurements suggest that the mud belt is intimately coupled with suspended sediments derived largely from the Geum River.

Tidal flats on the west coast of Korea act as a principal repository for littoral sediments carried by macrotidal currents. Due to low sediment input from the hinterland, most tidal flats have formed a retrogradational, coarsening-upward pattern during the Holocene sea-level rise. Sedimentation in the macrotidal flats is controlled mainly by the combined effect of waves and tides with distinctive seasonal cycles in sedimentary facies owing to the monsoonal climate: mud-flat-dominated facies form mainly by tidal processes in summer and sand-flat-dominated facies mainly by waves in winter. Sedimentary facies analysis for the preserved sequence indicates that winter storms play a major role in sedimentation in intertidal flats. Quantitative measurements of sediment transport on tidal flats indicate that wind-generated waves during winter can intensively interrupt the tidal-flat sedimentation, otherwise governed by dominant macrotidal currents. Ebb currents from the tidal flat, often more turbid than flood currents when waves are high, appear to be a major source for the nearshore suspended plume developed during winter.

ACKNOWLEDGMENTS: For this study Chough was supported by the Korea Science and Engineering Foundation (No. 2003-16) and BK21 project, Ministry of Education and Human Resources, and Chun was supported by the Korea Science and Engineering Foundation (R01-2001-000-00081-0). We thank Drs. W.R. Fitches and Y.K. Sohn for critical review of the manuscript.

REFERECES

Alexander, C.R., DeMaster, D.J. and Nittrouer, C.A., 1991, Sediment accumulation in a modern epicontinental-shelf setting: the Yel-

low Sea. Marine Geology, 98, 51−72.
Allen, J., 1980, Sand waves: a model of origin and internal structure. Sedimentary Geology, 26, 281−328.
Amos, C.L., 1978, The post-glacial of the Minas Basin, Nova Scotia: a sedimentological interpretation. Journal of Sedimentary Petrology, 48, 965−982.
Amos, C.L. and Long, B.F.N., 1980, The sedimentary character of the Minas Basin, Bay of Fundy. In: McCann, S.B. (ed.), The Coastline of Canada. Geological Survey of Canada, Paper 80-10, p.153−180.
Amos, C.L. and Zaitlin, B.A., 1985, The effect of changes in tidal range on a sub-littoral macrotidal region, Bay of Fundy, Canada. Geo-Marine Letters, 4, 161−169.
Arnott, R.W.C., 1995, The parasequence definition¶°Are transgressive deposits inadequately addresses? Journal of Sedimentary Research, B65, 1−6.
Ashley, G.M., 1991, Classification of large-scale subaqueous bedforms: a new look at an old problem. Journal of Sedimentary Petrology, 60, 160−172.
Bahng, H.K., Lee, C.W. and Oh, J.K., 1994, Origin and characteristics of sand ridges in the western continental shelf of Korean Peninsula. Journal of the Korean Society of Oceanograhpy, 29, 217−227.
Beardsley, R.C., Limeburner, R., Yu, H. and Cannon, G.A., 1985, Discharge of the Changjiang (Yangtze River) into the East China Sea. Continental Shelf Research, 4, 57−76.
Beets, D.J., Van der Valk, L. and Stive, M.J.F., 1992, Holocene evolution of the coast of Holland. Marine Geology, 103, 423−443.
Belderson, R.H., Johnson, M.A. and Kenyon, N.H., 1982, Bedforms. In: Stride, A.H. (ed.), Offshore Tidal Sands: Processes and Deposits. Chapman and Hall, New York, p. 27−57.
Berné, S., Lericolais, G., Marsset, T., Bourillet, J.-F. and De Batist, M., 1998, Erosional offshore sand ridges and lowstand shorefaces: examples from tide- and wave-dominated environments of France. Journal of Sedimentary Research, 68, 540−555.
Bloom, A.L. and Park, Y.A., 1985, Holocene sea-level history and tectonic movements, Republic of Korea. Quaternary Research of Japan, 24, 77−84.
Boyd, R., Dalrymple, R.W. and Zaitlin, B.A., 1992, Classification of clastic coastal depositional environments. Sedimentary Geology, 80, 139−150.
Butenko, J., Ye, Y. and Milliman, J.D., 1983, Morphology, sediments and Late Quaternary history of the East China Sea. In: Acta Oceanologica Sinica (ed.), Proceedings of the International Symposium on Sedimentation on the Continental Shelf, with Special Reference to the East China Sea, 2. China Ocean Press, Beijing, p. 725−751.
Chang, J.H. and Choi, J.Y., 2001, Tidal-flat sequence controlled by Holocene sea-level rise in Gomso Bay, west coast of Korea. Estuarine, Coastal and Shelf Science, 52, 391−399.
Chang, J.H., Lee, C.W., Jin, J.H., Kim, S.P., Park, Y.S., Shin, W.C., Kim, W.S., Kim, C.K., Bong, P.Y., Lee, H.Y., Choi, S.J., Park, Y.A., Park, S.C. and Yoon, H.S., 1996, Yellow Sea Drilling Program for Studies on Quaternary Geology (Analyses of YSDP-102, YSDP-103, YSDP-104, YSDP-105 Cores). Report KR-96(T)-18, Korea Institute of Geoscience and Mineral Resources, Daejeon, 595 p. (in Korean with English abstract)
Chappell, J. and Grindrod, J., 1984, Chenier plain formation in Northern Australia. In: Thom, B.G. (ed.), Coastal Geomorphology in Australia. Academic Press, Sydney, p. 197−231.
Chen, Z. and Stanley, D.J., 1998, Sea-level rise on eastern Chinas's Yangtze delta. Journal of Coastal Research, 14, 360−366.
Choi, B.H., 1980, A tidal model of the Yellow Sea and the Eastern China Sea. KORDI report 80-02, Korea Ocean Research and Development Institute, Ansan, 80 p.
Choi, B.H. and Lee, H.S., 2003, Changes in tidal current regime and sedimentation at Saemangeum. In: Choi, B.H. and Park, Y.A. (eds.), Sedimentation in the Yellow Sea Coasts: Proceedings of KSCOE Workshop. KSCOE/KAOSTS, Seoul, p. 97−115.
Chough, S.K., Lee, H.J. and Yoon, S.H., eds., 2000, Marine Geology of Korean Seas. Elsevier, Amsterdam, 313 p.
Chough, S.K., Kim, J.W., Lee, S.H., Shinn, Y.J., Jin, J.H., Suh, M.C. and Lee, J.S., 2002, High-resolution acoustic characteristics of epicontinental sea deposits, centraleastern Yellow Sea. Marine Geology, 188, 317−331.
Chun, S.S., Yang, B.C., Lee, I.T. and Lee, H.J., 2000, Non-barred, open macrotidal flats strongly influenced by wave action, Gomso Bay and Baeksu Coast, Southwest Korea: Depositional processes, seasonal evolution and transgressive stratigraphy. Field Guide Book (B2), Tidalite 2000, 5th International Conference on Tidal Environments, Seoul, 101 p.
Dalrymple, R.W., 1992, Tidal depositional systems. In: Walker, R.G. and James, N.P. (eds.), Facies Models: Response to Sea-Level Change. Geological Association of Canada, p. 195−218.
Dalrymple, R.W., Knight, R.J., Zaitlin, B.A. and Middleton, G.V., 1990, Dynamics and facies model of a macrotidal sand-bar complex, Cobequid Bay-Salmon River Estuary (Bay of Fundy). Sedimentology, 37, 577−612.
Dalrymple, R.W., Makino, Y. and Zaitlin, B.A., 1991, Temporal and spatial patterns of rhythmite deposition on mud flats in the macrotidal Cobequid Bay-Salmon River Estuary, Bay of Fundy, Canada. In: Smith, D.G., Reinson, G.E., Zaitlin, B.A. and Rahmani, R.A. (eds.), Clastic Tidal Sedimentology. Canadian Society of Petroleum Geologists, Memoir, 16, p. 137−160.
Damuth, J.E. and Hayes, D.E., 1977, Echo character of the east Brazilian continental margin and its relationship to sedimentary processes. Marine Geology, 24, 73−95.
Davis, R. A., Jr., ed., 1985, Coastal Sedimentary Environments. Springer-Verlag, New York, 716 p.
DeJong, J.D., 1977, Dutch tidal flats. Sedimentary Geology, 18, 13−23.
DeMaster, D.J., Mckee, B.A., Nittrouer, C.A., Qian, J.G., Cheng, G.D., 1985, Rates of sediment accumulation and particle reworking based on radiochemical measurements from continental shelf deposits in the East China Sea. Continental Shelf Research, 4, 143−158.
Eisma, D., 1981, Supply and deposition of suspended matter in the North Sea. In: Nio, S.D., Shuttenhelm, R.T.E. and Van Weering, T.C.E. (eds.), Holocene Marine Sedimentation in the North Sea Basin. International Association of Sedimentologists, Special Publication, 5, 415−428.
Emery, K.O., 1968, Relict sediments on continental shelves of world. American Association of Petroleum Geologists Bulletin, 52, 445−464.
Eo, D.S. and Kim, J.S., 2003, Hydraulic studies and engineering application for Saemangeum project. In: Choi, B.H. and Kioka, W. (eds.), Hydro-Environmental Impacts of Large Coastal Developments: Proceedings of ACECC-TCI Workshop. KSCOE/JSCE, Seoul, p. 11−23.
Fairbanks, R.G., 1989, A 17,000-year glacio-esustatic sea-level record: Influence of glacial melting rates on the Younger Dryas event and deep-ocean circulation. Nature, 342, 637−642.
Feng, H. and Wang, Z., eds., 1986, Holocene sea-level changes and

coastline shifts in Zhejiang province. Department of Geography, Hangzhou University, 23 p.

Folk, R.L., 1954, The distinction between grain size and mineral composition in sedimentary rock nomenclature. Journal of Geology, 62, 334–359.

Frey, R.W., Dorjes, J. and Howard, J.D., 1989, Coastal sediments and patterns of bioturbation, eastern Buzzards Bay, Massachusetts. Journal of Sedimentary Petrology, 59, 1022–1035.

Guan, B.-X., 1994, Patterns and structures of the currents in Bohai, Huanghai and East China seas. In: Zhou, D., Liang, Y. and Tseng C.K. (eds.), Oceanology of China Seas, vol. 1. Kluwer Academic Publishers, Dordrecht, p. 17–26.

Hayes, M.O., 1979, Barrier island morphology as a function of tidal and wave regime. In: Leatherman, S.P. (ed.), Barrier islands. Academic Press, New York, p. 1–27.

Houbolt, J.J.H.C., 1968, Recent sediments in the Southern Bight of the North Sea. Geologie en Minbouw, 47, 245–273.

Hsueh, Y. and Romca, R.D., 1986, Winter winds and coastal sea-level fluctuations in the northeast China Sea, Part II, Numerical model. Journal of Physical Oceanography, 16, 241–261.

Jin, J.H., 2001, A sedimentological Study of Long Sediment Cores in the Eastern Yellow Sea. Ph.D. thesis, Seoul National University, Seoul, 176 p.

Jin, J.H. and Chough, S.K., 1998, Partitioning of transgressive deposits in the southeastern Yellow Sea: a sequence stratigraphic interpretation. Marine Geology, 149, 79–92.

Jin, J.H. and Chough, S.K., 2002, Erosional shelf ridges in the mid-eastern Yellow Sea. Geo-Marine Letters, 21, 219–225.

Jin, J.H., Chough, S.K. and Ryang, W.H., 2002, Sequence aggradation and systems tracts partitioning in the mid-eastern Yellow Sea: roles of glacio-eustasy, subsidence and tidal dynamics. Marine Geology, 184, 249–271.

Johnson, H.D. and Baldwin, C.T., 1996, Shallow clastic seas. In: Reading, H.G. (ed.), Sedimentary Environments: Processes, Facies and Stratigraphy. Blackwell Science, p. 232–280.

Jung, W.Y., Suk, B.C., Min, G.H. and Lee, Y.K., 1998, Sedimentary structure and origin of a mud-cored pseudo-tidal sand ridge, eastern Yellow Sea, Korea. Marine Geology, 151, 73–88.

Kim, J.-M. and Kennett, J.P., 1998, Paleoenvironmental changes associated with the Holocene marine transgression, Yellow Sea (Hwanghae). Marine Micropaleontology, 34, 71–89.

Kim, J.W., 2003, Late Quaternary depositional processes of the central-eastern Yellow Sea: Chirp acoustic characteristics. Ph.D. thesis, Seoul National University, Seoul, 87 p.

Kim, Y.H., Lee, H.J., Chun, S.S., Han, S.J. and Chough, S.K., 1999, Holocene transgressive stratigraphy of a macrotidal flat in the southwestern Yellow Sea: Gomso Bay, Korea. Journal of Sedimentary Research, 69, 328–337.

Klein, G.D., ed., 1977, Clastic tidal facies. Continuing Education Publication Company, Illinois, 149 p.

Klein, G.D.,1985, Intertidal flats and intertidal sandbodies. In: Davis, R.A.Jr. (ed.), Coastal Sedimentary Environments. Springer-Verlag, New York, p. 187–224.

Korea Meteorological Administration, 1997, Automatic Weather Station Data. Annual Report 09200-73320-26-13, 698 p.

Korea Meteorological Administration, 1998, Automatic Weather Station Data. Annual Report 09200-73320-26-13, 724 p.

Korea Ocean Research and Development Institute, 1994, Quaternary sea-level changes and their implication in the evolution of coastal depositional environments (III). KORDI Report BSPG 00223-732-5, Korea Ocean Research and Development Institute, Ansan, 315 p.

Kröel, F. and Flemming, B.W., 1998, Evidence for temperature-adjusted sediment distributions in the back-barrier tidal flats of the East Frisian Wadden Sea (Southern North Sea). In: Alexander, C.R., Davies, R.A. and Henry, V.J. (eds.), Tidalites: processes and products. Society of Economic Paleontologists and Mineralogists, Special Publication, 61, 31–41.

Larsen, L.H., Cannon, G.A. and Choi, B.H., 1985, East China Sea tidal currents. Continental Shelf Research, 4, 77–103.

Lee, H.J. and Chough, S.K., 1989, Sediment distribution, dispersal and budget in the Yellow Sea. Marine Geology, 87, 195–205.

Lee, H.J. and Chu, Y.S., 2001, Origin of inner-shelf mud deposit in the southeastern Yellow Sea: Huksan Mud Belt. Journal of Sedimentary Research, 71, 144–154.

Lee, H.J. and Jo, H.R., 2003, Sedimentological and hydrodynamical monitoring of modern sediments in Garolim Bay on the west coast of Korea. In: Choi, B.H. and Park, Y.A. (eds.), Sedimentation in the Yellow Sea Coasts: Proceedings of KSCOE Workshop. KSCOE/KAOSTS, Seoul, p. 323–344.

Lee, H.J. and Yoon, S.H., 1997, Development of stratigraphy and sediment distribution in the northeastern Yellow Sea during Holocene sea-level rise. Journal of Sedimentary Research, 67, 341–349.

Lee, H.J., Chough, S.K., Jeong, K.S. and Han, S.J., 1987, Geotechnical properties of sediment cores from the southeastern Yellow Sea: effects of depositional processes. Marine Geotechnology, 7, 37–52.

Lee, H.J., Chun, S.S., Chang, J.H. and Han, S.J., 1994, Landward migration of isolated shelly sand ridge (chenier) on the macrotidal flat of Gomso Bay, west coast of Korea: Controls of storms and typhoon. Journal of Sedimentary Research, A64, 886–893.

Lee, H.J., Chu, Y.S. and Park, Y.A., 1999, Sedimentary processes of fine-grained material and the effect of seawall construction in the Daeho macrotidal flat-nearshore area, northern west coast of Korea. Marine Geology, 157, 171–184.

Lee, H.J., Park, K.S., Jo, H.R., Chu, Y.S., Sun, S.O., Kim, D.H., Park, E.S., Han, C.K., Kim, M.J., Jeong, K.H., 2002, Modeling of sedimentary dynamical behavior of coastal suspended sediments. NRL Report 2000-N-NL-01-C-264, Korea Institute of Science and Technology Evaluation and Planning, Seoul, 323 p.

Lee, H.J., Jo, H.R., Chu, Y.S. and Bahk, K.S., 2004, Sediment transport on macrotidal flats in Garolim Bay, west coast of Korea: significance of wind waves and asymmetry of tidal currents. Continental Shelf Research, 24, 821–832.

Lee, J.C., and Jung, K.T., 1999, Application of eddy viscosity closure models for the M_2 tide and tidal currents in the Yellow Sea and the East China Sea. Continental Shelf Research, 19, 445–475.

Li, C., Wang, P., Daidu, F., Bing, D. and Tiesong, L., 2000, Open-coast intertidal deposits and the preservation potential of individual laminae: a case study from east-central China. Sedimentology, 47, 1039–1051.

Li, C.X., Zhang, J.Q., Fan, D.D. and Deng, B., 2001, Holocene regression and the tidal radial sand ridge system formation in the Jiangsu coastal zone, east China. Marine Geology, 173, 97–120.

Li, M.Z. and Amos, C.L., 2001, SEDTRANS96: the upgraded and better calibrated sediment-transport model for continental shelves. Computers and Geosciences, 27, 619–645.

Lie, H.-J., 1985, Wintertime temperature-salinity characteristics in the southeastern Hwanghae (Yellow Sea). Journal of the Oceanographical Society of Japan, 41, 291–298.

Lie, H.-J., Cho, C.-H., Lee, J.-H. and Lee, S., 2001, Does the Yellow

Sea Warm Current really exist as a persistent mean flow? Journal of Geophysical Research, 106, 22199–22210.
Lie, H.-J., Cho, C.-H., Lee, J.-H. and Lee, S., 2003, Structure and eastward extension of the Changjiang River plume in the East China Sea. Journal of Geophysical Research, 108 (C3), 3077, doi:10.1029/2001JC001194.
Lim, D.I., 2001, Late Quaternary Stratigraphy and Sedimentology of Tidal-flat Deposits, Western Coast of Korea. Ph.D. thesis, Seoul National University, Seoul, 303 p.
Liu, J.P. and Milliman, J.D., 2004, Western Pacific post-glacial rapid and stepwise sea-level rise. 5th International Conference on Asian Marine Geology (Abstract), Bangkok, Jan. 13–18, p. 99.
Liu, J.P., Milliman, J.D. and Gao, S., 2002, The Shandong mud wedge and post-glacial sediment accumulation in the Yellow Sea. Geo-Marine Letters, 21, 212–218.
Liu, Z.X., 1997, Yangtze Shoala modern tidal sand sheet in the northwestern part of the East China Sea. Marine Geology, 137, 321–330.
Mask, A.C., O'Brien, J.J. and Preller, R., 1998, Wind-driven effect on the Yellow Sea Warm Current. Journal of Geophysical Research, 103, 30713–30729.
McCave, I.N., 1970, Deposition of fine grained suspended sediment from tidal currents. Journal of Geophysical Research, 75, 4151–4159.
Milliman, J.D. and Meade, R.H., 1983, Worldwide delivery of river sediment to the oceans, Journal of Geology, 91, 1–21.
Milliman, J.D., Beardsley, R.C., Yang, Z.S. and Limeburner, R., 1985, Modern Huanghe-derived muds on the outer shelf of the East China Sea: identification and potential transport mechanisms. Continental Shelf Research, 4, 175–188.
Milliman, J.D., Qin, Y.S., Ren, M.E. and Saito, Y., 1987, Man's influence on the erosion and transport of sediment by Asian rivers: the Yellow River (Huanghe) example. Journal of Geology, 95, 1–21.
Milliman, J.D., Qin, Y.S. and Park, Y.A., 1989, Sediment and sedimentary processes in the Yellow and East China Seas. In: Taira, A. and Masuda, F. (eds.), Sedimentary Facies in the Active Plate Margin. Terra Scientific Publishing Company, Tokyo, p. 233–249.
Mukherjee, K.K., Das, S. and Chakrabarti, A., 1987, Common physical sedimentary structure in a beach-related open-sea siliciclastic tropical tidal flat at Chandipur, Orissa, India and Evaluation of the Weather conditions through discriminant analysis. Senckenbergiana Maritima, 19, 261–293.
National Fisheries Research and Development Institute, 1997, Oceanographic observations. Annual Report, 46, Busan, 545 p.
National Fisheries Research and Development Institute, 1998, Oceanographic observations. Annual Report, 47, Busan, 327 p.
National Geographic Institute, 1978, Basic Research Report on Nearshore Environments of Korea (Asan Bay and adjacent areas). Seoul, 63 p.
National Geographic Institute, 1979, Basic Research Report on Nearshore Environments of Korea (Geunheung area). Seoul, 37 p.
National Geographic Institute, 1980, Basic Research Report on Nearshore Environments of Korea (Ungcheon area). Seoul, 64 p.
National Geographic Institute, 1981, Basic Research Report on Nearshore Environments of Korea (Seokpo area). Seoul, 56 p.
National Geographic Institute, 1982, Basic Research Report on Nearshore Environments of Korea (Mokpo area). Seoul, 70 p.
National Geographic Institute, 1983, Basic Research Report on Nearshore Environments of Korea (Beopseongpo area). Seoul, 60 p.
Nittrouer, C.A., Demaster, D.J. and McKee, B.A., 1984, Fine-scale stratigraphy in proximal and distal deposits of sediment dispersal systems in the East China Sea. Marine Geology, 61, 13–24.
Nummedal, D. and Swift, D.J.P., 1987, Transgressive stratigraphy at sequence bounding unconformitiessome principles derived from Holocene and Cretaceous examples. In: Nummedal, D., Pilkey, O.H. and Howard, J.D. (eds.), Sea-Level Fluctuation and Coastal Evolution. Society of Economic Paleontologists and Mineralogists, Special Publication, 41, 241–260.
Park, S.-C., Lee, H.-H., Han, H.-S., Lee, G.-H., Kim, D.-C. and Yoo, D.-G., 2000, Evolution of late Quaternary mud deposits and recent sediment budget in the southeastern Yellow Sea. Marine Geology, 170, 271–288.
Park, Y.A. and Khim, B.K., 1992, Origin and dispersal of recent clay minerals in the Yellow Sea. Marine Geology, 104, 205–213.
Park, Y.-H., 1986, A simple theoretical model for the upwind flow in the southern Yellow Sea. Journal of the Korean Society of Oceanography, 21, 203–210.
Pirazzoli, P.A., ed., 1991, World atlas of Holocene sea-level changes. Elsevier, Amsterdam, 300 p.
Posamentier, H.W., Jervy, M.T. and Vail, P.R., 1988, Eustatic controls on clastic deposition I-conceptual framework. In: Wilgus, C.K., Hastings, B.S., Kendall, C. G.S.C., Posamentier, H.W., Ross, C.A. and Van Wagoner, J.C. (eds.), Sea-Level Changes: An Intergrated Approach. Society of Economic Paleontologists and Mineralogists, Special Publication, 42, 109–124.
Reading, H.G., ed., 1996, Sedimentary environments: processes, facies and stratigraphy. Blackwell Science, Oxford, 688 p.
Reineck, H.E., ed., 1963, Sedimentgefuge im Bereich der sudichen Nordsee. Senckenberg Natural History Society, 505, Germany, 138 p.
Reineck, H.E., 1972, Tidal flats. In: Rigby, J.K. and Hamblin, W.K. (eds.), Recognition of Ancient Sedimentary Environments. Society of Economic Paleontologists and Mineralogists, Special Publication, 16, 146–159.
Reineck, H.E. and Cheng, Y.M., 1978, Sedimentologische und faunistische untersuchungen an Watten in Taiwan. I. Aktuogeologische untersuchungen. Senckenbergiana Maritima, 10, 85–115.
Reineck, H.E. and Singh, I.B., eds., 1980, Depositional Sedimentary Environments. Springer-Verlag, New York, 430 p.
Reynaud, J.-Y., Tessier, B., Berné, S., Chamley, H. and Debatist, M., 1999, Tide and wave dynamics on a sand bank from the deep shelf of the Western Channel Approaches. Marine Geology, 161, 339–359.
Ryu, S.O., 2003, Seasonal variation of sedimentary processes in a semi-enclosed bay: Hampyeong Bay, Korea. Estuarine, Coastal and Shelf Science, 56, 481–492.
Ryu, S.O., Lee, H.J. and Chang, J.H., 2004, Seasonal cycle of sedimentary process on mesotidal flats in the semienclosed Muan Bay, southern west coast of Korea: culminating summertime erosion. Continental Shelf Research, 24, 137–147.
Saito, Y., 1998, Sea levels of the last glacial in the East China Sea continental shelf. Quaternary Research of Japan, 37, 237–242 (in Japanese with English abstract).
Schlager, W., 1993, Accommodation and supply: a dual control on stratigraphic sequences. Sedimentary Geology, 86, 111–136.
Scott, D.B. and Greenberg, D.A., 1983, Relative sea-level rise and tidal development in the Fundy tidal system. Canadian Journal of Earth Sciences, 20, 1554–1564.
Shinn, Y.J., 2003, High-Resolution Seismic Reflection Studies of Late Quaternary Sediments in the Southern Yellow Sea and Northern East China Sea, M.Sc. thesis, Seoul National University, Seoul, 65 p.

Shinn, Y.J., Chough, S.K., Kim, J.W., Lee, S.H., Woo, J., Jin, J.H., Hwang, S.Y., Choi, S.H. and Suh, M.C., 2004, High-Resolution Seismic Reflection Studies of Late Quaternary Sediments in the Eastern Yellow Sea. In: Ocean-Continent Interactions within the East Asian Marginal Seas. American Geophysical Union Monograph (in press).

Short, A.D., 1991, Macro-meso tidal beach morphodynamics: an overview. Journal of Costal Research, 7, 417–436.

Song, W.-O., Yoo, D.-H., Dyer, K.R., 1983, Sediment distribution, circulation and provenance in a macrotidal bay: Garolim Bay, Korea. Marine Geology, 52, 121–140.

Soulsby, R., 1997, Dynamics of Marine Sands: a Manual for Practical Applications. Thomas Telford, London, 249 p.

Stride, A.H., Belderson, R.H., Kenyon, N.H. and Johnson, M.A., 1982, Offshore tidal deposits: sand sheet and sand bank facies. In: Stride, A.H. (ed.), Offshore Tidal Sands: Processes and Deposits. Chapman and Hall, London, p. 95–125.

Su, Y.-S. and Weng, X.-C., 1994, Water masses in China seas. In: Zhou, D., Liang, Y. and Tseng C.K. (eds.), Oceanology of China Seas, vol. 1. Kluwer Academic Publishers, Dordrecht, p. 3–16.

Thorne, J.A. and Swift, D.J.P., 1991, Sedimentation on continental margin, VI: a regime model for depositional sequences, their component systems tracts, and bounding surfaces. In: Swift, D.J.P., Oertel, G.F., Tillman, R.W. and Thorne, J.A. (eds.), Shelf Sand and Sandstone Bodies. International Association of Sedimentologists, Special Publication, 14, 189–255.

Uehara, K. and Saito, Y., 2003, Late Quaternary evolution of the Yellow/East China Sea tidal regime and its impacts on sediments dispersal and seafloor morphology. Sedimentary Geology, 162, 25–38.

Uehara, K., Saito, Y. and Hori, K., 2002, Paleotidal regime in the Changiang (Yangtze) Estuary, the East China Sea, and the Yellow Sea at 6 ka and 10 ka estimated from a numerical model. Marine Geology, 183, 179–192.

Van de Plassche, O., and Roep, T.B., 1989, Sea-level changes in the Netherlands during the last 6,500 years: Basal peat vs. coastal barrier data. In: Scott, D.B., Pirazzoli, P.A. and Honig, C.A. (eds.), Late Quaternary Sea-Level Correlation and Applications. Amsterdam, Elsevier, p. 41–56.

Van der Spek, A.J.F. and Beets, D.J., 1992, Mid-Holocene evolution of a tidal basin in the western Netherlands: A model for future changes in the northern Netherlands under conditions of accelerated sea-level rise. Sedimentary Geology, 80, 185–197.

Van Wagoner, J.C., Mitchum, R.M., Campion, K.M. and Rahmanian, V.D., 1990, Siliciclastic sequence stratigraphy in well logs, cores, and outcrops. American Association of Petroleum Geologists, Methods in Exploration Series, 7, 55 p.

Walker, R.G. and James, N.P., eds., 1992, Facies models: Response to Sea Level Changes. Geological Association of Canada, 407 p.

Walker, R.G. and Plint, A.G., 1992, Wave- and storm-dominated shallow marine systems. In: Walker, R.G. and James, N.P. (eds.), Facies Models: Response to Sea-Level Change. Geological Association of Canada, p. 219–238.

Wang, P., Min, Q. and Gao, J., 1985, A preliminary study of foraminiferal and ostracod assemblages in the Huanghai Sea. In: Wang, P. (ed.), Marine Micropaleontology of China. China Ocean Press, Beijing, p. 115–132.

Wang, Y. and Aubrey, D.G., 1987, The characteristics of the China coastline. Continental Shelf Research, 7, 329–349.

Wells, J.T., 1988, Distribution of suspended sediment in the Korea Strait and southern Yellow Sea: onset of winter monsoons. Marine Geology, 83, 273–284.

Woodroffe, C.D., Curtis, R.J. and McLean, R.F., 1983, Development of a chenier plain, firth of Thames, New Zealand. Marine Geology, 53, 1–22.

Wright, L.D. and Short, A.D., 1984, Morphodynamic variablility of surf zones and beaches: a synthesis. Marine Geology, 56, 339–364.

Yang, B.C., 2000, Seasonal cycle of surface sediment distribution and evolution of sedimentary facies on the Baeksu intertidal flat, southwestern open coast of the Korean Peninsula. M.Sc. thesis, Chonnam National University, Gwangju, 147 p.

Yang, B.C. and Chun, S.S., 2001, A seasonal model of surface sedimentation on the Baeksu open-coast intertidal flat, southwestern coast of Korea. Geosciences Journal, 5, 251–262.

Yang, B.C., Dalrymple, R.W., Chun, S.S. and Kim, J.K., 2003a, Characteristics of storm deposits in open-coast tidal flats, southwestern coast of Korea: Rising-tide and falling-tide sequence. 2003 Spring Meeting of Korean Society of Oceanography (Abstract), Jeju, May 15–16, p. 216–218.

Yang, B.C., Dalrymple, R.W. and Chun, S.S., 2004, Sedimentation on a wave-dominated, open-coast tidal flat, southwestern Korea: summer tidal flat - winter shoreface, Sedimentology, 51 (in press).

Yang, C.-S., 1989, Active, moribund and buried tidal sand ridges in the East China Sea and the southern Yellow Sea. Marine Geology, 88, 97–116.

Yang, H. and Xie, Z., 1984, Sea-level changes in East China over the past 20,000 years, In: Whyte, R.O. (ed.), The Evolution of Eastern Asian Environment. University of Hong Kong, p. 288–308.

Yang, S.Y., Li, C.X., Jung, H.S. and Lee, H.J., 2002, Discrimination of geochemical compositions between the Changjiang and the Huanghe sediments and its application for the identification of sediment source in the Jiangsu coastal plain, China. Marine Geology, 186, 229–241.

Yang, S.Y., Jung, H.S., Lim, D.I. and Li, C.X., 2003b, A review on the provenance discrimination of sediments in the Yellow Sea. Earth Science Reviews, 63, 93–120.

Yeo, R.K. and Risk, M.J., 1981, The sedimentology, stratigraphy, and preservation of intertidal deposits in the Minas Basin System, Bay of Fundy. Journal of Sedimentary Petrology, 51, 245–260.

Yoo, D.G., Lee, C.W., Kim, S.P., Jin, J.H., Kim, J.K. and Han, H.C., 2002, Late Quaternary transgressive and highstand systems tracts in the northern East China Sea mid-shelf. Marine Geology, 187, 313–328.

Zong, Y., 2004, Mid-Holocene sea-level highstand along the southeast coast of China. Quaternary International, 117, 55–67.

Manuscript received May 28, 2004
Manuscript accepted June 15, 2004